A Self-Controlled Master-Slave Upper Limb Rehabilitation Robot

Li Chunguang

A dissertation submitted to
Kochi University of Technology
in partial fulfillment of the requirements
for the degree of

Doctor of Philosophy

Special Course for International Students
Graduate School of Engineering
Kochi University of Technology
Kochi, Japan

February 2011

Abstract

Numerous upper limb rehabilitation robots have been developed to deliver therapy for hemiplegic patients with a unilateral-disabled limb or for aged persons with motor-function degenerated limbs. Rehabilitation robots supporting different training modes (for treating patients with different residual motor capabilities) and self-controlled exercises (for motivating active participation of patients in rehabilitation therapy) have attracted much attention recently. Particularly, many bilateral arm rehabilitation robots were developed because that bimanual coordinated training may motivate cerebral activation in both hemispheres and promote recovery process.

An innovative master-slave self-controlled upper-limb rehabilitation robot was introduced in this paper. Two identical DC motors with a wired connection are located in the master and slave manipulator sites respectively. A subject controls master and slave terminal handles with his/her two limbs. Based on the acting forces of two limbs, the motor attached with a larger torque works in generating state (master) and powers the other one, which works in electromotive state (slave) to overcome an external load induced by one limb. The robot implements force sensing without using a force sensor or an impedance controller. It is also characteristic by energy recycling and bidirectional controllability. The robot supports bimanual-coordinated exercises in passive-driven, active-assisted, and active-resisted training modes (the first and second patterns before and after the hyphen denote the states of the more impaired limb in point of itself and the less impaired or healthy limb, respectively). No matter in which mode, the required force for the more impaired limb is provided by the less impaired or healthy limb.

Three prototypes of mater-slave devices were developed. The first prototype was designed with a microprocessor realizing master-slave motion tracking control. Experiments performed on this

prototype validated the feasibility of the proposed master-slave mechanism and preliminarily confirmed the capabilities of the system in force sensing and energy recycling. In the second prototype, motors with higher efficiency were used to reduce energy loss in the master-slave circuit. Encoders with higher accuracy and a dSPACE control platform (DS1104) were applied to realize master-slave control and to increase motion tracking precision. As well, torque transducers were adopted to measure terminal torques and to confirm the force sensing capability of the system more fully. Experiments conducted on this prototype further confirmed the capability of force sensing and energy recycling, and demonstrated bidirectional controllability of the system.

The third prototype increased the driving power of the system and is capable of supporting bilateral arm coordinated training. A master-slave system model was provided and verified. Stability analysis revealed that this prototype can respond to a subject's commands safely if the rotational velocity was within a frequency range of 30 Hz. Training experiments in different training modes were performed simultaneously with the measurement of hemoglobin concentration (using near-infrared spectroscopic (NIRS) imaging system). The concentration of oxygenated hemoglobin was used to reflect cerebral activation level (CAL). Group analysis revealed that CAL and motion tracking capability of subjects increased after training. This demonstrated a positive training effect of the robot. In addition, bimanual training induced greater brain activation than single limb training. This indicated that the bilateral arm coordinated exercises supported by the robot may stimulate the functional integrity of two hemispheres. Therefore, the robot has a potential for promoting motor function improvement.

Contents

1. Introduction

1.1 Development of Rehabilitation Robots

Nowadays stroke or brain injury is a common disease, which results in an increasing number of hemiplegic patients with unilateral limb impairment. Meanwhile, the percentage of aged persons is continuously increasing in many countries. In the elderly, the prevalence of physical deterioration is very high, and their physical deterioration generally leads to degeneration of motor function. Thereby, motor function recovery and strength enhancement are necessary in our aging society. This emerging requirement has stimulated considerable interest in the development of upper limb rehabilitation robots, which can act as a therapeutic aid for therapists under existing conditions in many countries where the physical therapy resources are quite limited.

Numerous robots were developed to deliver arm therapy, such as MIT-MANUS [1, 2], ARM-GUIDE [3, 4], MIME [5, 6] and ARMin [7], which are representative robotic devices that have been tested extensively on hemiplegic patients and achieved good results in improving arm function. MIT-MANUS, which is a 2 degrees-of-freedom assisted robot, can support patients in executing reaching movements in a horizontal plane. In order to achieve a better improvement in shoulder strength and function, ARM-GUIDE, MIME and ARMin were developed to give training in a three-dimensional workspace. ARM-GUIDE allows subjects to perform active-assisted reaching movements against gravity. It can be used as both a diagnostic tool and a treatment tool for addressing arm impairment in hemiparetics. MIME supports unilateral training in passive, active-assisted, and active-constrained modes. Furthermore, it can assist the affected limb to move with the same manner of motion as the contra-lateral limb, with the two limbs performing bilateral mirror image movements. The results of clinical evaluation with FM (Fugl-Meyer) scale and MSS (Motor status score) immediately before-treatment, immediately

post-treatment, and 6 months after treatment suggested that combining unilateral and bilateral training modes may accelerate impairment reduction, and that bilateral exercise may help to achieve reduced hypertonia and abnormal synergies. ARMin is robotic device that can deliver patient-cooperative arm therapy. It allows patients to play ball games or perform ADL-related tasks by combining an audiovisual display, which can motivate the activity of patients in exercises. However, these robots are relatively complex and difficult to set up by patients themselves. Besides, the supervision from a therapist is always required during the training process. Thus, the durations that patients spend in rehabilitation activities are limited and the economic burden to patients is increased.

A home-based rehabilitation makes treatments with relatively high intensity and frequency that are favorable for improving motor recovery [8]. Therefore, the development of telerehabilitation robots which can be used in patients' homes is a new tendency recently. A portable telerehabilitation system [9–11] with haptic feeling was developed for the treatment and assessment of elbow deformity of stroke patients. A real-time control strategy and a teach-and-replay control method are achieved for tasks involving slow movements and fast movements, respectively. And the torque and position control modes for the master and slave devices can be exchanged for passive and active movements. Thus the system supports both the passive and the active movements including slow and fast tasks. However, the teach-and-replay control does not actually accomplish transparent haptic feeling. Otherwise, the control strategy is complex since a hybrid force-position controller is employed and a separate control method is required for the master and slave devices. Furthermore, the operator is a therapist rather than patients themselves. Patients are trained passively or with insufficient initiative (visual/video feedback). This is unfavorable to acquire a good recovery effect. Even though therapists can optimize the therapy scheme according to the feedback force, the degree of comfort of patients cannot be sensed, so it is possible to make patients feel pain in the process of training. Therefore, many self-controlled upper limb rehabilitation robots were developed for use at home [12–15].

Popescu and Burdea introduced a PC-based rehabilitation system to support home-based VR (virtual-reality) exercises [16]. The included networking allows clinic to telemonitor the training process and to change the difficulty level of exercises. And the rehabilitation component can apply resistive forces to patients. However, no experimental results were presented. Colombo and Pisano presented two robots for home-based upper limb rehabilitation training [17]. Particularly, a new evaluation metrics was proposed for observing the improvement rate and selecting the targeted rehabilitative strategies. During exercise, patients themselves control the handle of the device to track a target position repeatedly. The experimental results demonstrate the validity of this rehabilitation technique both in recent and in chronic post-stroke patients.

Meanwhile, in order to motivate much more activation of patients in exercises and facilitate the motor recovery, some robots that support bimanual training were introduced. In bilateral arm training with rhythmic auditory cueing (BATRAC) [18], the less impaired arm provided minimal assistance for the more impaired arm when necessary. Results of Fugl-Meyer Motor Performance Test and the Wolf Motor Arm Test (WMAT) suggested that BATRAC yielded significant and durable functional gains in patients even with serious upper extremity hemiparesis. The assessment with functional magnetic resonance imaging (fMRI) [19] gave evidence that BATRAC may lead to reorganization of brain regions involved in motor control. Hesse [20] proposed a portable robot for training the bilateral forearm and wrist of hemiparetic patients. Bimanual mirror symmetric movements can be realized with the healthy arm providing an assistant force for the paretic one or with the robot attaching a resistant force to the paretic arm. 12 chronic hemiparetic patients performed bimanual training. Significantly decreased Modified Ashworth Scale (MAS) score revealed a reduction of wrist and finger spasticity, but minimally increased Rivermead Motor Assessment (RMA) score could not reveal a significant improvement of motor function. A subsequent trial [21] on 44 acute stroke patients revealed that the robot-trained group produced a superior enhancement in upper limb motor control and power compared with the group that practiced with electrical simulation of the paretic wrist extensor. This is

probably explained by the bilateral practice and extensive repetitions of the robot therapy.

1.2 Rehabilitation of Brain Function

As for hemiplegic patients and aged persons with degenerated motor function, there is always functional disorder in some regions or a hemisphere of brain. Therefore, more and more researches studied brain mechanism during the process of motor function recovery. Commonly used methods in brain research include electroencephalography (EEG), magneto encephalography (MEG), functional magnetic resonance imaging (fMRI), and near infrared spectroscopy (NIRS). The comparison among these methods is introduced in [22]. MEG and fMRI have limited application environment because movement is restrained seriously in these methods. EEG is a neuroimaging method that has high temporal resolution but relatively poor spatial resolution. NIRS imaging technique is a non-invasive approach for monitoring cerebral activation and is capable of continuous data collection during dynamic movements. It is less susceptible to data corruption by movement and has a higher spatial resolution than EEG. It has been applied for studying the mechanism underlying the recovery of motor functions [23–27], and its validity and merits has been verified with the achieved positive results. Researches [28, 29] have confirmed that during the process of motor function recovery, the cerebral activation in impaired regions or hemisphere usually increased and the asymmetry of regional activation improved. A skilled reaching test on rats [30] demonstrated that the coordination of two forearms may induce the functional integrity of two hemispheres and contribute to motor function recovery.

1.3 Research Goals

It is widely accepted that force feedback is desirable in rehabilitation robotic systems because a kinesthetic feel of interaction forces can guide human operators to determine an appropriate input force according to various handling environments. However, the robotic systems mentioned above realize force feedback/sensing with torque/force sensors or impedance controllers, which increase the difficulty of hardware mounting or control complexity of the system. In our research,

a self-controlled master-slave robot was developed for supporting rehabilitation training in a home environment. The robot realized bilateral force sensing without using any force sensor. It was also characteristic by master-slave motion tracking, energy recycling, and bidirectional controllability with a compact structure. Master and slave units were controlled by a subject with two limbs. This avoided the time-delay caused by distance between the master and slave devices (tele-rehabilitation). The robot supported bimanual training in passive-driven, active-assisted, and active-resisted modes for patients with different residual motor functions. Different modes are realized with the healthy limb providing a suitable force (a driving force in passive mode, an assistant force in active-assisted mode, or a resistant force in active-resisted mode) for the impaired limb. On the other hand, it is impossible to avoid subjective factors of therapists when evaluates recovery effect by using the traditional assessment methods such as Fugl-Meyer (FM) scale, Motor status score (MSS), Modified Ashworth Scale (MAS) score, and so on. In this paper, training effect was objectively assessed based on the variation of movement performance and cerebral activation concentration that measured with NIRS imaging technique.

The paper is organized as follows: Section 2 presents theoretical materials of the proposed master-slave robot; Section 3 introduces the designed three prototypes and the corresponding validation experiments; Section 4 introduces motion tracking experiments, and confirms the training effect and the advantages of the proposed bimanual training in view of movement performance and CAL; Section 5 shows conclusions.

2. Methods and Materials

In the designed master-slave robot, two DC motors are utilized to construct a closed-loop circuit by a wired connection: the negative power input terminals of the two motors are connected directly, while their positive power input terminals are connected with an H-bridge driver, which supplement a certain amount of energy for the circuit. Two operating handles in the master and slave terminals are controlled by two upper limbs of a subject. Schematic diagram of upper limb rehabilitation training is shown in Fig. 2-1. One limb exerts a force on one handle and drives the ipsilateral motor to generate electric energy. Based on the closed-loop current, this energy is recycled to power the other motor to output one force. This force assists the contra-lateral limb or balances the force of the contra-lateral limb to implement desired movements. Based on movement intention, desired training mode (passive-driven, active-assisted, or active-resisted), force sensation, and the state of the more impaired limb, the subject regulates the force of the healthy or less impaired limb to assist or resist the more impaired one in motion imitation. No matter in which mode, two limbs perform symmetric mirror image movement.
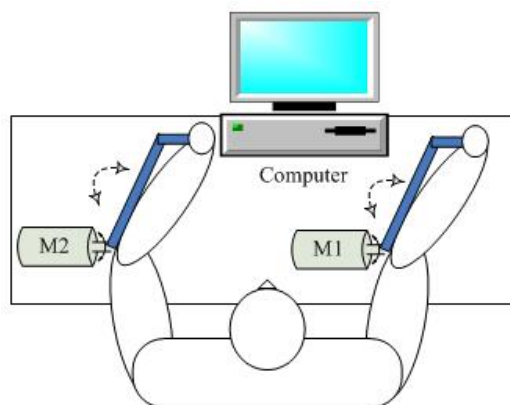

Fig. 2-1 Schematic diagram of upper limb rehabilitation training

2.1 Theoretical Analysis

Equivalent closed-loop circuit of the system is given in Fig. 2-2, in which M_m and M_s represent the two motors. In this paper, the subscripts $_m$ and $_s$ mean the master and the slave respectively, and the parameters with subscripts $_{in}$ and $_{out}$ denote the terminal variables in the master and slave sites respectively. Based on the dynamics mechanism, the motion equations are written as Eq. (1) when two terminal torques have an opposite direction. In the case when two terminal torques possess the same direction, the motion equation in the slave site is re-written as Eq. (2).

$$\begin{cases} \dfrac{T_{in}\eta_m}{N_m} = T_M + T_{0\_m} + J_m N_m \dfrac{d\omega_{in}}{dt} \\ \dfrac{T_{out}}{N_s\eta_s} = T_M - T_{0\_s} - J_s N_s \dfrac{d\omega_{out}}{dt} \\ T_M = C_T i \end{cases} \tag{1}$$

$$-\frac{T_{out}\eta_s}{N_s} = T_M - T_{0\_s} - J_s N_s \frac{d\omega_{out}}{dt} \tag{2}$$

where T_{in} and T_{out} stand for terminal torques; T_M denotes electromagnetic torque, the two motors possess identical electromagnetic torque since the same torque constant C_T and the shared closed-loop current i; T_{0_m} and T_{0_s} are motor no-load torques caused by no-load losses including mechanical loss, magnetic core loss, and additional loss in the motors; J_m and J_s are motor inertial moments; ω_{in} and ω_{out} are terminal velocities; N_m, N_s and η_m, η_s represent the gear ratios and working efficiencies of the gearboxes. According to Eq. (1), the relationship between the torques in the two sites can be written as:

$$\begin{cases} T_{in} = \lambda_T T_{out} + \dfrac{N_m}{\eta_m}(T_{0\_m} + T_{0\_s} + J_m N_m \dfrac{d\omega_{in}}{dt} + J_s N_s \dfrac{d\omega_{out}}{dt}) \\ \lambda_T = \dfrac{N_m}{N_s}\dfrac{1}{\eta_m\eta_s} \end{cases} \tag{3}$$

where λ_T is defined as force sensing coefficient, which expresses force sensing capability

towards the force variation in slave site. For the case that two terminal torques have the same direction, the force sensing coefficient is expressed as:

$$\lambda_T = -\frac{N_m}{N_s}\frac{\eta_s}{\eta_m} \tag{4}$$

Eqs. (3) and (4) indicates that the torques in the two terminals correspond to each other. This is realized due to the closed-loop current. When an active force or an impedance in one site increases/reduces, the current as well as the electromagnetic torques of the two motors increases/reduces, then, the other limb can immediately sense this variation in the contra-lateral site and regulate the resistant, assistant, or driving force accordingly, further to achieve a new balance between the torques in the two sites. Meanwhile, the limb that exerts an active force can also sense the variation of the resistant or assistant force. This means that the system is capable of mirroring the force in each site to the contra-lateral site (bilateral force sensing) without a force sensor. However, the no-load torques and inertial torques of the motors increase the requirement for the torque of the healthy limb. But this can not affect a correct force sensation because the no-load torques and inertial torques of the motors are almost constant when the rotational velocities have not big change, which is the case in rehabilitation application.
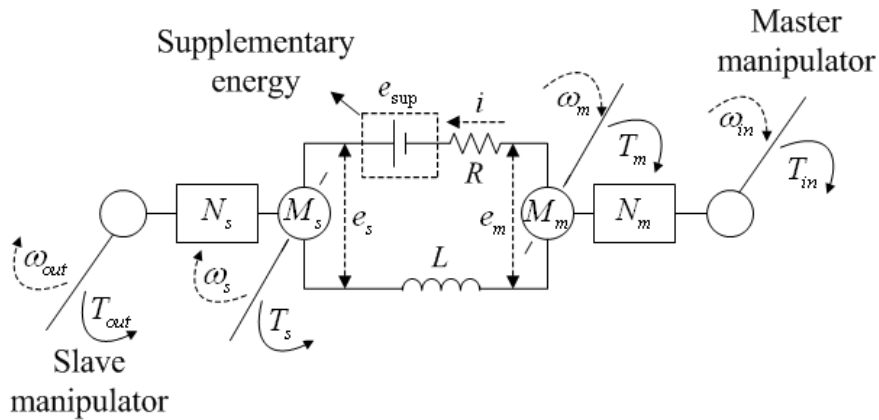

Fig. 2-2 Equivalent closed-loop circuit of the master-slave system

Under the control of a subject, the master motor generates electric energy and transmits it to the

slave motor, and the slave motor is driven to move with the motion trend of the master motor. However, the energy losses in the circuit make it impossible to realize accurate motion tracking. This is especially the case when a large resistance is attached to the slave site, a large current and therefore large energy losses in the circuit will result, further, the two motors will have a big difference in velocities and positions. And usually, the rotational velocity of the master should be very high to actuate the slave. In order to realize master-slave symmetric movement accurately and make it possible to actuate the slave with a slow input velocity, a certain amount of energy is compensated for the circuit to offset the energy losses. Based on the electrical mechanism, the voltage balance equation of the circuit can be written as:

$$
\begin{cases}
2Ri + 2L\dfrac{di}{dt} = e_m + e_{\sup} - e_s \\
e_m = C_T N_m \omega_{in}, e_s = C_T N_s \omega_{out}
\end{cases}
\tag{5}
$$

where R and L denote the motor resistance and inductance, since the two motors are connected in series, a factor of 2 is needed here; e_m and e_s are motor armature voltages, which depend on the motor torque constant and the velocities of the motors. e_s is referred to as counter EMF (electromotive force) since it has an opposite direction with the current; $e_{\sup}$ is the supplementary voltage (how to supplement a proper amount of energy will be introduced in chapter 3). The energy generated by the master motor, together with the supplementary energy, enables the slave/gear unit to reproduce the movement of the master/gear unit. That is, the system achieves a kind of energy recycling. When accurate motion tacking is realized ($\omega_{in} = \omega_{out}$), the supplementary voltage can be expressed as:

$$
e_{\sup} = 2(Ri + L\frac{di}{dt})
\tag{6}
$$

On the other hand, if the master and slave motors have no connection, and an independent supply power is used to drive the slave/gear unit to accomplish motion imitation, the corresponding driving voltage (e_{dri}) in the slave site will be written as:

$$e_{dri} = e_s + Ri + L\frac{di}{dt} \tag{7}$$

in which the current is the same as that in Eq. (6) when the identical external force was attached and movement velocity was same. The armature voltage is usually larger than the energy losses in the resistance and inductance for a rehabilitation application (large load), thus the supplementary voltage in Eq. (6) is always less than the driving voltage in Eq. (7). That is, the required energy is reduced due to the recycled energy from the master motor.

According to the above analysis, the system is equivalent to a damping system, through which a subject can adjust the input force of one limb properly according to the variation of an active force in the contra-lateral side, even though there is frictional loss in the power transmission process. Whereas, a certain amount of energy is required for achieving the same motion manner of the two motors.

2.2 Gearbox Function

For a rehabilitation application, it is almost impossible to find motors with sufficient torques to support the impaired limb directly. Even if it is possible, high-power motors will increase the volume and weight of the device seriously. Thus, the gearbox mechanism is adopted here to increase the driving power of the system with small DC motors. With the gearboxes, the torques in the master and slave motor shafts are minified N_m and N_s times compared to the corresponding terminal torques, and the rotor velocities of motors are magnified N_m and N_s times compared to the terminal velocities. This causes that the current is minified and that the armature voltage generated by the master motor is N_m-times magnified (refer to Eqs. (1) and (5)), while the electric power is kept nearly constant. Thus, the energy loss in the energy transfer circuit (depends on the closed-loop circuit) can be reduced. This can increase the energy recycling efficiency in the electronic circuit, and is advantageous to realize master-slave motion imitation. However, the no-load loss will be increased slightly due to the magnified velocities in motor

shafts. Additionally, there is energy loss in the gearboxes. That is, two limbs should deliver more input power to overcome mechanical loss and further coordinate with each other.

2.3 Training Modes

The force sensing mechanism and the symmetric structure make the system have bidirectional controllability. The motor attached with a larger force acts as the master motor, no matter on which side it is located; accordingly, the other motor acts as the slave motor. With this characteristic, different training modes can be implemented for patients no matter which limb is impaired. A simple introduction is given as follows:

Passive-driven mode: The impaired limb has an extremely weak motor capacity and is moved passively by the healthy limb, which exerts a driving force to overcome the resistant force produced by the impaired one. Therefore, the motor controlled by the healthy limb behaves as the master while the other motor behaves as the slave. Movement trajectory and velocity are controlled by the healthy limb, and are subject to the acceptable motor capacity of the impaired limb. During exercise, a patient feels resistant force from the impaired limb, and adjusts the driving force of the healthy limb properly to implement an expected movement within the range of motor capacity of the impaired limb.

Active-assisted mode: The impaired limb has a mild motor capacity and starts movement with an active force. Nevertheless, the force is insufficient to accomplish movements. The healthy limb provides an auxiliary force to help the impaired limb complete movements by feeling how the impaired limb moves or according to the movement intent (the active force of the impaired limb is too weak to be sensed in the other site). The magnitude of the assistant force depends on the impaired limb's residual motor capacity and the desired movement range or velocity. Thereby, the working states of the motors depend on the magnitudes of the acting forces in the two sites and are not fixed. The electric power generated by the master as auxiliary input electric energy is provided for the slave motor, to reduce the input force requirement in slave terminal.

Active-resisted mode: The impaired limb is able to complete movements, while the healthy limb imparts a reverse force to increase the difficulty level of movements and to make the impaired limb perform tasks with maximal effort. This mode was used to perform strength enhancement training. The motor operated by the impaired limb behaves as the master, while the motor controlled by the healthy limb behaves as the slave. The master motor provides negative electric power for the slave to resist movement of the affected limb. Similarly, movement trajectory and velocity rely on the forces from the impaired and healthy limbs.

No matter in which training mode, the required driving force, assistant force or resistant force is provided by the healthy limb. Therefore, the system can support real bimanual-training. In the process of self-controlled bimanual training, the magnitudes of imposed forces from the two limbs are determined by subjects themselves. The subjects can control the assistant/resistant force from the healthy limb as small/large as possible with the consciousness of achieving function recovery quickly. And the assistant/resistant force can be increased/reduced properly when the impaired limb is too tired, further to avoid producing tired feeling in exercises.

2.4 Power Transmission Flow

For the passive-driven and active-resisted modes, the forces produced at the two terminals have opposite directions. The corresponding power transmission flowchart is shown in Fig. 2-3, in which P_{in} and P_{out} denote the input and output power in the terminals; P_{in_m}, P_{M_m}, and P_{out_m} represent input mechanical power, electromagnetic power, and output electrical power of the master motor, respectively; P_{in_s}, P_{M_s}, and P_{out_s} are input electrical power, electromagnetic power, and output mechanical power of the slave motor, respectively; and P_{sup} is the compensatory energy power. Various energy losses in the system are listed in Table I. Gear loss is caused by coulomb friction in gearboxes. Mechanical loss, magnetic core loss and excitation loss, which are mainly caused by mechanical friction and the alternative magnetic field towards the armature core, are called the no-load loss in general and are primarily related to the

velocity. Resistance loss and contact loss, which are caused by the armature current, are called load loss. The load loss and excitation loss are energy losses in the circuit. As shown in Fig. 2-3, the power balance equation in the circuit is given by:

$$P_{M\_m} + P_{\text{sup}} = P_{M\_s} + 2(p_a + p_b + p_f)$$ (8)

When the system achieves motion tracking accurately, ω_{out} equals ω_{in}, the compensatory energy power can be expressed as:

$$P_{\text{sup}} = C_T i \omega_{out}(N_s - N_m) + 2(p_a + p_b + p_f)$$ (9)

where the resistance loss accounts for the main part of the energy losses. This suggests that the compensatory energy relies on the gear ratios of two gearboxes and the energy losses in circuit. Based on Eqs. (3) and (9), the gearboxes with different gear ratios affect the requirements for the input power from the healthy limb and the supplementary energy. There are two cases as follows:

- $N_m > N_s$: As indicted in Eq. (3), a larger input torque/power is required to drive the same load compared to the system using identical gearboxes with the gear ratio of N_s, and the force sensing coefficient is increased. In contrast, the demand for the supplementary energy is reduced because the master can generate more electromagnetic power than that required in the slave site (refer to Eqs. (8) and (9)). Actually, the two motors do not achieve motion tracking, whereas the two terminals can realize motion tracking due to the function of different gearboxes.

- $N_m < N_s$: This is a reverse case of $N_m > N_s$. Compared with the case that two gearboxes have the same gear ratio of N_s, a smaller input torque/power is required, while the demand for the compensatory energy is increased.

TABLE I. VARIOUS LOSSES IN THE CONTROL SYSTEM

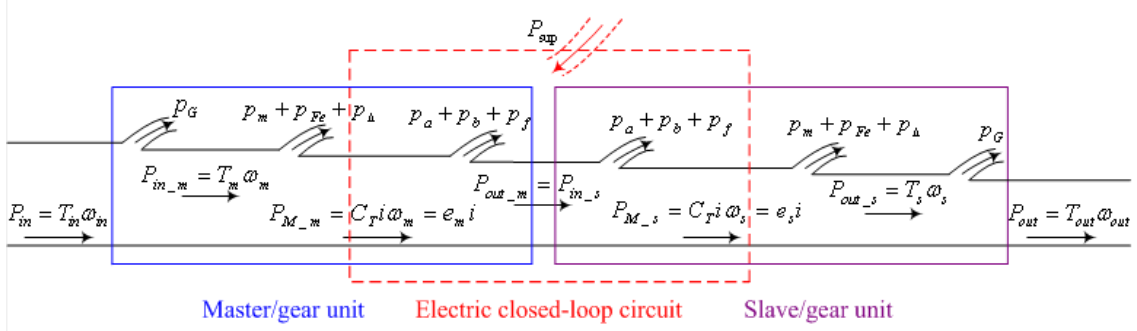| gear loss	mechanical loss	core loss	added loss	resistance loss	contact loss	excitation loss
p_G	p_m	p_{Fe}	p_Δ	p_a	p_b	p_f

Fig. 2-3 Power transmission flowchart of the system in passive-driven and active-resisted modes

In active-assisted mode, the forces attached to the master and slave sites have the same direction. Therefore, the power transmission flow differs from the other two training modes. The corresponding diagram is shown in Fig. 2-4. The dashed arrowheads represent the torque balance relationship. The smaller (active or assistant) torque overcomes the frictional torque caused by the gearbox in slave site fully or partly, further to reduce the impedance of the master motor.

The corresponding power balance equations are the same as Eqs. (8) and (9). Thus, the gearbox influence on the requirement for supplementary energy is the same as that introduced above. However, the relationship between two terminal torques in active-assisted mode is written as:

$$\frac{T_{in}\eta_m}{N_m} + \frac{T_{out}\eta_s}{N_s} = T_{0\_m} + T_{0\_s} + J_m N_m \frac{d\omega_{in}}{dt} + J_s N_s \frac{d\omega_{out}}{dt} \tag{10}$$

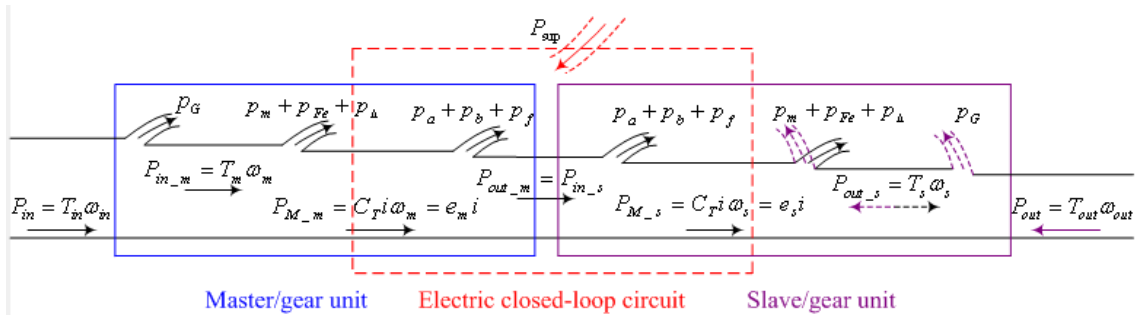The demand for the input torque/power will increase no matter that the gear ratio of which gearbox is increased.

Fig. 2-4 Power transmission flowchart of the system in active-assisted modes

3. Prototype Design

In this study, three prototypes were constructed. The first one was used to validate the feasibility of the proposed master-slave mechanism. Tests on prototype No. 1 preliminarily demonstrated the force sensing and energy recycling capability of the master-slave device. The second one applied higher-accuracy encoders and realized master-slave motion tracking with increased precision. Tests on prototype No. 2 completely confirmed force sensing and energy recycling capability, and demonstrated the feature of bidirectional controllability. The third one increased the driving power of the system. Combined with an additional visual interface, it was capable of supporting bimanual coordinated exercises. Except for a further verification on force sensing and energy recycling, multiple training modes and system stability were also confirmed and analysed on prototype No.3.

3.1 Prototype No. 1

At first, we proposed a master-slave control device: two DC motors are wired connected directly. We hypothesized that when one external force drives one DC motor, it can generate electrical energy (generator) and power another DC motor (actuator) to rotate. And in the generator terminal, the limb can sense the external force attached in the actuator terminal without using any force sensors. The first platform was designed in order to verify the feasibility of this working mechanism.

3.1.1 Hardware Design

Fig. 3-1 shows the first prototype. It was composed of two identical DC motors (geared DC motor, 1271 series, N=43, McLennan co. UK), an H-bridge driver (TA7267BP, Toshiba co. Japan), two photoelectric encoders (BTE030, 90 code tracks, Best-technology co. Japan), and a

microprocessor (MC9S08QG8, Freescale co. USA). In order to carry out system performance analysis easily, a DC driving motor (82861010, Crouzet Co. France) instead of a human operator was used for driving the master motor in a constant velocity. It was powered by a DC power module directly, and was coaxially connected to the master motor.
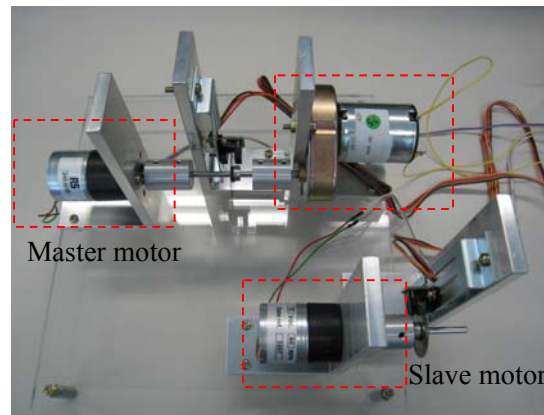

Fig. 3-1 The first platform of the master-slave control system

3.1.2 Master-Slave Motion Controller

Master-slave motion control is aimed at achieving precise master-slave motion imitation, and thus the input velocity and position are considered the tracking objectives of the output site in the controller. The amount of compensatory energy is regulated according to the difference between two terminals' velocities and the difference between two terminals' positions. Here a PID (proportional-integral-differential) control is used to construct a basic position-velocity feedback controller. Since the input velocity is controlled by an operator, it is not a constant. If the differential control is applied to the velocity difference between the input and output site directly, the fluctuation of the input velocity may lead to overshoot and oscillation of the whole system. Therefore, the differential control is applied only to the output velocity.

The regulation of supplementary energy is realized by adjusting the duty cycle of a pulse-width modulated (PWM) signal, which is fed to an H-bridge driver to provide moderate energy for the

closed-loop circuit. The compensated voltage, e_{sup}, can be calculated using:

$$e_{\text{sup}} = (2\alpha - 1)U_s \qquad (11)$$

where α is the duty cycle of the PWM signal, and U_s is the supply voltage of the H-bridge driver. In the design, a bipolar driving mode is adopted to drive the H-bridge driver. Therefore, when $\alpha = 50\%$, the e_{sup} equals to zero; when $\alpha > 50\%$, the e_{sup} is positive; when $\alpha < 50\%$, the e_{sup} is negative. The amount as well as the direction of the compensated energy can be controlled by the magnitude of α directly. During operation, the energy is compensated in the form of increments. There are three cases as follows:

- When motors rotate with a positive direction (clockwise), $\alpha_{new} = \alpha_{old} + \Delta\alpha$.

- When motors rotate with a negative direction (counter- clockwise), $\alpha_{new} = \alpha_{old} - \Delta\alpha$.

When motors converse their direction, α is needed to carry out complementation calculation: $\alpha_{new} = 1 - \alpha_{old}$, where α_{old} and α_{new} represent the duty cycles before the adjustment and after the adjustment, respectively.

3.1.3 Validation Experiments

A. Force sensing test

In this experiment, different loads were attached to the slave site (40-120 g, with an increment of 40g), and the input voltage of the driving motor was constant (12V). The input power of the driving motor and the rotational velocity of the master motor were tested for different loads. The input torque of the master motor was calculated by dividing the tested velocity into its corresponding input power, which was deduced from the input power of the driving motor (82861010) and its work efficiency (about 39%) roughly.

The results regarding the relationship between the input and output torques are given in Fig. 3-2. It can be seen that the input torque increased following the increment of the load torque, verifying that the system has force sensing capability. However, there was a large difference between the

input and output torques, this was caused by the no-load torque and inertial torque of two motors, as well as the amplification function of the gearboxes and the mechanical loss in gearboxes (refer to Eq. (3)). This torque difference will be nearly constant if the rotational velocity has no big change.
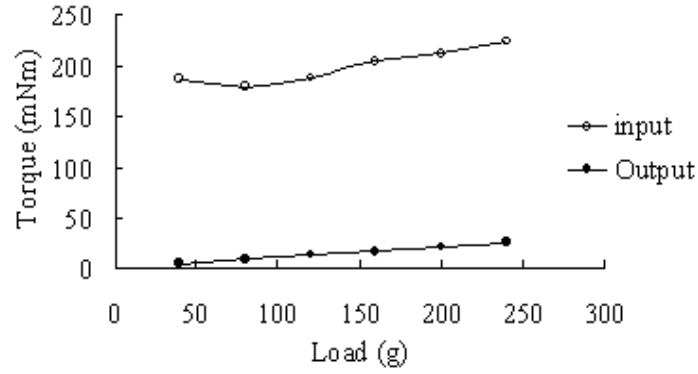

Fig. 3-2 The relationship between the input and output torques

B. Energy supplement test

In this experiment, the input voltage of the driving motor was increased from 8V to 12V with an increment of 0.5V. And a constant load of 44g (around 4.7mNm) was attached to the slave side. An appropriate amount of energy was compensated for the system with a PID controller for achieving good motion tracking performance. The relationship among the resistance loss (p_a) in the circuit, compensatory energy (p_{sup}) and the electro-magnetic power of the slave motor, P_{M_s} (equals P_{M_m} in balance state), was determined by measuring the current, the duty cycle of the PWM signal and the rotational velocity of the two motors simultaneously.

The corresponding powers were calculated using

$$\begin{cases} p_{\text{sup}} = (2\alpha - 1)U_s i \\ p_a = i^2 R \\ P_{M\_s} = e_s i = C_T \omega_s i \end{cases} \tag{12}$$

where U_s was 12 volts. The calculated results are shown in Fig. 3-3. It is obvious that the supplementary energy was approximately coincident with the resistance loss. However, the

26

former was slightly larger than the latter because contact loss and excitation loss also occurred in the energy recycling circuit (refer to Eq. (9)). In addition, the electromagnetic power of the slave motor was larger than the supplementary energy, which confirms that the system has energy recycling capability.
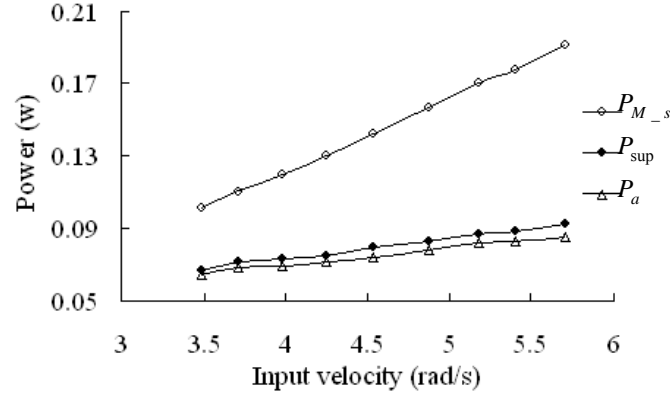

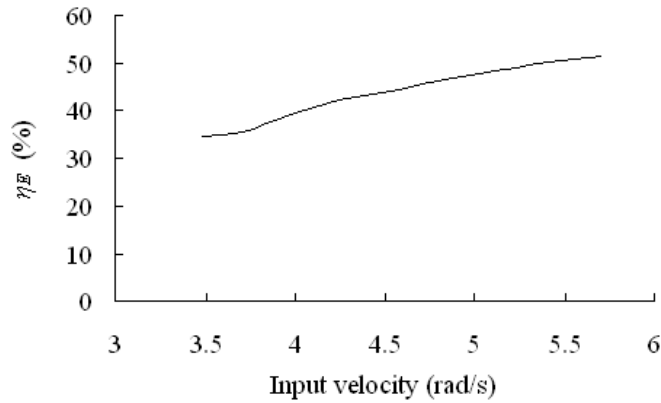Fig. 3-3 The relation curve of compensated energy and resistance loss

Fig. 3-4 The energy recycling efficiency curve

The energy recycling efficiency in the closed-loop circuit, η_E, was calculated as follows:

$$\eta_E = (P_{M\_s} - p_{\sup}) \times 100\% / P_{M\_s} \tag{13}$$

The corresponding curve is shown in Fig. 3-4. The energy recycling efficiency increased from 34.31% to 51.35% with the increment of the input velocity from 3.48 radians per second to 5.71 radians per second. The efficiency increased because the master motor generated more

electromagnetic power with greater velocity, meanwhile, the energy losses in the circuit remained nearly constant with fixed load (current).

When a step voltage of 8.5 V was provided for the driving motor, the sample results of system responses are given in Fig. 3-5. The system realized velocity tracking with the steady-state errors that were less than 0.3 radian per second.
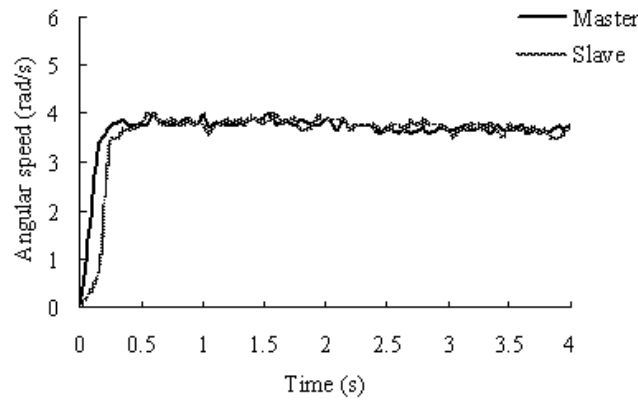

Fig. 3-5 Velocity tracking curves of one sample step response

3.2 Prototype No. 2

In prototype No.1, the required input torque was a few times larger than the load torque. This was mainly caused by the mechanical losses in DC motors (p_m , p_{Fe} , and p_Δ) and friction loss in gearboxes (working efficiency: 50%). Otherwise, the steady-state errors in master-slave motion tracking were relatively large due to the low measurement accuracy of the encoders. In order to reduce the force requirement in the master site and increase master-slave motion tracking precision, prototype No. 2 was designed using motors and gearboxes with higher working efficiency (reduced mechanical and friction losses in motors and gearboxes) and applying encoders with higher measurement accuracy. In addition, torque sensors were applied to collect torque information in two terminals so as to verify force sensing capability more reliably. Furthermore, dSPACE control platform was applied to realize semi-physical simulation in real time (RTW).

3.2.1 Hardware Design

The second prototype is shown in Fig. 3-6. It is mainly composed of two identical motor/gear units (A-max 32 motor, combined with Planetary Gearhead GP 32 A, N=4.8 and Encoder HEDL 5540, maxon, Switzerland), an H-bridge driver (LMD18200, National Semiconductor, U.S.A.), and a dSPACE control platform (DS1104, dSPACE, Germany). In addition, two torque transducers (TP-20KCE, Kyowa, Japan) and a torque signal amplifier were applied to measure the input and output torques for verifying force feedback capability. However, they are not required in real applications.
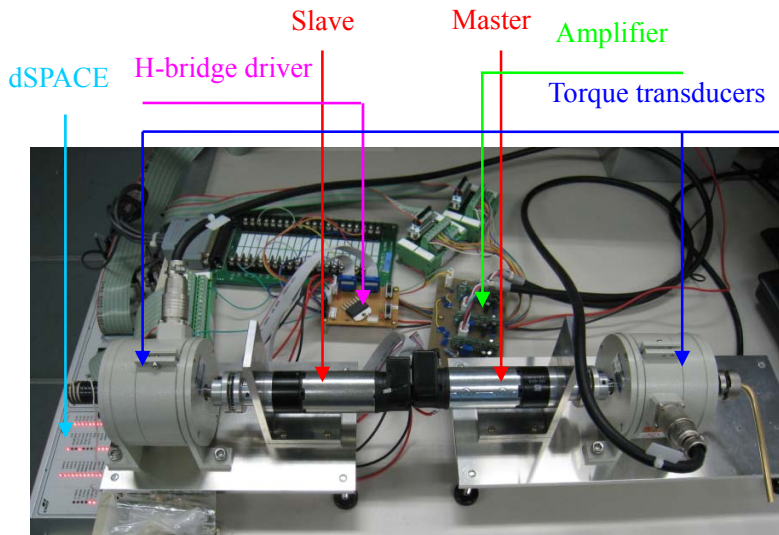

Fig. 3-6 Experimental platform of the master-slave system

3.2.2 Master-Slave Motion Controller

The supplementary energy is supplied for the closed-loop circuit with an H-bridge driver. The hardware connection is given in Fig. 3-7. Since the working states of the two motors are not unchanging, in order to specify the fixed hardware connection, M_1 and M_2 are used to represent the two motors, and the variables with subscripts $_1$ and $_2$ are used to represent the parameters in the corresponding sites. The control inputs of the H-bridge driver are a

pulse-width-modulated (PWM) signal and a direction control signal, which are used to regulate the magnitude and direction of the supplementary voltage. Based on the velocity difference and position difference between the two terminals, a motion tracking controller regulates the control signals of the H-bridge driver with a PID control method, and enables the driver to supply an appropriate amount of energy for the master-slave circuit.
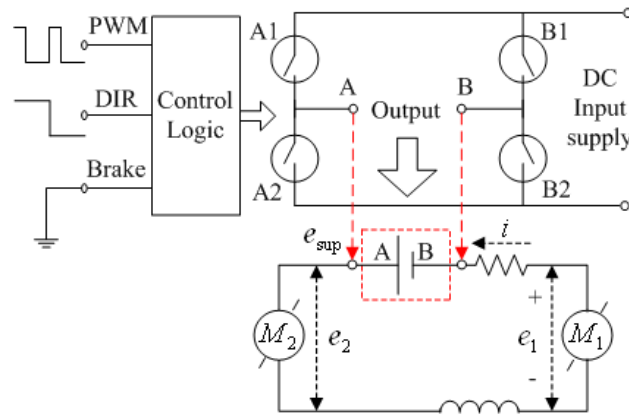

Fig. 3-7 Connection of the H-bridge driver and the two motors

The motion tracking direction is decided based on the training modes. In passive-driven mode, the movement is completely controlled by the healthy limb and thus, the motion of the healthy limb is the tracking objective. In active-assisted or active-resisted mode, the movement is started by the impaired limb and thus, the motion of the impaired limb is the tracking objective. No matter which training mode is active, the initial velocity of the motor (the tracking objective) attached with an active force is larger than that of the follower on the contra-lateral side. Therefore, initial velocities were used to determine the master-slave motion tracking direction.

In the paper, the terminal velocity/position of the motor/gear unit attached with an active force is defined as the reference velocity/position, and that on the contra-lateral side is defined as the following velocity/position. Also, in order to avoid overshoot and fluctuation of the system, a differential forward PID operation is applied in the design. The block diagram of the motion controller is shown in Fig. 3-8.

The motion control equations are given as follows:

$$\begin{cases} \alpha = \alpha^{\omega} + \alpha^{\theta} \\ \alpha^{\omega} = K_P^{\omega}((\omega_1 - \omega_2) + K_I^{\omega}\int(\omega_1 - \omega_2) - K_D^{\omega}\dfrac{d\omega_f}{dt}) \\ \alpha^{\theta} = K_P^{\theta}((\theta_1 - \theta_2) + K_I^{\theta}\int(\theta_1 - \theta_2) - K_D^{\theta}\dfrac{d\theta_f}{dt}) \end{cases} \qquad (14)$$

$$\begin{cases} \omega_f = \begin{cases} \omega_2, & |\omega_1^0| > |\omega_2^0| \\ -\omega_1, & |\omega_2^0| > |\omega_1^0| \end{cases} \\ \theta_f = \begin{cases} \theta_2, & |\omega_1^0| > |\omega_2^0| \\ -\theta_1, & |\omega_2^0| > |\omega_1^0| \end{cases} \end{cases} \qquad (15)$$

where K_P, K_I and K_D denote the proportional, integral and differential coefficients, respectively; the superscripts ω and θ mean the velocity and the position; the variables with the subscript f represent the following velocity or position; and ω_1^0 and ω_2^0 denote the initial velocities of two motors. The inputs of the differential operation are decided according to the magnitudes of the initial velocities, which reflect the motion tracking direction. The sign and the magnitude of α are used to switch the direction and adjust the duty cycle of the PWM signal respectively.
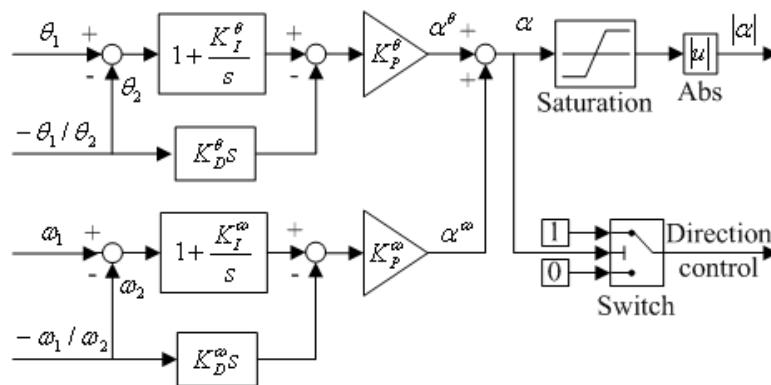

Fig. 3-8 Block diagram of the motion tracking controller

During operation, the supplementary voltage should have the same direction as the armature

voltage of the master motor, further to offset the voltage drop (energy losses) in the circuit and to increase the equivalent voltage provided for the slave motor. Considering the hardware connection shown in Fig. 3-7, when M_1 acts as the master, the supplementary energy should have the same direction with e_1 (the armature voltage of M_1); when M_1 acts as the slave, the supplementary energy should have an opposite direction to e_1, which is the back EMF in this case, therefore, the inputs of the differential operation should be the negative velocity and position of the motor M_1, as expressed in Eq. (15). As for the motion tracking controller, the corresponding cases are generalized in Table II. The velocity relation denotes the state when there is no supplementary energy. The direction of the master motor's armature voltage is consistent with that of the rotational velocities, whereas the direction of the slave motor's back EMF is opposite to that of the rotational velocities (refer to Eq. (5)). The direction signal is determined from the sign of α. Overall, the motion tracking controller can provide the correct control signals whatever the working states and rotational directions of the two motors.

TABLE II. DIRECTIONS OF THE COMPENSATED ENERGY IN DIFFERENT SITUATIONS

Working state	Rotational direction	Velocity relation	e_1	Direction signal
M_1: master M_2: slave	clockwise	$\omega_1 > \omega_2 > 0$	positive (EMF)	positive
	counter-clockwise	$\omega_1 < \omega_2 < 0$	negative (EMF)	negative
M_1: slave M_2: master	clockwise	$\omega_2 > \omega_1 > 0$	positive (back EMF)	negative
	counter-clockwise	$\omega_2 < \omega_1 < 0$	negative (back EMF)	positive

3.2.3 Validation Experiments

Three test experiments were performed. One is force feedback test, which is used to testify the capability of force feedback and acceptable feedback performance; the second is energy recycling test, which is used to appraise the energy recycling capability of the new prototype; the last is bidirectional control test, which is used to confirm the characteristic of bidirectional

controllability and the same working performance in the two control directions.

In the first and second experiments, in order to simplify system performance analysis, a DC driving motor was used to drive the master/gear unit instead of a human operator. It was coaxially connected to the master/gear unit and was driven by another H-bridge driver, here referred to as driver 2, while the driver connected with the master-slave circuit was referred to as driver 1. The input voltage of the driving motor was adjusted based on the difference between a predefined reference velocity and the velocity in the master terminal. The schematic diagram is shown in Fig. 3-9. In the third experiment, an operator exerted forces in the both sites with the two hands and without using the DC driving motor and the H-bridge driver 2. The corresponding diagram is shown in Fig. 3-10. In the figures, the master/slave unit and the motor 1 or motor 2 unit mean the combination of the motor, gearbox, encoder, and the torque transducer. The torque information given with dashed lines indicates that it is not required in real applications.

The DS1104 collected the velocity and position information though the incremental encoder interface, worked out the control signals for the H-bridge driver 1 with the motion tracking controller, enabled the driver to supply a proper amount of energy for the closed-loop circuit. The energy generated by the master motor, together with the supplementary energy, drove the slave motor to track the motion of the master motor. In addition, the torque information was collected through AD modules of the DS1104 for verifying the force feedback capability and bidirectional controllability. For the first and the second experiments, the DS1104 also calculated the control signals for the H-bridge driver 2 and regulated the input voltage of the DC driving motor, which further rotated the system with the reference velocity. Meanwhile, the closed-loop current obtained with the H-bridge driver 1 was sampled through the AD modules of the DS1104, and the control output of the motion tracking controller (α) was recorded for testifying the characteristic of energy recycling. All the information mentioned above is sampled every 1 millisecond.
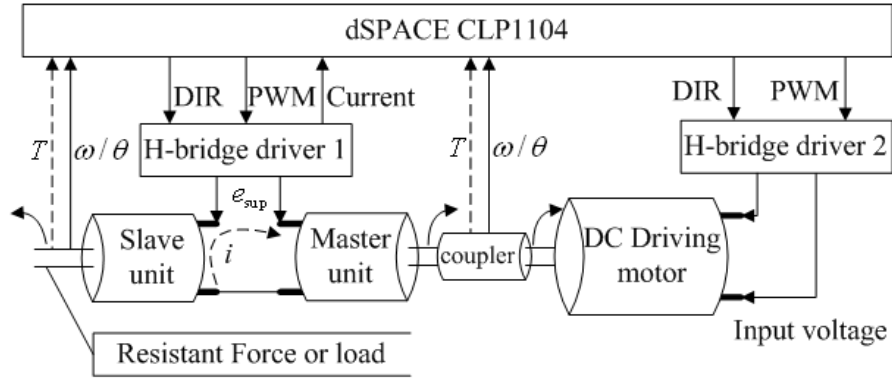
Fig. 3-9 Schematic diagram of the experiments with DC driving motor on prototype No. 2
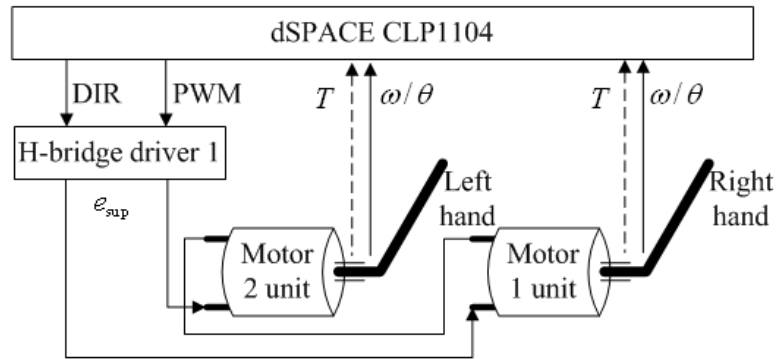

Fig. 3-10 Schematic diagram of the experiment performed with the two hands on prototype No. 2

A. Force sensing test

The regulation of the input torque following the variation of resistant torque was used to verify the force sensing capability. We attached an increased resistant force to the slave site with one hand, and verified the force feedback capability based on the concomitant regulation of the force in the master site. The resistant force was intentionally exerted with a certain fluctuation so as to testify the force feedback performance. The reference velocity was set as 250 degrees/second. The tested results are given in Fig. 3-11, in which the opposite sign symbols denote the opposite directions of the two torques. The torque difference (T_{dif}) was the summation of the torques in the two terminals. It actually represented the difference between the two torques. In this experiment, the motion tracking was realized with the maximum tracking errors of positions and velocities

being 2.91 degrees/second and 0.52 degree, respectively. The motion tracking precision was greatly increased compared to the prototype No. 1.

As shown in Fig. 3-11 (a), the control torque produced in the master site (controlled by the DC driving motor) increased following the increment of the resistant torque, thus the force feedback capability of the system was demonstrated. Besides, the control torque was regulated accordingly even though the variation of the resistant torque was small. Therefore, a good force feedback performance was confirmed. Even though the control torque in the master site was larger than the resistant torque, their difference was less than the resistance force in the slave site. This reflected that negative effect caused by the no-load torques of the motors and the frictional torques of the gearboxes (working efficiency) was reduced greatly compared to prototype No. 1. In addition, the torque difference kept nearly constant even though the forces exerted in the two terminals were increased. This indicated that the varying external acting force had unnoticeable impact on the unload torques and gearboxes' frictional torques so long as the rotational velocities were kept constant. It was true that the torque difference (mainly caused by the working efficiency of the gearboxes) had a slight change following the variation of the velocity, whereas in rehabilitation applications, the variation of the torque difference was small compared to the variation of the external torque. Additionally, the system was mainly aimed at achieving force sensing while the force transparency was less essential. Therefore, the torque difference was acceptable for the considering system.

In order to quantify the force feedback capability of the system towards the external impedance variation in the slave site, we defined force feedback coefficient as:

$$\lambda_T = \frac{\Delta T_{in}}{\Delta T_{out}} = \frac{T_{in}^k - T_{in}^0}{T_{out}^k - T_{out}^0} \tag{16}$$

where T_{out}^0 and T_{in}^0 represent the initial torques when there was no external resistant force and the system was rotated with the velocity of 250 degrees/second. T_{out}^0 (0.032 Nm) was used to

drive the worm gear at the slave site. T_{in}^0 (0.048 Nm) was used to overcome the frictional torques in the gearboxes and the unload torques in two motors, further to drive the two motors to rotate; the variables with the superscript ^{k} denote the sampling values in the k time. The initial torques were excluded in the calculation for eliminating the effect of no-load torques. The force feedback coefficient curve is shown in Fig. 3-11 (b), the system realized force feedback with an approximately constant reflecting coefficient. The average coefficient was 1.445. It was larger than unit one, the cuase of this is considered to be the frictional torques induced by the gearboxes.
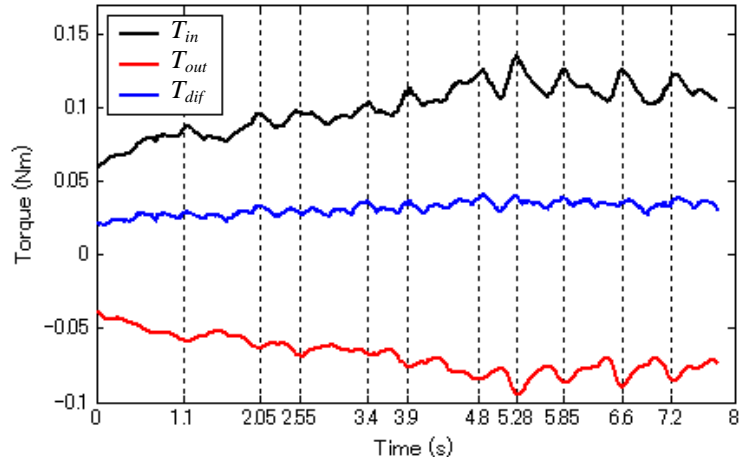
(a) Torque variation curves
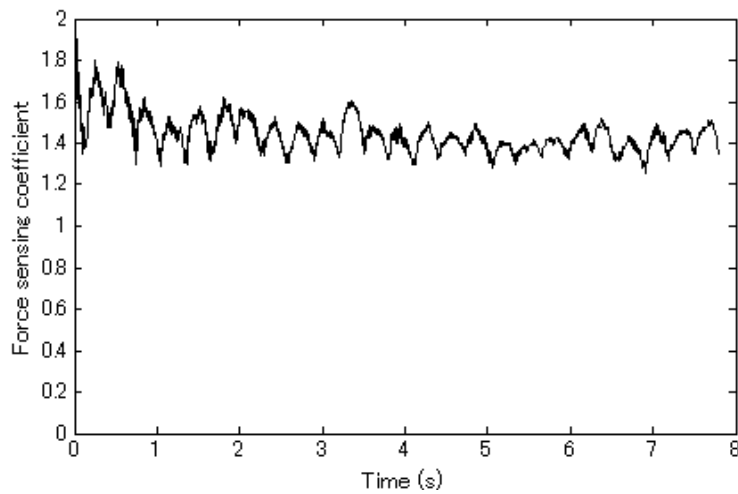
(b) Force feedback coefficient

Fig. 3-11 Torque variation curves in prototype No. 2

B. Energy recycling test

In order to verify the energy recycling capability, the reference velocity was set as a sine signal with an increasing magnitude in different periods. That is, the system was rotated with clockwise and counter-clockwise direction periodically. No external load was attached in the slave site. The electromagnetic power, supplementary energy power, and the power of the resistance loss were calculated with:

$$\begin{cases} P_M = C_T i N_s \omega_{out} = i e_s \\ P_{\text{sup}} = \alpha U_s i \\ P_R = i^2 R \end{cases} \tag{17}$$

where U_s denotes the supply voltage of the H-bridge driver. U_s was 12 volts and R was 6.04 ohms. Since $\omega_m = \omega_s$ when the system achieved motion tracking and the system was configured with a symmetrical structure (the corresponding coefficients in the two sites are almost identical), P_M represented the electromagnetic power of the two motors actually. The inductance loss was not considered because that it was very small and negligible compared to the resistance loss. The electromagnetic power and the supplementary energy power were used to verify the energy recycling capability; the supplementary energy power and the resistance loss were used to confirm the function of the supplementary energy.

The results corresponding to the energy recycling test are given in Fig. 3-12, in which P_δ denotes the power difference between the compensated energy and resistance loss. Seeing Fig. 3-12 (a), it can be concluded that accurate motion tracking was realized in both rotational directions. In this test, the maximum velocity and position errors were 4.06 degrees/second and 0.5 degree respectively. As can be seen from Fig. 3-12 (a) and (b), the electromagnetic power of the slave motor (represents the electromagnetic power of the two motors) increased with the variation of the velocity (the powers were always positive even though the velocity was negative), whereas the compensated energy had unnoticeable changes among different periods. This indicated that the driving power of the slave motor came from the electric energy generated by
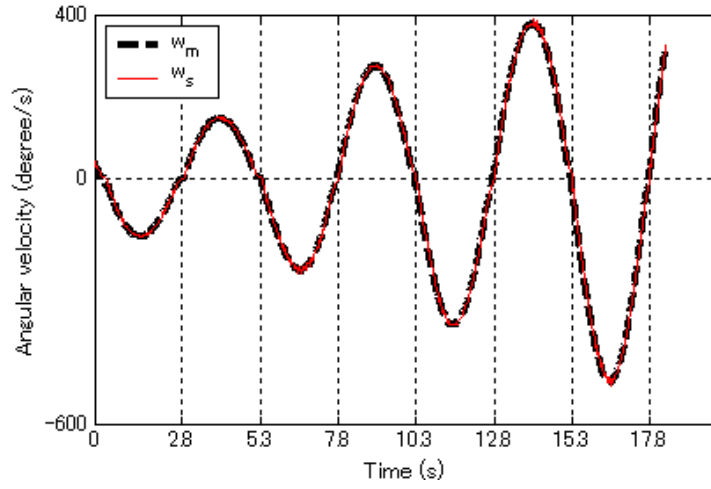
(a) Velocity tracking curves
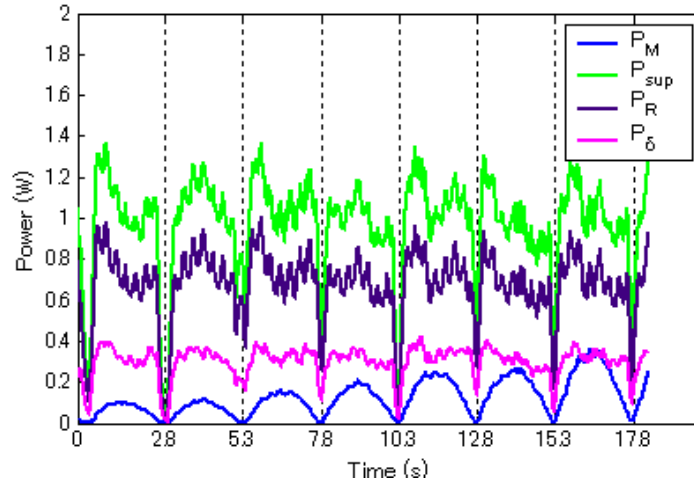
(b) Relationship between the motor electromagnetic power, supplementary energy and the resistance loss

Fig. 3-12 Results corresponding to the energy recycling test in prototype No. 2

the master motor other than from the compensated energy. Hence, the energy recycling capability is confirmed. Meanwhile, the compensated energy and the resistance loss had the same varying regulation in each period, this demonstrated that the compensated energy was used to offset the energy losses in the circuit. However, the former was larger than the latter because there were also inductance loss, as well as the contact loss and excitation loss that are caused by the armature current and alternative magnetic field. The resistance loss accounted a main part of the energy

losses and thus, P_R was relatively large compared to P_δ, which reflected the power of the other energy losses in the circuit. However, the compensated energy was larger than the electromagnetic power of the slave motor because of the large energy losses in the circuit. In order to reduce the energy losses in the circuit and enhance energy recycling efficiency, the gearboxes with larger gear ratio should be considered in the future applications.

C. Bidirectional controllability test

In order to verify the characteristic of bidirectional controllability, the DC driving motor that controlled the master unit and the H-bridge driver 2 were removed from the experimental platform. An operator attached forces to the two terminals with two hands. The exerted forces had opposite directions and different magnitudes with the smaller one defined as a resistance force and the larger one defined as a control force, and the two motors in the corresponding sites behave as the slave and the master respectively. In the experiment, the operator changed the magnitude of the resistant force periodically and regulated the control force according to force sensation, trying to achieve a movement with small variation among different periods.

The results coresponding to the two control directions are shown in Fig. 3-13 and Fig. 3-14 respectively. Fig. 3-13 gives the results of the test when the right hand provided a control force while the left hand imposed a resistant force with relatively small magnitudes. That is, the motor located in the right hand site acted as the master while the other motor acted as the slave; Fig. 3-14 gives the results of the test when the left hand provided a control force while the right hand imposed a resistant force with relatively small magnitudes, and the working states of the two motors were reversed compared to the former case. In the both figures, the black line represents the torque produced on the right hand side and the the red line represents the torque produced on the left hand side, the blue line represents the difference between the control torque and the resistant torque in the two terminals.

It can be seen that the accurate motion tracking was achieved in the both control directions. In the testing experiments, the maximum veloity and position errors were 11.67 degrees per second and
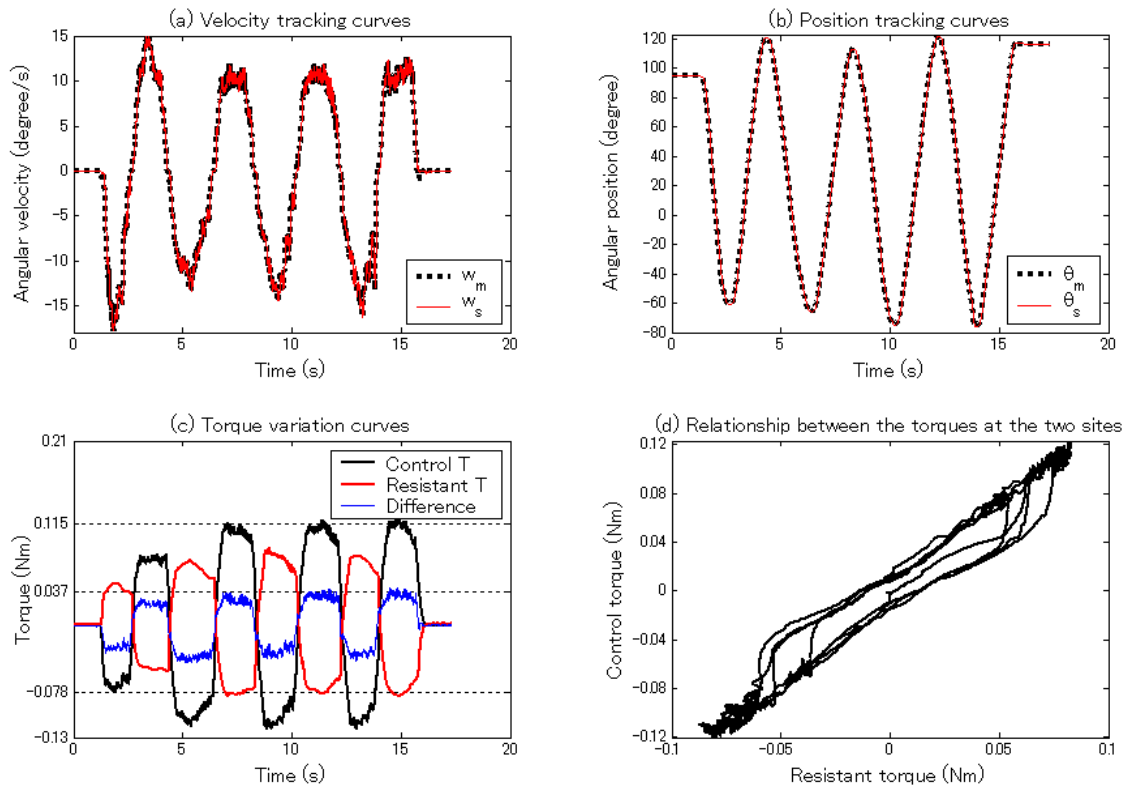
Fig. 3-13 Results of the test when the right hand controls the movements of the left hand
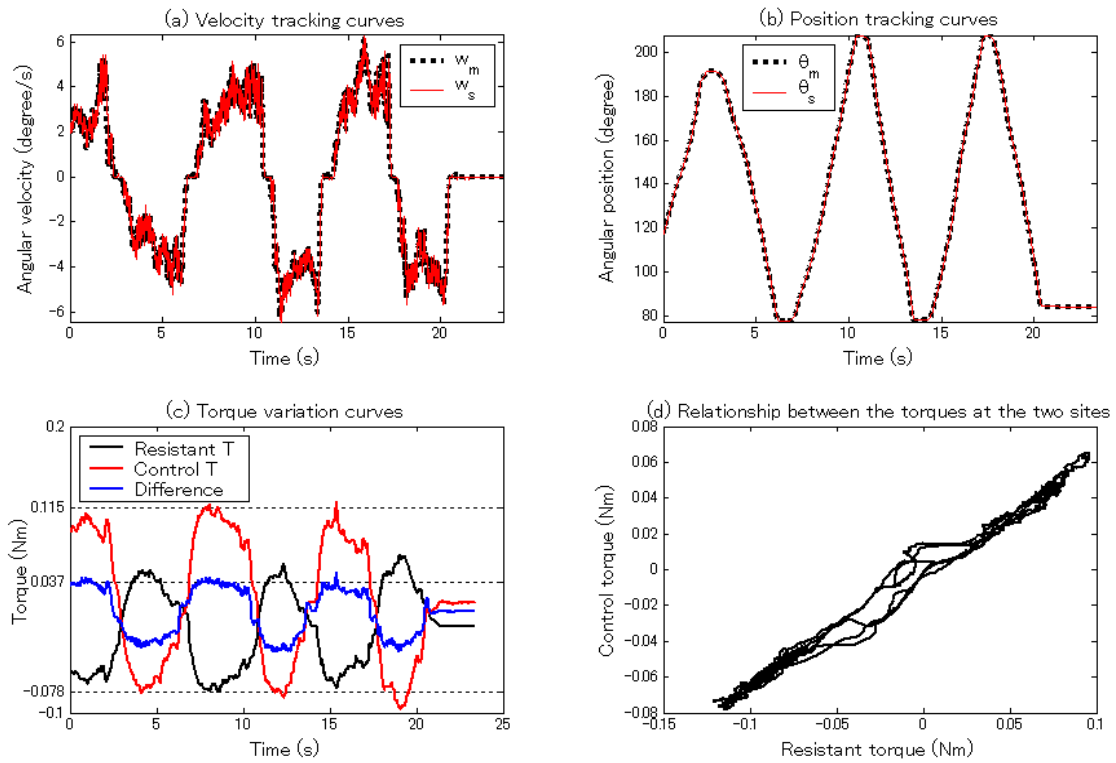

Fig. 3-14 Results of the test when the left hand controls the movements of the right hand

0.77 degree when the control direction was from right to left, and were 16.88 degrees per second and 0.41 degree when the control direction was from left to right. In addition, the control torque increased following the increment of the resistant torque in the two control directions. This confirmed that force feedback/sensing was realized in the both control directions and the operator was able to regulate the control force accordingly based on the sensation of the feedback force. Besides, by comparing Fig. 3-13 (c) and Fig. 3-14 (c), it can be concluded that when the resistant torques had the same magnitude (0.078 Nm), the control torques (0.115 Nm) as well as the torque differences (0.037 Nm) were approximately indentical for the two control directions. The resluts verified that the system implemented bidirectional control and achieved almost the same force feedback performance for the both control directions. As well, the relationship between the control torque and resistant torque are given in Fig. 3-13 (d) and Fig. 3-14 (d). We can see that there were hysteretic errors when the reciprocating motion was carried out for the both control directions. When the resistant torque was small, the no-load torques of the motors and the frictional torques caused by the gearboxes were too large compared to the resistant torque, thus the hysteretic errors were obvious. In the testing range of the resistant force, the average hysteretic deviations were 0.0051 Nm and 0.012 Nm respectively; and the standard deviations were 0.0092 and 0.015 respectively for the two control directions.

3.3 Prototype No. 3

In the prototype No. 2, due to the small gear ratio of gearboxes, the output torque was too small (0.183Nm) to drive a human limb in rehabilitation exercise and the energy recycling efficiency was low. Therefore, we designed prototype No. 3 using motors with a larger allowable maximum output torque and using high efficiency gearboxes with a larger gear ratio. In addition, a visual interface was added to the system to display motion tracking trajectories (using ControlDesk, a test and experiment software attached with dSPACE). Prototype No. 3 is capable of supporting bimanual coordinated training in passive-driven, active-assisted, and active- resisted modes.

3.3.1 Hardware Design

Prototype No. 3 is shown in Fig. 3-15. Two DC motors combined with planetary gearheads and encoders (motor 3863012C, gearhead 38/2 A, encoder IE2-512, Faulhaber Group, Germany) constructed master and slave units, which are manipulated by the two limbs of a subject. A desktop PC provided visual feedback and guided the subject to perform reference movements. The dSPACE control platform (DS1104) was used to implement master-slave motion tracking control and to ensure an accurately symmetric movement of the two limbs. Two handles were connected with mechanical terminals of the master and slave units. Two torque transducers and a torque signal amplifier were also applied to measure terminal torques and verify the torque relationship between the two terminals. The transducers were located at the handle bases near the gearhead shaft connections. Master and slave units were fixed to a height-adjustable and position-adjustable table. The detailed information of the employed devices is listed in Table III.

Visual feedback: dynamic tracking trajectory
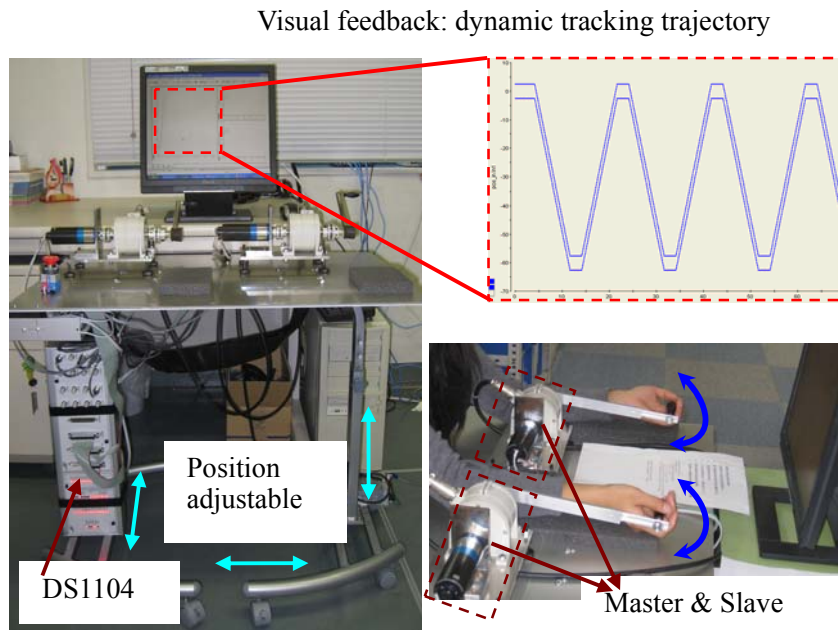
Fig. 3-15 Self-controlled bimanual training system. The height and position of the table were adjustable so as to make each subject feel comfortable; DS1104 is a single-board system with real-time hardware and comprehensive I/O for developing controllers, it was used to realize master-slave motion controller and to collect real-time data for visual interaction; the user coordinated the forces of two limbs and controlled the master and slave terminals to track predefined dynamic tracking trajectory.

TABLE III: INFORMATION OF THE APPLIED DEVICES.

DC motor	Max. torque: 110mNm	Max. current: 7.6A
Gearhead	Gear ratio: 66:1	Efficiency: 70%
Encoder	Pulse number: 512	Max. freq. response: 160KHz
H-bridge driver	Max. current: 3A	Supply voltage: 12 to 55V
Torque transducer	Rated capacity: 2Nm	Non-linearity: ±1%RO
Signal amplifier	Amplified factor: 2000	

Gearboxes with gear ratios of 43 and 66 were selected in different testing experiments. Considering the gearbox efficiency as the theoretical value of 0.7, the corresponding maximum output torques of the motor/gear units were 3.311 Nm and 5.082 Nm respectively, which will be sufficient to drive a forearm to perform elbow flexion/extension movement. The torque caused by gravity of a forearm was estimated for a human with a weight of 65 kilogram and height of 175 centimeter [31], and the result was 1.519 Nm. During operation, the unhealthy limb may produce impedance except the gravity due to its limited residual motor capability and movement positions. Therefore, gearboxes with larger driving torque were selected. The lengths of the two handles were adjustable. This made the system capable of supporting subjects with different limb lengths in performing forearm flexion/extension movement.

In order to insure safety throughout the training process, position limit can be regulated by setting parameters according to the motor capacity of patients. If one terminal is moved beyond the position limit, the H-bridge driver immediately stops compensating energy for the circuit and disconnects the master and slave motors. Accordingly, the slave unit stops movement immediately, and the two limbs are capable of free movement. Once the impaired limb is outside the position limit, it can return to a safe position spontaneously or with the help of the healthy one. In addition, if the actual current of the motors is larger than the allowable maximum value, the H-bridge driver also stops working to ensure the normal operation of the system. This can also prevent abnormal operation caused by the sudden and large forces that result from the spasticity of the impaired limb. Since the driving force in passive mode or the assistant/resistant force in active-

assisted/resisted mode is exerted by the healthy limb, patients can regulate the force according to force sensation and the feel of the impaired limb. Therefore, there is no need to set a torque limit based on the residual motor function of patients. Besides, a push-button can be manipulated by the subject to switch off the power of the system in case of emergency.

Information flow of the system is shown in Fig. 3-16, in which the dashed lines represent that the devices or the information are not needed in future applications. The function of DS1104 was the same as that introduced in prototype No. 2. Thus detailed description is not presented here.
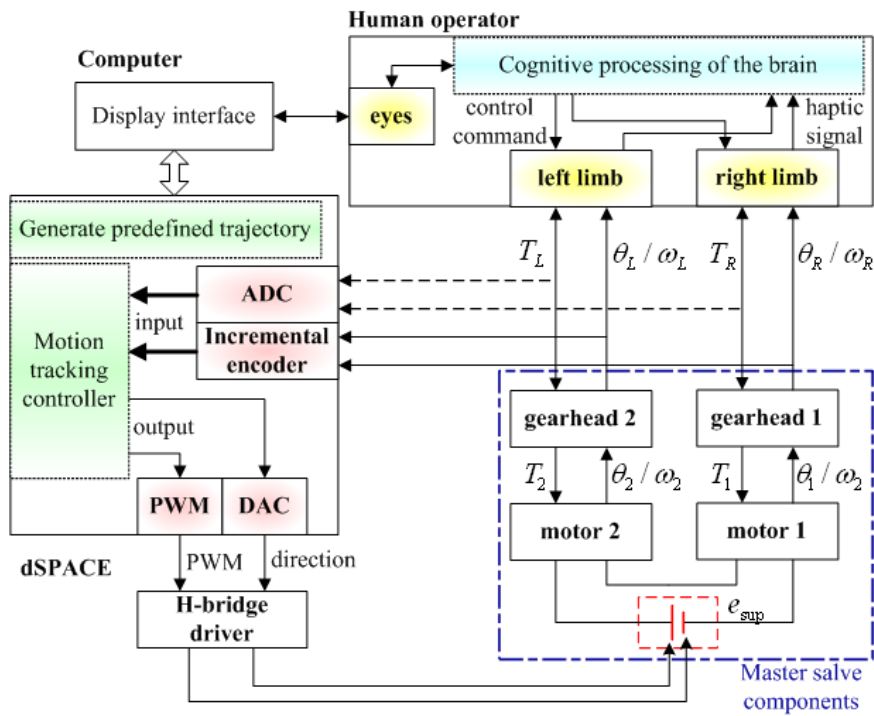
Fig. 3-16 Information flow of the master-slave system

3.3.2 System Control Model

The transfer function diagram of the system is shown in Fig. 3-17. The red block denotes the motion tracking controller, which had the same structure with that introduced in the design of prototype No. 2. The detailed derivation process of the transfer function diagram is given in appendix section. Fig. 3-18 gives a simplified transfer function diagram of the sub-model inside the yellow block.

Fig. 3-17 Transfer function diagram of the master-slave system.

Fig. 3-18 Simplified transfer function diagram of the sub-model inside the yellow block.

3.3.3 Stability Analysis
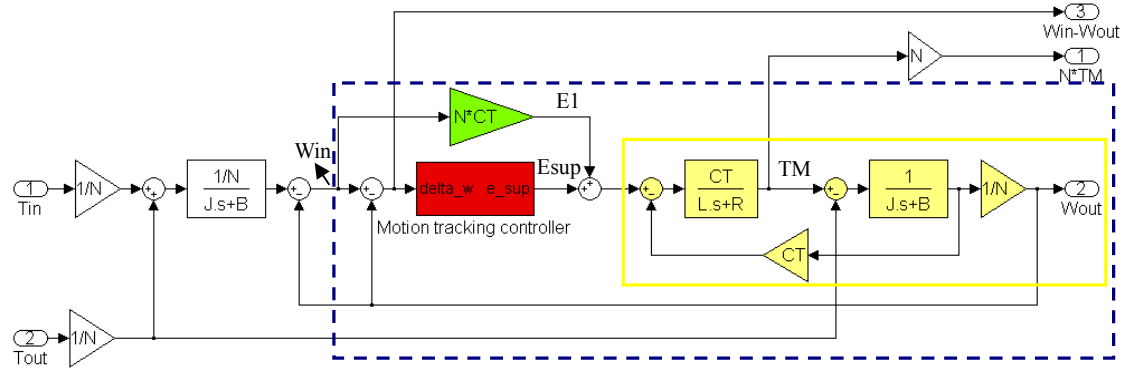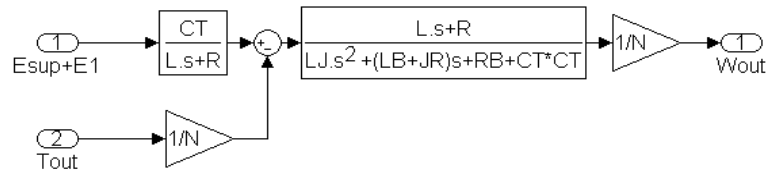
In order to simplify stability analysis, the coefficient of viscous friction was approximately deemed as a constant (the variation in viscous friction torque was negligible for the rehabilitation tasks with slow movement velocity). Firstly, the system model was converted into a discrete model with a sampling frequency of 1 KHz. Secondly, proper PID control parameters were selected to make the subsystem inside the dashed block in Fig. 3-17 stable. The velocities in the master and slave terminals were the input and output of the subsystem. Here the output torque was considered as a constant load, and further, a linear subsystem model was achieved. Therefore, the SISO design tool of MATLAB software (linear system analysis tool) was used to analyze the stability of the subsystem by selecting proper PID parameters. The selected control architecture for analyzing subsystem stability is shown in the upper left corner of Fig. 3-17. Thirdly, the stability of the whole system was verified with the simulation tool Simulink: two step signals were used as input torque and output torque (the torque produced in the slave terminal) in the

Simulink model, and simulation was performed to analyze the step response of the whole system. If the velocity output became unstable in the third step, the second and third steps would be repeated until the system achieved a stable output for both the SISO and simulation analyses. Fig. 3-19 shows the Bode diagram obtained with the SISO design tool when the proportional, integral, and differential coefficients of the velocity controller were 0.096, 40, and 0.006 and those of the position controller were 2, 50, and 0.0048, respectively. The amplitude margin and phase margin were 13 dB and 54.3 degrees, respectively, and the corresponding angular frequencies were 214 Hz and 5.35 Hz. Both the amplitude margin and the phase margin were larger than zero, and thus the subsystem was stable.

The corresponding step response acquired with the simulation tool Simulink is shown in Fig. 3-20. The results suggested that the whole system was stable with the employed control parameters. When T_{out} was positive, it denoted a resistant torque in the slave terminal, while when T_{out} was negative, it represented an assistant torque. We multiplied the electro-magnetic torque by gear ratio so as to compare it with the external torques clearly. The corresponding steady-state value (1.5 Nm) was half of the summation of T_{in} and T_{out} (2 Nm and 1 Nm). This agreed with the explanation given in the Appendix. Considering the input torque as the input of the whole model, the response times of electromagnetic torque and output velocity were around 0.195 s and 0.65 s, respectively, while the response time of output velocity towards the input velocity was 0.315 s. Overall, the system was quick enough to respond to an operator's commands.

However, there were overshoots in the simulation results. This indicated that when the system responded to a step variation in input or output torque, the controller regulated compensative energy to achieve mirror-symmetric movement of the two terminals and thus induced fluctuations in electromagnetic torque and velocity difference. These overshoots here were acceptable for our analysis. In real application, the torques in the two terminals are controlled by an operator and are not step signals, and thus overshoots may be avoided.
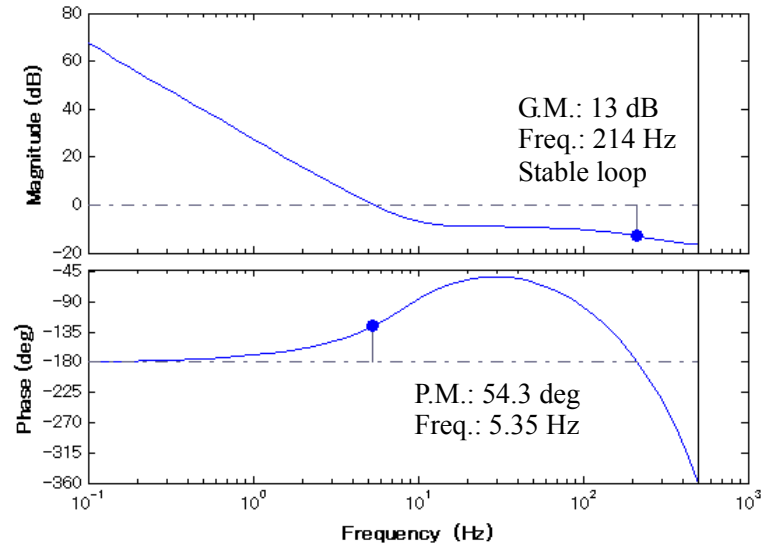
Fig. 3-19 Bode diagram of the subsystem model.
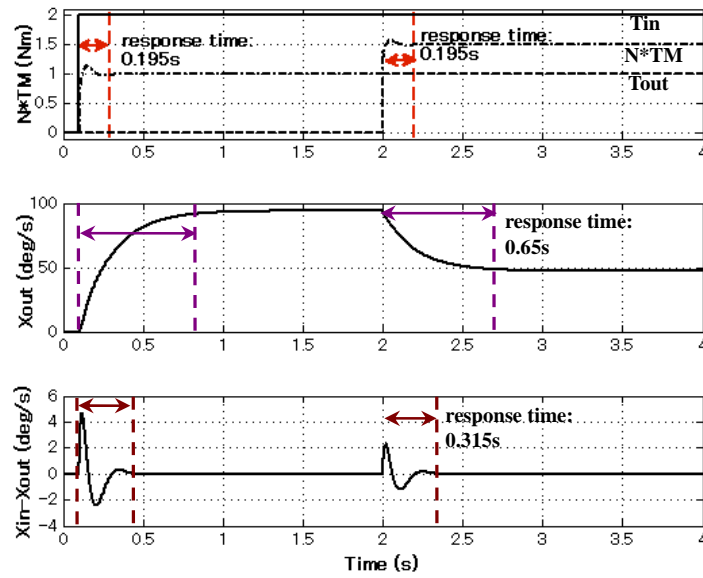
Fig. 3-20 Step response of the whole system in simulation.

3.3.4 Validation Experiments

Except for a further verification of force sensing and energy recycling, the influence of different gearbox combinations, the frequency response range of the system, and the capability of supporting different training modes were also confirmed. In the tests of force sensing, energy recycling, and gearbox influence, a DC driving motor, which was the same with that used in

prototype No.2, was also used to drive the master/gear unit. In the tests of system frequency response and different training modes, the DC driving motor was removed and two handles were attached to the terminal axes of the two torque transducers. An operator controlled the two handles with two limbs.

A. Energy Recycling Test

Two identical gearboxes with the gear ratio of 66 were employed and a constant load of 500 gram (the corresponding resistant torque was 0.0492 Nm) was attached to the slave site. During the test, the reference velocity increased with an angular acceleration of 1 degree/second^2. In order to confirm the capability of energy recycling and the function of supplementary energy, two experiments were carried out: in the first experiment, the two motors were connected directly and there was no supplementary energy; in the second experiment, the H-bridge driver was connected with the two motors and supplied supplementary energy for the circuit. And the armature voltages of the two motors and the supplementary voltage were calculated with:

$$\begin{cases} e_m = C_T N_m \omega_{in} \\ e_s = C_T N_s \omega_{out} \\ e_{\sup} = \alpha U_s \end{cases} \tag{18}$$

where U_s was 12 volts. The comparison of the two motors' armature voltages, which also represent velocities according to Eq. (10)), was carried out for each experiment. As well, the two motors' armature voltage difference in the first experiment, which actually was the voltage drop in the resistance and inductance and indirectly reflected the amount of energy losses in the circuit, was calculated and compared with the compensated voltage in the second experiment.

The example results for the two experiments are given in Fig. 3-21 (a) and (b) respectively. From Fig. 3-21 (a) we can conclude that the master motor was able to drive the slave one even though there was no supplementary energy. This confirmed the energy recycling capability of the system. However, there was a big difference in the armature voltages (velocities), this was caused by the energy losses in the circuit. As for Fig. 3-21 (b), when the energy was compensated for the circuit,

the motor armature voltages (velocities) were basically identical. And that the compensated voltage showed agreement with the two motors' armature voltage difference given in the Fig. 3-21 (a) . This demonstrated that the supplementary energy was used to offset the energy losses in the circuit and as a result, accurate motion tracking was achieved. In addition, if an independent supply power was applied to drive the slave unit for implementing symmatrical movements, the driving voltage will equal the summation of the e_s and half of the two motors' armature voltage difference (the voltage drop in the resistance and inductance of one motor, refer to Eq. (7)). The amount will be about 2.25V at the beginning and increase following the increment of the velocity.
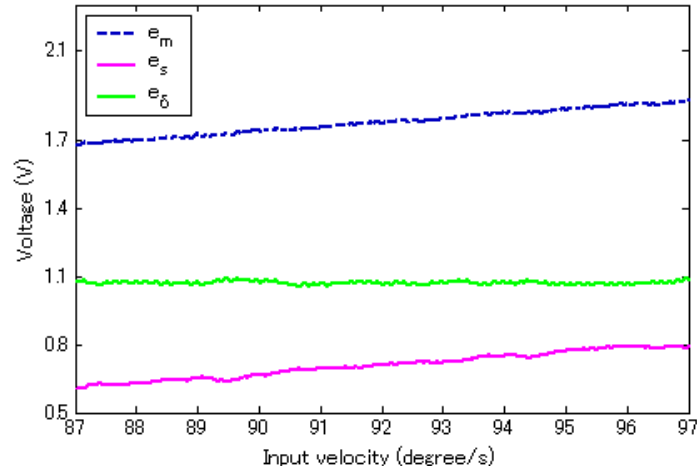
(a) Two motors' armature voltages and their difference: without supplementary energy
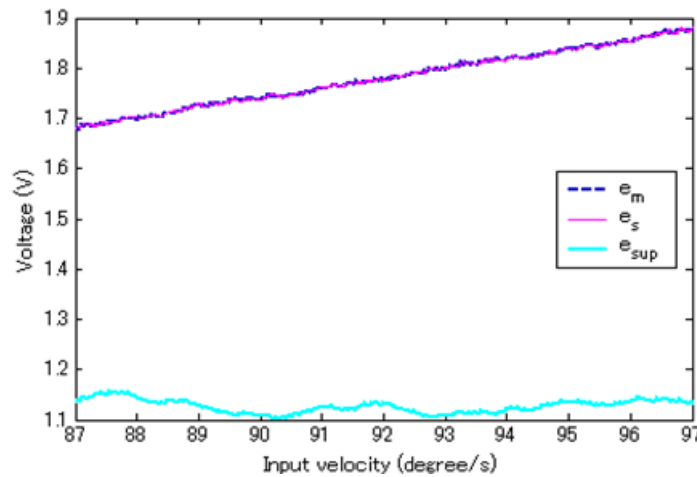
(b) Two motors' armature voltages and the supplementary voltage: with supplementary energy

Fig. 3-21 Results of the energy recycling test on Prototype No. 3

This will be larger than the compensated voltage (around 1.1V). Therefore, it can be concluded that a certain amount of energy can be saved with the function of energy recycling.

B. Force Sensing Test

In this experiment, the gearboxes with the same gear ratios as the energy recycling test were employed. The DC driving motor provided a control force for the master-slave device and rotated the master terminal with a reference velocity of 100 degrees per second. The constant velocity was used to minimize the variation of the no-load/inertial torques of motors and thus to acquire force sensing coefficient accurately. With the supplementary energy from the H-bridge driver, the slave motor was rotated in the same velocity of the master. In the process of rotation, an operator exerted an increasing resistant force in the slave site with one hand for a moment. In this period, the corresponding force information was used to analyze force sensing performance.

The corresponding results are shown in Fig. 3-22. As can be seen from Fig. 3-22 (a), the input torque increased linearly following the increment of the resistant torque. This demonstrated that the system realized force sensing without a force sensor. The actual force sensing coefficient calculated with Eq. (16) was approximately constant even though a varying resistant torque was attached to the slave terminal ($T_{out}^0 \approx 0.014$ Nm and $T_{in}^0 \approx 0.665$ Nm), as shown in Fig. 3-22 (b). the corresponding average value was 1.626, which was larger than unit one due to the frictional loss in the gearboxes. This result shows agreement with Eq. (3). Combining Eqs. (3) and (16), the force sensing coefficient can be expressed as:

$$\lambda_T = \frac{N_m}{N_s}\frac{1}{\eta_m\eta_s} + \frac{N_m}{\eta_m}\frac{(\Delta T_{0\_m} + \Delta T_{0\_s} + \Delta J_m N_m \frac{d\omega_{in}}{dt} + \Delta J_s N_s \frac{d\omega_{out}}{dt})}{\Delta T_{out}} \tag{19}$$

In reference to Fig. 3-22 (c), the terminal velocities in the master and the slave sites had a small fluctuation, thus the no-load and inertial torques were not constant. That is, the second item in Eq. (19) varied slightly. As well, the gearbox efficiency was not unchanged for the increased resistant force. Therefore, the calculated force sensing coefficient was not a constant. In this test, the

maximum change rate of the force sensing coefficient was 0.04 within the velocity varying range of 1.625 degrees per second. This fluctation can be ignored for a human-controlled operation. And the force sensing coefficient of 1.626 was enough for human operators to sense the variation of the acting force in the slave site.

Fig. 3-22 (c) and (d) give the results of velocity tracking and position tracking. The maximum velocity error was 0.5987 degree per second and the maximum angular position error was 0.0719 degree. This demonstrates that high motion tacking performance was achieved.
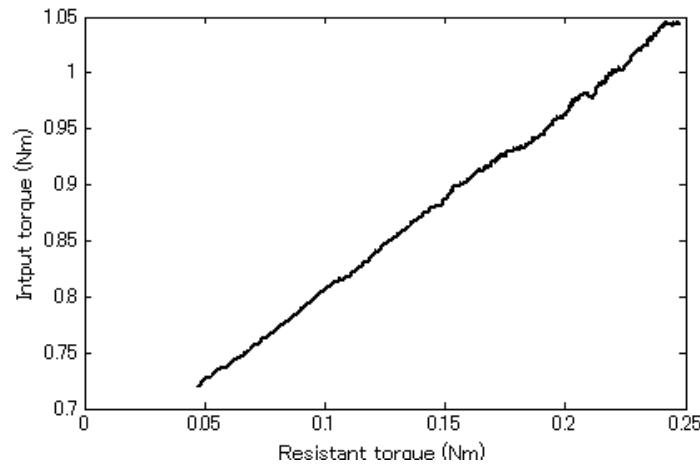
(a) Relationship between the input and output torque
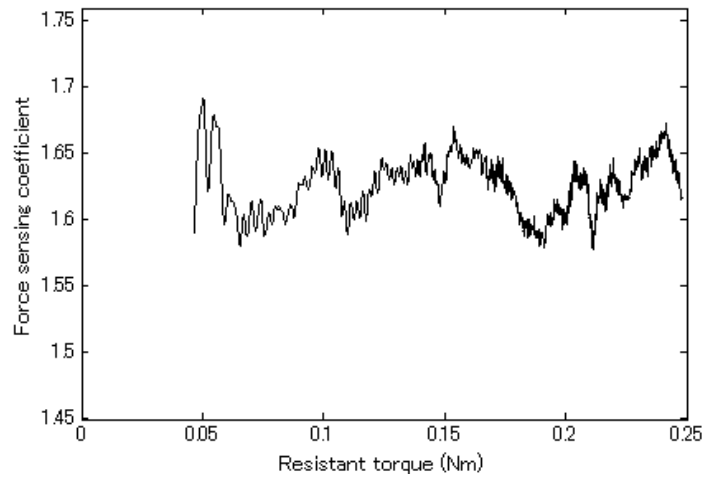
(b) Force sensing coefficient versus resistant torque
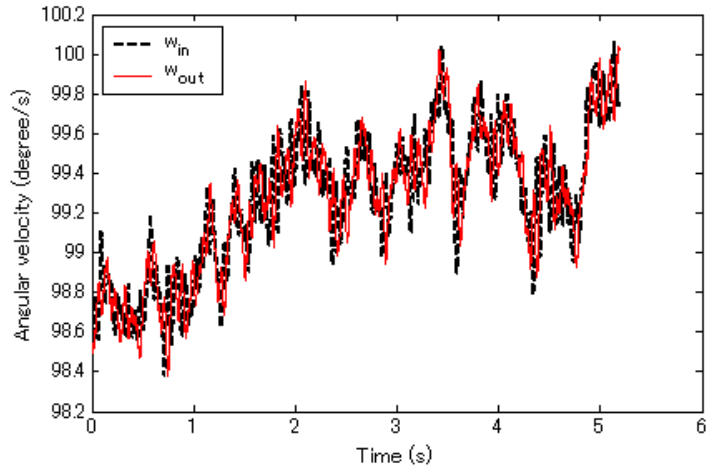
(c) Velocity tracking curve
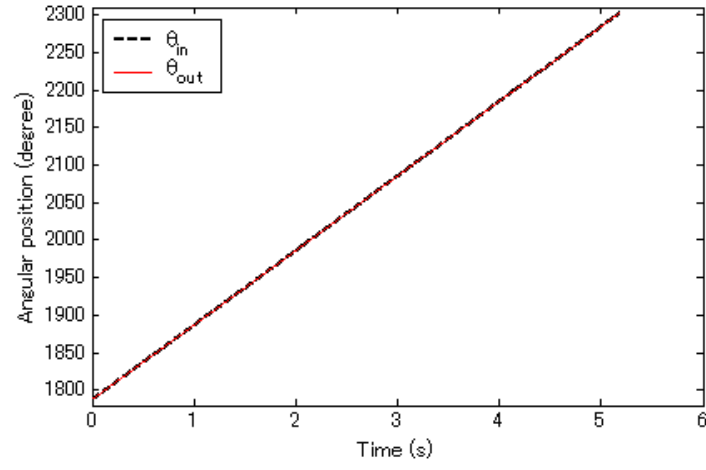
(d) Position tracking curve
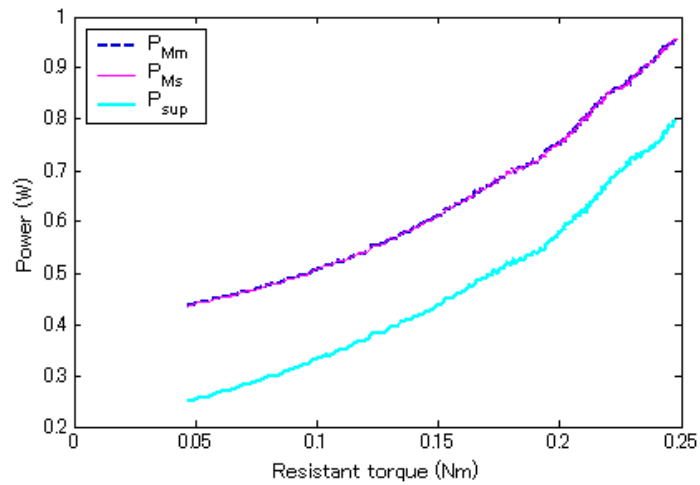
(e) Two motors' electromagnetic powers and the supplementary energy power

Fig. 3-22 Results of the force sensing test on prototype No. 3.

The electromagnetic powers of the two motors and the supplementary energy power were given in Fig. 3-22 (e). In the experiment, the system realized velocity tracking and the gearboxes in both sites had a symmetric structure (identical gear ratio), thus the electromagnetic powers of the two motors were basically identical. This confirms that the energy losses in the circuit were compensated completely (refer to Eqs. (8) and (9)). Otherwise, the supplementary energy power was less than the electromagnetic power of the slave motor, which further confirms that the master motor provided energy for the slave motor.

C. Influence of Different Gearbox Combinations

As for the gearboxes in the master and slave sites, four sets of gear ratio combinations were employed, as listed in Table IV. With each combination, two experiments were carried out, the testing objectives and the experimental conditions are also listed in Table IV, in which η_{sys} represents system efficiency, it was defined as:

$$\eta_{sys} = \frac{P_{out}}{P_{in} + P_{sup}} * 100\% \tag{20}$$

where P_{in}, P_{out} and P_{sup} were calculated by:

$$\begin{cases} P_{in} = T_{in}\omega_{in} \\ P_{out} = T_{out}\omega_{out} \\ P_{sup} = \alpha U_s i \end{cases} \tag{21}$$

The first experiment was aimed at testing gearboxes' influence on force sensing capability, as well, aimed at confirming the relationship of the two motors' electromagnetic powers and the supplementary energy power when gearboxes had different gear ratios. The velocity was fixed and the resistant force attached to the slave site was increased, which was the same as that in the force sensing test. The second experiment was used to test gearboxes' effect on system efficiency as well as the requirements for input power and compensatory energy. In order to carry out a comparison between the different gear ratio combinations easily, the output power was controlled with a constant value by attaching a load of 500 gram to the slave site and setting a reference

velocity of 100 degrees per second. The corresponding output power was 0.085 watt.

TABLE IV. TESTING OBJECTS AND EXPERIMENTAL CONDITIONS

Gear ratio combination		experiment	Testing objectives	Testing conditions
N_m	N_s			
66	66	1	λ_T	● Constant velocity: 100 degrees/s; ● The impedance in the slave site was increased.
66	43			
43	66	2	P_{in}, P_{sup}, η_{sys}	● Constant velocity: 100 degrees/s; ● Constant load: 500 g.
43	43			

For the gearbox combination with different gear ratios, the relationship of the two motors' electromagnetic powers and the compensated energy power obtained in the first experiment are shown in Fig. 3-23. It can be seen that when N_m was larger than N_s, the electomagnetic power of the master motor was more than that of the slave motor when the two terminals achieved motion tracking. That is, the master generated more energy than that required in the slave site. Therefore, the amount of the compensated energy decreased even though there were energy losses in the circuit. In contrast, when N_m was smaller than N_s, the electomagnetic power of the master motor was less than that of the slave motor. Thus, the supplementary energy was also used to provide extra energy for the slave motor except offsetting the energy losses in the circuit. Looking at the initial phase of Fig. 3-23 (b), the compensated energy power was less than the electromagnetic power of the slave motor, this verifies that the energy generated by the master motor was recycled even though it was less than that reqired in the slave site.

In addition, for each gear ratio combination, the average values of the testing results were calculated and listed in Table V. By comparing the case of $N_m = N_s = 43$ with that of $N_m = 66$, $N_s = 43$, we can see that the force sensing coefficient and the demand for the input power increased distinctly when the gear ratio of the master/gear unit was increased, in contrast, the compensated energy decreased significantly. Whereas by comparing the case of $N_m = N_s = 66$
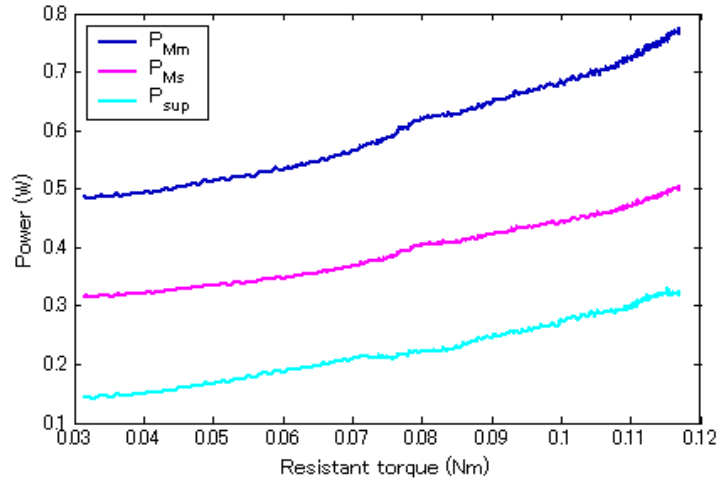
(a) $N_m = 66$, $N_s = 43$
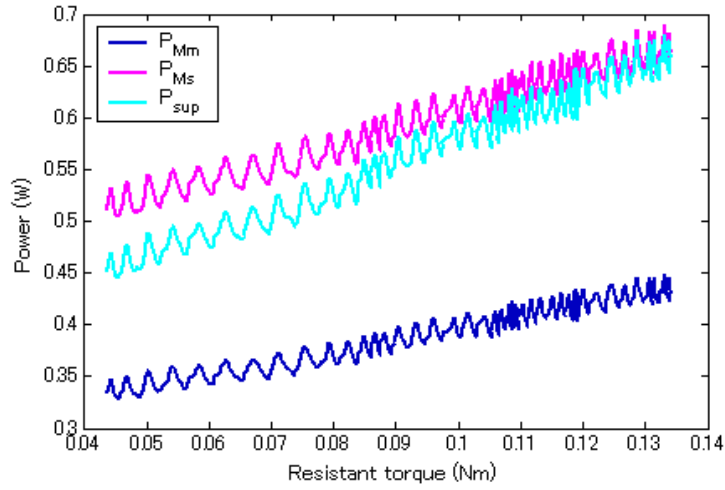
(b) $N_m = 43$, $N_s = 66$

Fig. 3-23 Two motors' electromagnetic powers and the supplementary energy power when system employed gearboxes with different gear ratios

TABLE V. RESULTS OF THE COMPARISON EXPERIMENTS

N_m	N_s	λ_T	P_{in}	P_{sup}	η_{sys}
66	66	1.534	1.265	0.330	5.481
66	43	2.442	1.302	0.196	5.468
43	66	0.862	0.771	0.443	7.338
43	43	1.498	0.788	0.344	7.412

with that of $N_m = 43$, $N_s = 66$, it can be conclued that when the gear ratio of the master/gear unit was reduced, the force sensing coefficient and the demand for input power declined while the supplemetary energy increased. The results fully appraised the theoretical analysis introduced in section 2.4. As for the cases of $N_m = N_s = 43$ and $N_m = N_s = 66$, the compensated energy had no obvious change, while the need for the input power increased with the increment of the gear ratios. It was because that the actual working efficiency of the gearboxes decreased with the increment of gear ratios. Furthermore, it can be concluded that the system efficiency mainly depended on the gear ratio of the master motor: the larger the gear ratio of the master, the lower the system efficiency will result.

D. Stability Test in Hardware

The test was aimed at investigating the stability of the system when the motion velocity was increased and verifying the same working performance of the system for both control directions. This experiment was performed with the same platform as that used in the different operating modes test. Firstly, upward and downward movements were carried out by attaching an increased force to the right site, while no external load/force was attached to the left site. Thus, the left motor/gear unit tracked the movements of the right motor/gear unit with an increased velocity. The attached force was increased until there was a sudden change in the sensed force, that is, the master and slave terminals could not mirror each other in motion behavior, and then stopped the movement immediately. Secondly, the above process was repeated for the reverse control direction: the control force was attached to the left site and no external load/force was attached to the right site. After the experiment, in order to confirm the stable frequency response range of velocity, a FFT (Fast Fourier Transform) analysis was carried out with the velocity information collected from the two terminals during the period that the master and slave made mirror symmetric movements.

Fig. 3-24 gives the frequency response result of velocity when the control force was exerted by

the right limb. When the velocity was varied above the frequency of around 30 Hz, the slave could not mirror the movement of the master any more, and there was a sudden change in the sensed force. Because that in a sampling period, the velocity/position difference between the two terminals became larger when the rotational velocity had a higher frequency, and resulted in a larger control output of the master-slave motion tracking controller. Further, the two terminals had larger differences in motion velocities and positions, which easily lead to a movement fluctuation of the slave terminal and a great change in the current and the sensed force. Almost the same result was obtained when the control force was exerted by the left limb. This confirmed the same operational performance in the two control directions and thus made the system have potential in training patients no matter which limb is impaired. Overall, the system can maintain stable if the rotational velocity was kept within the frequency range of 30 Hz. This frequency range of velocity was sufficient for patients to perform rehabilitation training.
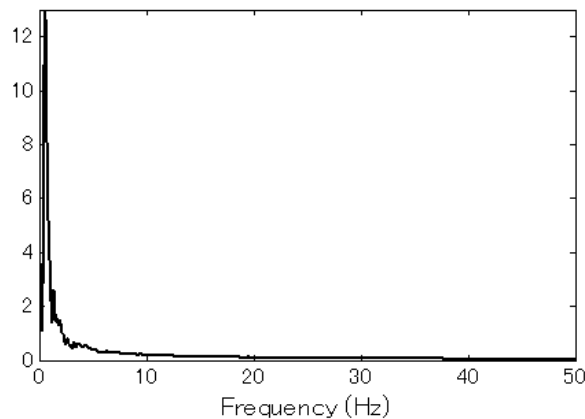
Fig. 3-24 Frequency response result of velocity for: control force was exerted by the right limb

E. Working Efficiency Test

This test included two sub-experiments: (1) there was no supplementary energy provided for the master-slave circuit; (2) a certain amount of energy was compensated for the circuit to implement master-slave symmetric movement. In each sub-experiment, a subject attached a force to one handle and drove the system to rotate the other handle, which was not attached with any force. In

order to test the change of working efficiency following the variation of output power, the control force was increased at first (phase 1). Then, the control force was reduced to avoid a collision of the handles and the tabletop (phase 2). This movement process was repeated five times for the both control directions in each sub-experiment.

An example of velocity curves in two terminals is given in Fig. 3-25. When there was no supplementary energy, the two terminal velocities had an obvious difference and the slave motor could not be actuated when the input velocity in the master side was small. As well, there was a delay in the output velocity. When there was supplementary energy, the slave reproduced the movement of the master accurately and quickly, which verified the function of the supplementary energy in ensuring master-slave symmetric movement and further confirmed quick response performance of the system in real application. As for the working efficiency of the system, there was no obvious difference between two control directions in both sub-experiments. Fig. 3-26 presents the preventative results when the control direction was from right to left. $\omega_{\max}$ denoted the maximum output velocity in the left side. Considering the case that there was no supplementary energy, when the maximum output velocity was low, the working efficiency had the same variation trend with the output power; when the maximum output velocity was high, the working efficiency increased as the increase of the output power in phase 1, whereas it still increased or had no distinct change in phase 2. The difference of the working efficiency between the low and high velocities in phase 2 can be explained by the slave unit's inertial movement, which was obvious when the slave unit was rotated with a high velocity. For the case that there was supplementary energy, the working efficiency increased to a certain value quickly and kept the corresponding value without obvious change in phase 1, whereas the working efficiency in phase 2 increased continuously even though the output power decreased. The variation of the working efficiency in phase 2 can also be explained with the inertial movement of the slave unit. Overall, the working efficiency of the system with supplementary energy had relatively small change with the variation of output power. In addition, the working efficiency of the system with

supplementary energy was higher than that without supplementary energy.

(a) Without supplementary energy.   (b) With supplementary energy.
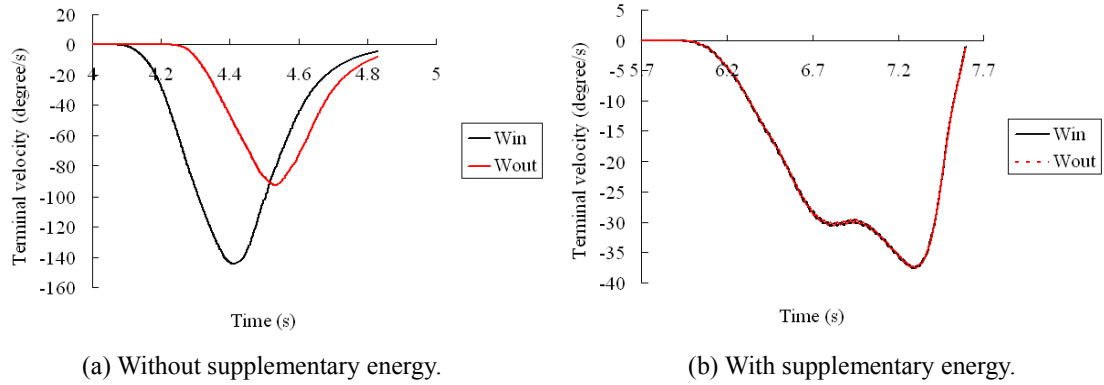
Fig. 3-25 An example of terminal velocities in two sub-experiments.

(a) Without supplementary energy.

(b) With supplementary energy.
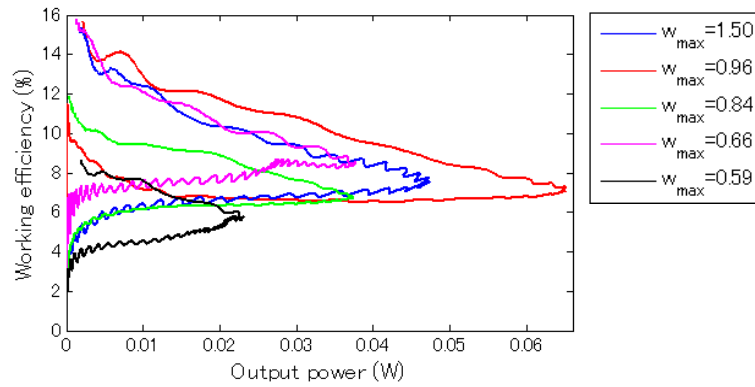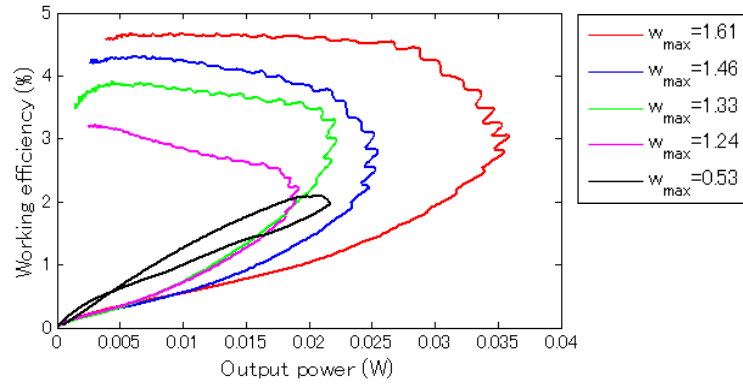
Fig. 3-26 Working efficiency of the system.

F. Different Operating Modes Test

In this test, the two handles were controlled by the two limbs of an operator. In order to confirm

that the system can support training in different operating modes, the test was performed in two steps. Firstly, the left limb provided a small force actively, and the right limb gave an assistant force to assist the left one to accomplish movements. Secondly, the left limb started movements with a larger force, while the right limb exerted a resistant force to increase the burden on the left one. The two cases were used to imitate active-assisted and active-resisted modes, respectively. Besides, the second case can also be used to imitate passive mode if the resistant force of the right limb is considered as impedance caused by an impaired limb with no motor function and the active force of the left limb is considered as a driving force from the healthy limb. In order to compare the torque relationship the same upward and downward movements (elbow flexion and extension) were performed for the two cases.
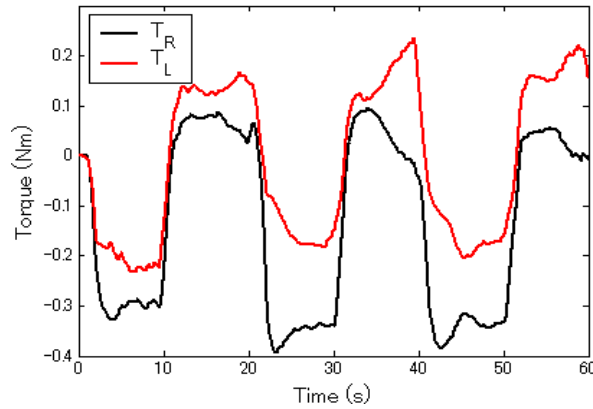
(a) Left limb: active force, right limb: assistant force
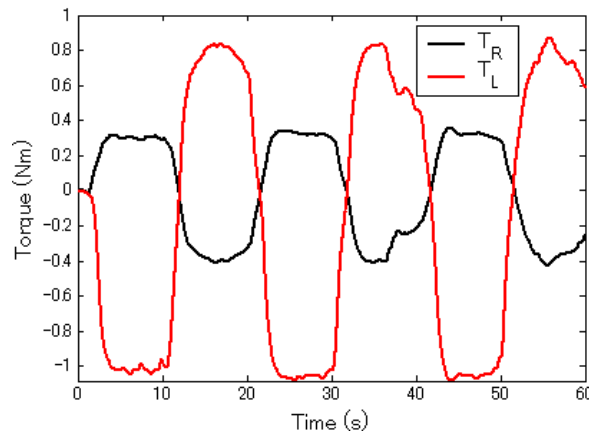
(b) Left limb: active force, right limb: resistant force

Fig. 3-27 Torque relations for different operating modes

The torque relations for the two cases are presented in Fig. 3-27, where T_L denotes the produced torque in the left site, and T_R represents the produced torque in the right site. In active-assisted mode, the torques in the two sites had the same direction, while in the active-resisted mode, the torques in the two sites had a reverse direction. Besides, the active torque exerted by the left limb in the former case was very small compared to that in the later case. Additonally, high motion tracking performance was achieved, the corresponding maximum velocity and position errors were 0.5926 degree per second and 0.0613 degree in the active-assisted mode and were 0.2373 degree per second and 0.024 degree in the active-resisted mode. The results demonstrated that the system can support different operating modes by coordinating the forces of the two limbs, and no matter in which mode, high motion tracking performance could be achieved.

4. Training Experiments

In order to confirm the effectiveness of the proposed robot, bimanual motion tracking trainings in active-resisted and active-assisted modes were firstly performed on 11 healthy subjects. After training, the movement coordination capability of the two arms of the subjects increased obviously; and active-resisted training achieved a greater improvement than active-assisted training. However, the training effect was evaluated only based on motion tracking precision. Motion tracking training No. 2 was performed on 14 healthy volunteers in bimanual active-resisted, bimanual active-assisted and single-limb training modes, simultaneously with movement information of the master-slave terminals and concentration of hemoglobin in brain being recorded. After bilateral arm coordinated training, significantly increased motion tracking precision and CAL fully demonstrated the positive training effect of the robot. A higher CAL induced in bimanual tasks indicated that bimanual training may motivate the functional integrity of two hemispheres and may be more favorable for improving motor function than single hand training. However, no resistant or assistant force comparative to that exerted in bimanual active-resisted or active-assisted mode was provided in single-limb trainings. Therefore, in motion tracking training No. 3, a resistant or assistant force was attached by another person in single-limb training. Statistical analyses completely confirmed that bimanual tasks activated both hemispheres to a significantly higher level than single-limb tasks and reveled that bimanual training achieved a relatively better hemispheric asymmetry of cerebral activation compared to unilateral-limb training.

4.1 Motion Tracking Training No. 1

A bimanual-coordinated training test was performed on 11 healthy subjects (the students at Kochi

University of Technology: 5 female and 6 male; mean age: 27.4) to preliminarily reflect the availability of the system for supporting healthy subjects in performing exercise. The subjects sat before the table and put their forearms on the table naturally with two hands holding the handles. The height and position of the table were adjusted to make each subject feel comfortable. Based on haptic feel and visual feedback, the subjects controlled the forces of two limbs and drove the two handles to perform upward and downward movement repeatedly (elbow flexion and extension).

4.1.1 Training Mode

There were two bimanual training modes. The first was active-resisted mode: the left limb started the movement actively while the right limb attached a resistant force to increase the impedance of the left one. The second was active-assisted mode: the left limb provided an active force and the right limb exerted an auxiliary force to assist the left one in motion tracking tasks. No matter in which mode, the subjects regulated the forces of the two limbs based on force sensation and visual feedback, and controlled the two handles (implementing mirror symmetric movement) to track reference movement trajectories that were displayed on the PC.

4.1.2 Training Task

Seven motion tracking tasks were included in each training mode. Every task lasted 70 seconds, and was alternated with a 30-s rest period. Before the recorded experiment in each training mode, each subject practiced the first motion tracking task three times to become familiar with the operation. After that, the training was performed. After each tracking task, a corresponding score was presented on the PC to reflect the corresponding motion tracking result. This could motivate the subjects' interest in exercises and was favorable for improving motor agility. If the score was less than 60 points, the same motion tracking task had to be performed repeatedly until the score was not less than 60 points. That is, the score was also used to define an acceptable limit to the results of a motion tracking task.

The motion information and torque information were collected for the first and seventh tasks. The motion information in the first and last tasks was compared to evaluate the training effect, and further to verify the availability of the system for supporting bimanual-coordinated training modes. The torque information was used to confirm the relationship between the terminal forces in different training modes.

4.1.3. Instructions for Subjects

The subjects were instructed to coordinate the forces of two limbs and to try to keep the actual trajectories in the center of the two reference trajectories. The subjects should try their best to concentrate attention during the period of each motion tracking task. Before the training, the subjects did not know the experimental objective, in order that they would not make more effort during the last motion tracking task. Thereby, an objective result could be obtained.

4.1.4. Reference Movement

The reference movements were displayed in the form of dynamic trapezoid trajectories with the height representing the movement angle, as shown in Fig. 4-1. Upward and downward movements denoted elbow extension/flexion movements. Two synchronously dynamic reference trajectories were displayed to define a motion fluctuation range (the distance between two reference trajectories: d and $d * \cos \alpha$, in which $\alpha = tg^{-1} \omega_{out}$). At the moment of changing rotational direction, the position change of the actual trajectories was usually larger than that in other periods, and thus a larger fluctuation range of d compared to $d * \cos \alpha$ was defined. In addition, at the moment of changing rotational direction, a transmit time was given to avoid a sharp variation in velocity. The central positions of two reference trajectories were ideal tracking targets.

In all the tasks, the motion velocity was the same with a magnitude of eight degrees per second. The first and seventh tasks had the same reference trajectories with identical maximum rotational angles (determined from the central position of two reference trajectories) in all the reciprocating

motion periods. However, the reference trajectories in the other tasks were different: the maximum rotational angles were varied in different reciprocating motion periods; besides, the varying amplitude and order were different. That is, the tracking tasks were not only repetitions of the same movement. This characteristic and dynamic feature of reference trajectories can activate the subjects' close attention in the process of training. In addition, the maximum rotational angle, movement velocity, and motion fluctuation range can be set independently for each tracking task. Since this experiment was aimed at confirming the feasibility of the system for bimanual-coordinated training preliminarily, fixed parameters were used to reduce movement difficulty. In order to further concentrate the subject's attention, before the test, the subjects were informed that the reference trajectories had a varying maximum rotational angle in different periods, whereas the concrete values were not imparted. In the process of training, the subjects coordinated the forces of the two limbs to perform upward and downward movements repeatedly and tried to keep the actual trajectories in the center of the two reference trajectories.

Fig. 4-1 Schematic diagram of movement tracking

4.1.5 Evaluation Metrics

For each task, a score was calculated based on the difference between the actual positions of two

terminals and the ideal position, which was defined as the central position of two reference trajectories. Since the two terminals realized symmetric movement accurately, here, the position of the slave terminal was used to denote the actual position. The calculation formula is:

$$\begin{cases} score = 100 - \dfrac{40\theta_{rms}{}'}{2d/3} \\[4mm] \theta_{rms}{}' = \sqrt{\dfrac{\sum\limits_{i=1}^{N}(\theta_{ref}^{i} - \theta_{s}^{i})^2}{N}} \end{cases} \tag{22}$$

where θ_{ref} denotes ideal position; θ_s is the position of slave (right) terminal; $\theta_{rms}{}'$ is position RMS (root mean square); N is the number of the sampled data in one task. When $\theta_{SD}{}'$ equals $2d/3$, the score is 60 points; when $\theta_{SD}{}'$ equals zero, the score is 100 points; for other values of $\theta_{SD}{}'$, the score is calculated linearly. The comparison value of $\theta_{SD}{}'$ ($2d/3$) to acquire 60 points was preliminarily selected depending on the feedback information of another two healthy subjects, who performed the first three motion tracking tasks in the two training modes. In each mode, the two subjects practiced the first motion tracking task three times firstly to get familiar with the operation. Then, they performed the first three tracking tasks. After each task, the comparison value of $\theta_{SD}{}'$ was regulated to make the corresponding score of each task just slightly larger than 60 points. Finally, $2d/3$ was selected as the comparison value of $\theta_{SD}{}'$ to acquire 60 points, which further was considered an acceptable limit to the results of each task for all the subjects.

The score was used to reflect the extent of fluctuation between the actual trajectories and the ideal one, and to motivate the subjects to try their best to keep the two terminals in the central position of two reference trajectories. However, the ideal trajectory was only derived from two references but was not displayed on the PC. It could not reflect the mean error of position tracking and the fluctuation of movement velocity. Therefore, it was not enough to evaluate the training effect by only using the score. Here, we further defined revaluation metrics so as to assess the training effect completely. The mean value and standard deviation of the position errors between the

reference and actual positions ($\bar{\theta}$, θ_{SD}), along with the standard deviation of the velocity errors (ω_{SD}) between the reference and actual velocities, were firstly calculated for the first and last motion tracking tasks. Then, the corresponding values were compared between the first and the last tasks. The formulas for calculating mean value and standard deviations are given as:

$$\bar{\theta} = \frac{\sum\limits_{i=1}^{N} \delta_\theta}{N} \tag{23}$$

$$\theta_{SD} = \sqrt{\frac{\sum\limits_{i=1}^{N} \delta_\theta{}^2}{N}} \tag{24}$$

$$\omega_{SD} = \sqrt{\frac{\sum\limits_{i=1}^{N} (\omega_{ref} - \omega_s)^2}{N}} \tag{25}$$

$$\delta_\theta = \begin{cases} \theta_s - \theta_{Uref}, & \theta_s > \theta_{Uref} \\ \theta_{Lref} - \theta_s, & \theta_s < \theta_{Lref} \\ 0, & \theta_{Lref} \leq \theta_s \leq \theta_{Uref} \end{cases} \tag{26}$$

ω_{ref} and ω_s denote the ideal velocity that induced from the dynamic reference movement and the actual velocity in the slave terminal. θ_{Uref} and θ_{Lref} represent the position values of the upper and lower reference trajectories. To compare $\bar{\theta}$, θ_{SD}, and ω_{SD} between the first and last tasks and to evaluate the training effect statistically, one-way multivariate analysis of variation (MANOVA1) on 'time' (first and last) was performed with SPSS software (PASW Statistics 18). Statistical significance was set at $p < 0.05$.

4.1.6 Results and Discussion

The comparison results of $\bar{\theta}$, θ_{SD}, and ω_{SD} for all the subjects in the two training modes are given in Figs. 4-2, 4-3, and 4-4. In active-resisted mode, nine subjects completed the last task with obviously reduced $\bar{\theta}$, θ_{SD}, and ω_{SD} compared to the first task. The second subject

performed the last task with a slightly reduced standard deviation of velocity errors, whereas the mean value and standard deviation of position errors increased. The sixth subject finished the last task with a decreased average position error, but the standard deviation of position errors and velocity errors increased somewhat. In active-assisted mode, all the subjects accomplished the last task with reduced mean value and standard deviation of position errors, whereas five subjects (numbers 1, 4, 8, 9, and 11) finished the last task with an increased standard deviation of velocity errors. As for the group analysis of MANOVA1, the results revealed a significant main effect of 'time' on $\bar{\theta}$ and θ_{SD} in both training modes; the corresponding significant differences of $\bar{\theta}$ and θ_{SD} between the first and last tasks were $p \approx 0.015$ and $p \approx 0.040$ in active-resisted mode and $p \approx 0.009$ and $p \approx 0.022$ in active-assisted mode. However, there was not a main effect of 'time' on ω_{SD}. Table 2 summarizes the mean values of $\bar{\theta}$, θ_{SD}, and ω_{SD} of all the subjects and the changes in errors in the comparison between the first and the last task. In conclusion, after motion tracking training, there was a significant improvement in position tracking precision, whereas there was no obvious enhancement in velocity tracking precision. During the task periods, the volunteers controlled two terminals to track predefined dynamic movement trajectories. That is, they mainly focused on position tracking rather than velocity tracking. The velocity deviation was calculated with the actual velocity and the induced velocity from the dynamic reference movement. Therefore, in the short training period, the position tracking achieved a greater enhancement in accuracy compared to velocity tracking. Overall, the subjects learned how to accomplish tasks with training practice and achieved an improved movement performance. Significant improvement in position tracking precision indicated that the bimanual training performed using our designed robot can enhance the bimanual-coordinated capability of healthy subjects. However, the validity of the bimanual training in improving the movement performance of hemiplegic patients should be further verified.
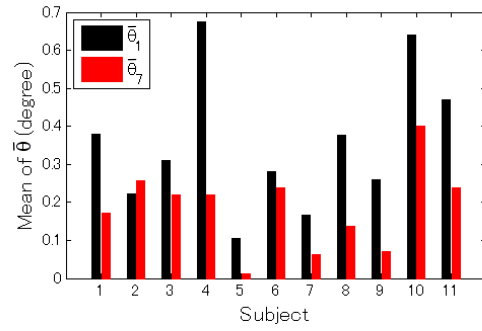
(a) Active-resisted mode
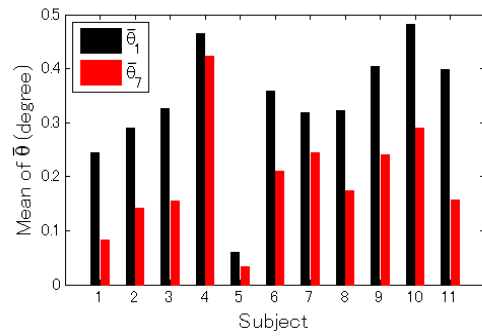
(b) Active-assisted mode

Fig. 4-2 Comparison of mean position error between the first and seventh tasks.
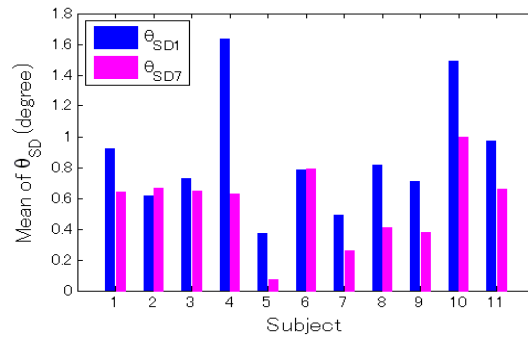
(a) Active-resisted mode
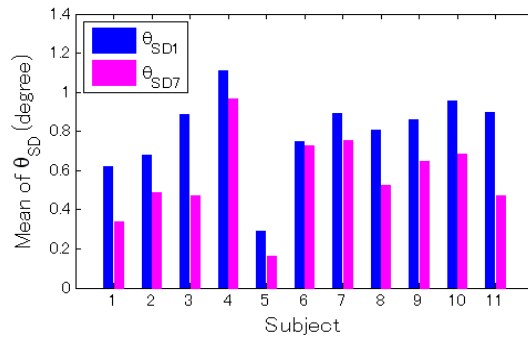
(b) Active-assisted mode

Fig. 4-3 Comparison of position standard deviation between the first and seventh tasks.
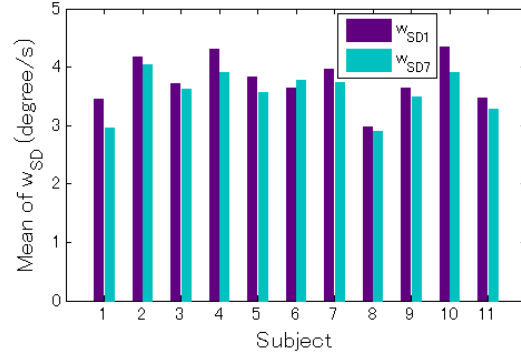
(a) Active-resisted mode
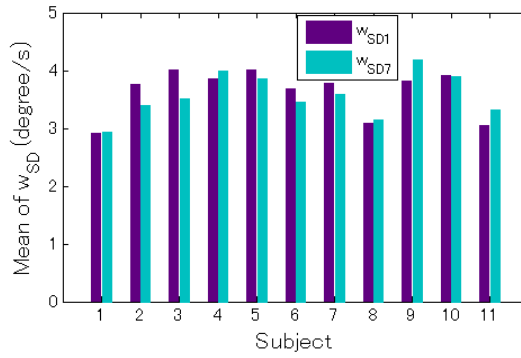
(b) Active-assisted mode

Fig. 4-4 Comparison of velocity standard deviation between the first and seventh tasks.

TABLE VI. MEAN VALUES OF MOTION TRACKING ERRORS OF ALL THE SUBJECTS AND THE ERROR CHANGES OF THE FIRST VERSUS LAST TASK COMPARISON.

Training mode	Parameter	First task (mean)	Last task (mean)	Change (mean)
	$\bar{\theta}$	0.3536	0.1841	0.1695
Active-resisted	θ_{SD}	0.8670	0.5591	0.3079
	ω_{SD}	3.7727	3.5612	0.2115
	$\bar{\theta}$	0.3334	0.1957	0.1377
Active-assisted	θ_{SD}	0.7956	0.5664	0.2292
	ω_{SD}	3.6275	3.5681	0.0594

4.2 Motion Tracking Training No. 2

In the first training experiment, the training effect was only evaluated based on motion tracking precision. Here, training experiment No. 2 was performed on 14 healthy volunteers in bimanual active-resisted, bimanual active-assisted and single-limb training modes, simultaneously with

movement information of the master-slave terminals and concentration of hemoglobin in brain being recorded. Training effect was fully verified based on the variations of motion tracking precision and CAL.

4.2.1 Subject

14 healthy volunteers (ten male and four female, age: 27.7±1.38 years old) at Kochi University of Technology participated in the motion tracking training. All the volunteers were right-handed. No volunteers had a history of physical or psychiatric disorder. Informed consent was obtained from each volunteer.

4.2.2 Training Task

Based on force sensation and visual feedback, the volunteers regulated the forces of two limbs and controlled two terminals to track desired movements in three phases, as shown in Fig. 4-5. (1) Active-assisted training: one limb provided an active force and meanwhile, the other limb exerted an assistant force. The forces of two limbs had the same direction as the reference movement; (2) Active-resisted training: one limb provided an active force with the same direction as the reference movement, while the other limb exerted a relatively small resistant force with a reverse direction as the reference movement; (3) Single-limb training: only one limb (the other limb was not attached to the handle) exerted a driving force on the corresponding terminal to control the movements of two motors and further to actuate the other handle in motion imitation.

(a) active-assisted phase   (b) active-resisted phase   (c) single-limb phase
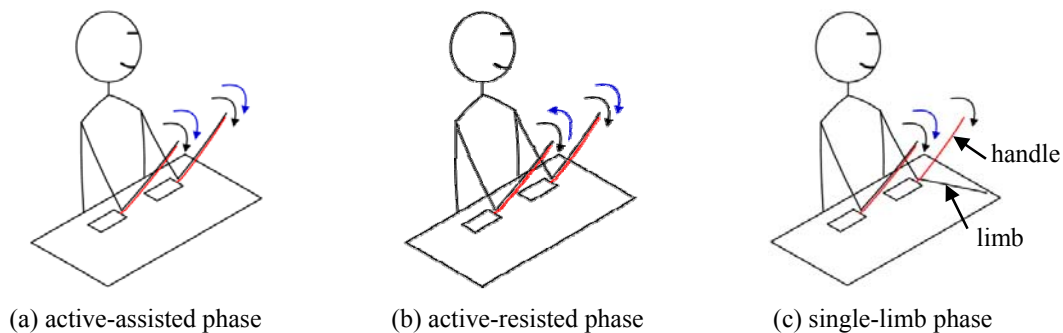
Fig. 4-5 Schematic diagram of the three training phases. Red lines represent two operation handles. Black arrowheads show the rotational directions of the two handles. Blue arrowheads show the directions of the forces exerted by the limbs.

Before the recorded experiment in each training phase, the volunteers practiced the first tracking task three times to get familiar with the operation. In the single-limb phase, three times of practices were performed with the right limb, and three times of practices were performed with the left limb. Then, a 90-s rest was given to make the volunteers rest themselves. After that, the motion tracking training was performed with the hemoglobin concentration of the volunteers and dynamic movement information of the two terminals (position and velocity) being recorded. In each training phase, there were six 70-s specific tracking tasks. Each task period was alternated with a 30-s rest period, as shown in Fig. 4-6. There was a beep to remind the volunteers of the start and end of each task.
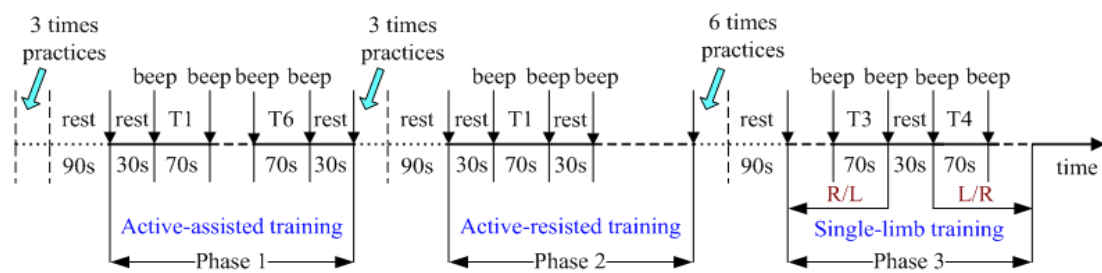
Fig. 4-6 Time sequence in three phases. Firstly, three times of practices were performed to make the volunteers get familiar with the operation in each training mode. In the single-limb phase, three times of practices were performed with the right limb, and three times of practices were performed with the left limb. Then, a 90-s rest was given before the recorded experiment. In each training phase, there were six 70-s motion tracking tasks alternated with a 30-s rest period. A beep was provided to remind the volunteers of the start and end of each task.

Since all the volunteers were healthy subjects, only one training period rather than many sections were selected. A 90-s rest between different training phases was enough for the volunteers to rest themselves. Hence the effects caused by the order of training modes could be avoided. However, in single limb phase, the right and left limb training modes were performed just with a 30-s interval (rest period). In order to avoid the training order effect of two single limb modes, seven volunteers performed the first three tasks and last three tasks with the right limb and left limb, respectively; while the other seven volunteers performed the single right-limb tasks and single

left-limb tasks (each single mode includes three tasks) in a reverse order. Only three tasks were performed in two single-limb training modes because the single-limb tasks were relatively easy and their many more repetition may cause the volunteers to pay less attention at last.

In all the tasks, the motion velocity was the same with a magnitude of eight degrees per second. In each task, there were three times of reciprocating upward and downward movements. In bimanual training phases, except for the first and last tasks, in which cerebral activation amount and motion tracking precision were compared, the tracking curves in other four tasks had different maximum rotational angles(the distance between the central positions of two reference trajectories) in the three reciprocating movement periods. And the variation order in rotational angle was different for the four tasks. But in the two bimanual training phases, the corresponding tasks had the same reference movement. As well, the three tasks in two single-limb modes had the same reference movements with the first three tasks in two bimanual modes. Varied reference movements in different tasks were designed so as to avoid mechanical motion-repetitions of arms and to achieve a virtual improvement in movement coordination function. While the same reference movement in the corresponding tasks of different training modes was defined so as to assure the comparability of the CAL in different training modes. In order to make the volunteers pay much more attention during training, before the experiment, they were informed that the reference trajectories had a varying maximum rotational angle in different reciprocating movement periods, whereas the concrete variation values were not imparted.

4.2.3 Cerebral Activation Measurement

Concentration changes of oxygenated hemoglobin (Oxy-Hb), deoxygenated hemoglobin (Deoxy-Hb), and total hemoglobin (Total-Hb) were measured using an ETG-7100 optical topography system (Hitachi Medical Corporation, Tokyo, Japan) [32], as shown in Fig. 4-7. The emitter and detector probes were arranged in a 30 mm square grid. Two wavelengths of the near-infrared light were 695 mm and 830 mm. Changes in the intensity at two wavelengths were

converted to relative changes in Oxy-Hb, Deoxy-Hb, and Total-Hb with the Beer Lambert law (BLL) [33]. The infrared light could detect the variation in cerebral blood volume at around 20 mm to 30 mm below the scalp [34]. The magnitudes of concentration changes in Oxy-Hb, Deoxy-Hb, and Total-Hb were displayed as a contour map (NIRS topography) during the process of training.
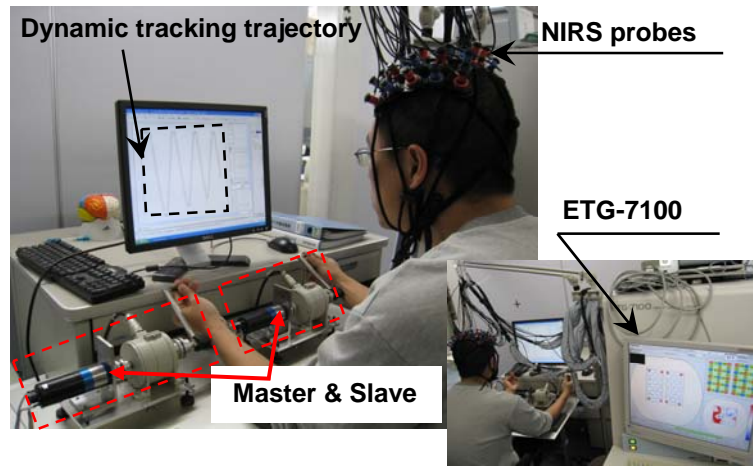
Fig. 4-7 Experimental scene

Two probe holders were placed on a volunteer's bilateral frontal areas according to the international 10-20 system [35–38] (Fig. 4-8). Each probe holder was mounted with 8 emitters and 7 detectors. Since the midpoint of each couple of emitter and detector was a test point, 22-channel (labeled as channels 1 to 22) signals was measured simultaneously with each probe. All the 44-channel signals covered sensorimotor cortices (SMC: channels 2, 6, 15, and 19 in the left hemisphere, and channels 3, 8, 17, and 22 in the right hemisphere), supplementary motor areas (SMA: channels 20 and 21 in both the left and right hemispheres), premotor cortices (PMC: channels 7, 11, and 16 in the left hemisphere, and channels 7, 12, and 16 in the right hemisphere), and somatosensory areas (SSA: channels 1, 10, and 14 in the left hemisphere, and channels 4, 13, and 18 in the right hemisphere). SMC mainly give movement commands to different physical parts; SMA and PMC are related to planning movement procedure. SSA is correlated with motor sense. The former three areas are considered as motor-control related regions, and all the four

Fig. 4-8 Placements of probe holders and measurement channels. (a) 10-20 system; (b) functional mechanism of human brain; (c) detected channels on (a) and (b); (d) distribution of detected channels in motor-related areas. Firstly, CZ portion was determined from the positions of nasion and inion of each

volunteer; secondly, C3 and C4 portions were confirmed based on the positions of A1, A2, and CZ; thirdly, two probe holders were positioned on head with channel 6 of the left holde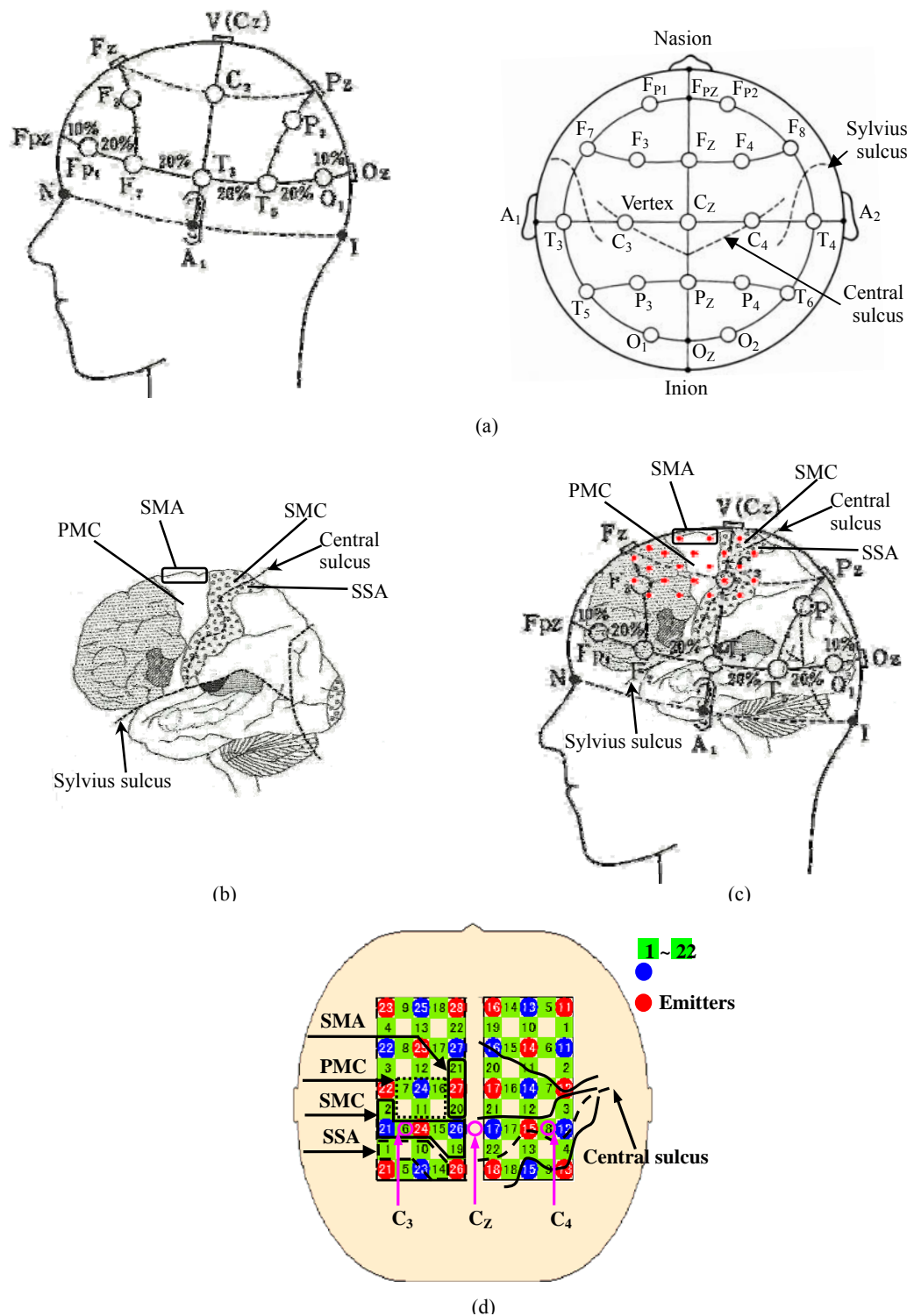r and channel 8 of the right holder being located in the C3 and C4 portions, and in the center column, with the midpoint of the two posterior detectors being located in the CZ portion. Each probe holder detected 22-channel signals (labeled as channels 1 to 22). ; SMC: sensorimotor cortices; SMA: supplementary motor areas; PMC: premotor cortices; SSA: somatosensory areas; SMC, SMA, and PMC were considered as motor control related regions.
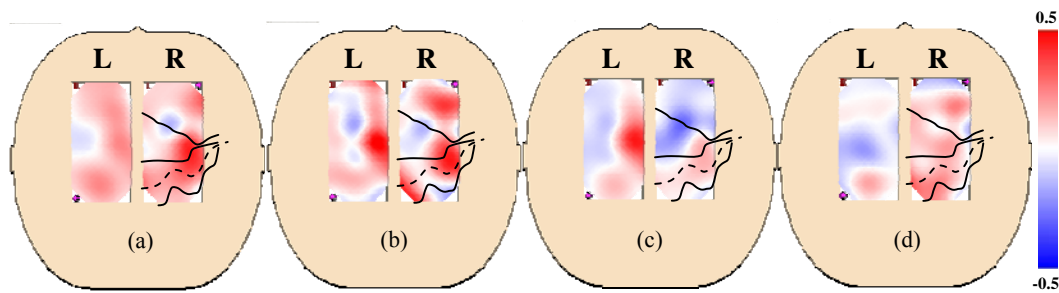
Fig. 4-9 Representative Oxy-Hb mappings on the head of a male in four training modes. (a) active-assisted mode; (b) active-resisted mode; (c) single right-limb mode; (d) single left-limb mode. L and R represent the left and right hemispheres. The Oxy-Hb mappings on head were captured in the 50th second of a representative task in each training mode. Color gradient bar indicates the relative concentration of cerebral activation.

areas are considered as motor related regions. The signals were sampled at 10 Hz. A smoothing operation with a 5-s moving average was performed to filter low-frequency noise that mixed in the channel signals.

Four representative Oxy-Hb mappings on the head of a male in the four training modes are shown in Fig 4-9. It can be seen that some or all the motor related regions were activated in different training modes. It was obvious that bimanual coordinated training modes induced greater cerebral activation in both hemispheres than single limb training modes. As well, the right limb training mainly activated the left hemisphere and the left limb training mainly activated the right hemisphere.

4.2.4. Instructions for Subjects

The volunteers were instructed to track desired movement carefully during each task and to avoid

head tilt during the whole process. During a rest period, they were instructed to stop the movements of two limbs and fully relax their brain without thinking, movement, and language before a new task. Evaluation method was not informed beforehand to avoid much more attention being paid in the last task.

4.2.5 Statistical Analyses

A. Cerebral Activation Amount

Compared with Deoxy-Hb and Total-Hb, Oxy-Hb has the most apparent changes corresponding to tasks [39]. Therefore, the concentration change in Oxy-Hb was used to reflect CAL. Firstly, the sampled data were analyzed in "integral mode" with ETG-7100 software. The data in the first and last tasks were analyzed for active-assisted and active-resisted modes. Meanwhile, the first three tasks in two bimanual-coordinated modes and the three tasks in two single limb modes were respectively analyzed using weighted mean method. The obtained Oxy-Hb was recorded with ΔOxy-Hb because it was a relative value to a baseline, which was determined from a predefined pre time, recovery time, and post time during data analysis [40]. Since there were low-frequency oscillations in the NIRS signals and the volunteers achieved a better rest of brain in different times during each rest period, the lengths of pre time, recovery time, and post time were randomized for different volunteers. Secondly, average ΔOxy-Hb in each channel was respectively calculated for the first and last tasks in two bimanual modes and for the task in four training modes. Finally, average ΔOxy-Hb was calculated for the regions of SMC, SMA, PMC, and SSA in the left and right hemispheres (8 regions altogether).

Three-way analysis of variation (ANOVA) on 'time' (first and last) $\times$ 'hemisphere' (right and left) $\times$ 'mode' (active-assisted and active-resisted) was performed to compare CAL difference between the first and last tasks in two hemispheres and in two bimanual training modes. In single-limb training phase, the first three tasks and the last three tasks were performed with different limbs. Thus, comparison between the last and first tasks was not performed for two single limb

training modes.

Three-way analysis of variation on 'hemisphere' (right and left) × 'region' (SMC, SMA, PMC, and SSA) × 'mode' (bimanual assisted, bimanual resisted, single right-limb, and single left-limb) was conducted to compare CAL in two hemispheres and four motor related regions among four training modes. As for the factors with significant main effect, post-hoc multiple comparison analysis using Tukey's least significant difference criterion was further performed. If interactions between two factors were significant, simple main effect for the interaction was analyzed to confirm the CAL differences among the four training modes on different levels of the other factor (hemisphere or region). All above analyses were performed with SPSS software (PASW Statistics 18). Statistical significance was set at $p < 0.05$.

B. Motion Tracking Precision

In order to observe the variation in motion tracking precision in two bimanual training modes, the mean deviations of the positions and velocities ($\overline{\theta_{MD}}$ and $\overline{\omega_{MD}}$) between the reference values and actual values were calculated for each task. Referring to the motion tracking trajectories shown in Fig. 4-10, the calculation equations were written as:

$$\overline{\theta_{MD}} = \frac{\sum_{i=1}^{N} \left| (\theta_{ref}^i - \theta_{act}^i) \cos\alpha \right|}{N} \tag{27}$$

$$\overline{\omega_{MD}} = \frac{\sum_{i=1}^{N} \left| \omega_{ref}^i - \omega_{act}^i \right|}{N} \tag{28}$$

where θ_{ref} denoted the reference position; θ_{act} was the actual position of the two terminals (two terminals achieved mirror movement accurately, and thus the position on the right side was considered as the actual position); and ω_{ref} and ω_{act} denoted the reference velocity induced from the dynamic reference movement and the actual terminal velocity on the right side. N was the number of data sampled in one task. Two-way multivariate ANOVA on 'time' (first and last) ×

'mode' (active-assisted and active-resisted) was performed to compare position mean deviation and velocity mean deviation between the last and first tasks in bimanual training modes. On the base of the explanation given above, the comparison of position mean deviation and velocity mean deviation between the last and first tasks was not performed for single limb training modes.
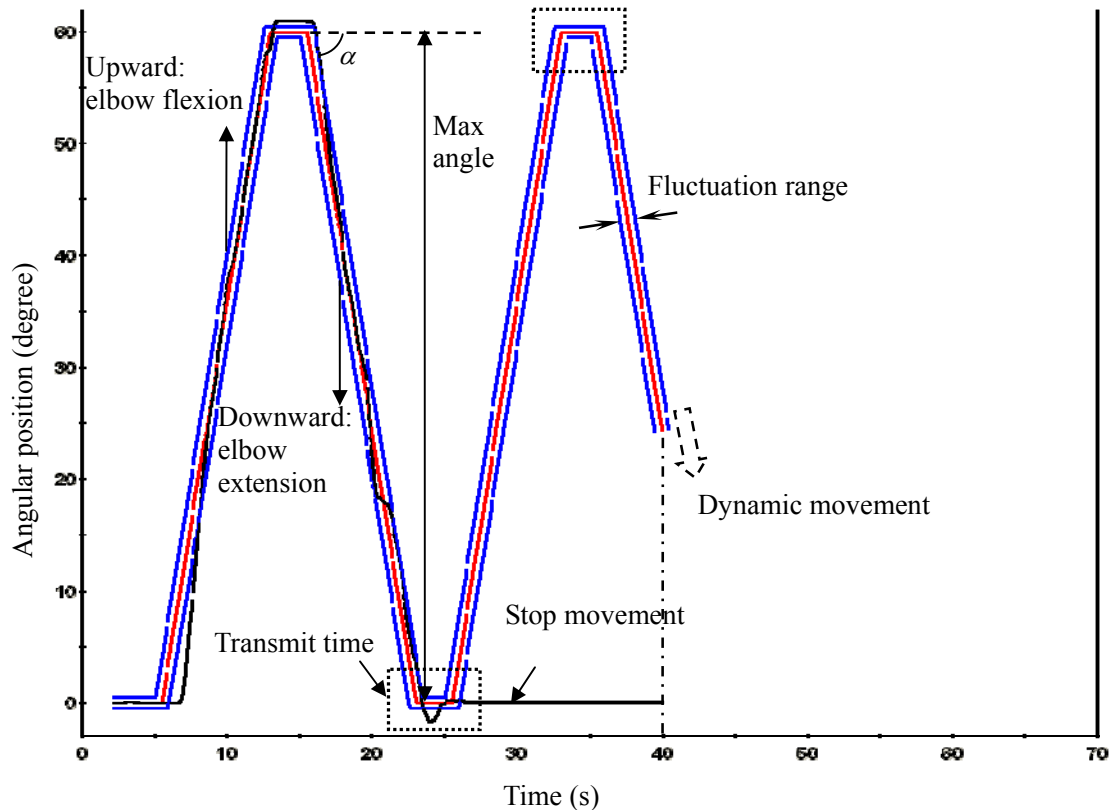
Fig. 4-10 The corresponding dynamic tracking trajectory when a task was executed till the 40 seconds. The black line was a representative movement trajectory in one terminal axis (two terminal axes have the same motion action), in order to give a clear explanation, the tracking movements of the two handles were stopped after one reciprocating period; the red line presents a desired tracking movement; two blue lines define a movement fluctuation range; both the red line and blue lines are predefined dynamic trajectories and synchronous with each other. At the moment of changing rotational direction, a transmit time is given to avoid a sharp variation of velocity. Both the reference trajectories and actual trajectory of the terminals were real-time displayed on the PC to realize a dynamic motion tracking. Vertical and horizontal ratios in this figure are different so as to give a clear image, the fluctuation range in the transmit periods is actually the same with that in other time periods.

4.2.6 Results

For one female, the feedback motion trajectories were not displayed correctly in the process of training. This resulted in an incorrect data collection of hemoglobin concentration and motion tracking information. For two males, the hemoglobin concentration sampled in some channels was unusable because some probes were not attached sufficiently firmly to the probe holders. Besides, their motion tracking information was not recorded completely. Another male performed tasks with hemoglobin concentration being recorded correctly whereas motion tracking information in active-resisted mode being unrecorded. Thereby, group analyses on cerebral activation amount were carried out on the residual 11 volunteers (eight males and three females, six performed single left-limb tasks firstly and five performed single right-limb tasks firstly), while the analyses on motion tracking precision were performed on 10 volunteers (seven males and three females, five performed single left-limb tasks firstly and five performed single right-limb tasks firstly).

A. Cerebral Activation Amount

Three-way ANOVA on 'time' $\times$ 'hemisphere' $\times$ 'mode' revealed a significant main effect of 'time' ($p = 0.027$). The estimated marginal means of ΔOxy-Hb amount in the first and last tasks were 0.089 and 0.126 mM·mm (number of molecules in one millilitre multiply the length of optical path). However, no significant interactions and main effects of 'hemisphere' and 'mode' were presented. The interactive graphs of estimated marginal means of cerebral activation concentration between 'hemisphere' and 'time' and between 'mode' and 'time' are given in Fig. 4-11 and Fig. 4-12. It can be seen that the left hemisphere achieved a greater increase in CAL than the right hemisphere, and the active-resisted training induced a greater increase in CAL than the active-assisted training.
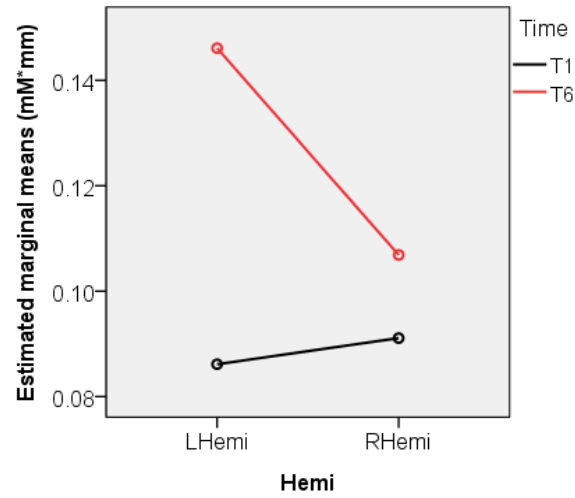
Fig. 4-11 Estimated marginal means of cerebral activation concentration for the interaction between 'hemisphere' and 'time'. The left hemisphere achieved a greater increase in cerebral activation concentration than the right hemisphere.
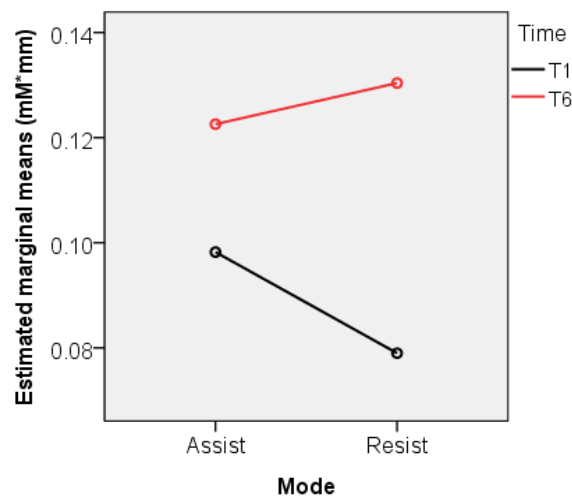
Fig. 4-12 Estimated marginal means of cerebral activation concentration for the interaction between 'mode' and 'time'. The active-resisted training mode induced a greater increase in cerebral activation concentration than the active-assisted training mode.

Three-way ANOVA on 'hemisphere' × 'region' × 'mode' revealed a significant main effect of 'region' ($p = 0.001$) and 'mode' ($p = 0.004$). Since the four training modes were compared together, and it has been confirmed that the right-limb or left-limb tasks mainly activated the contra-lateral hemisphere [23], the main effect of 'hemisphere' had no meanings. Otherwise, no significant interactions were presented. The estimated marginal means of cerebral activation
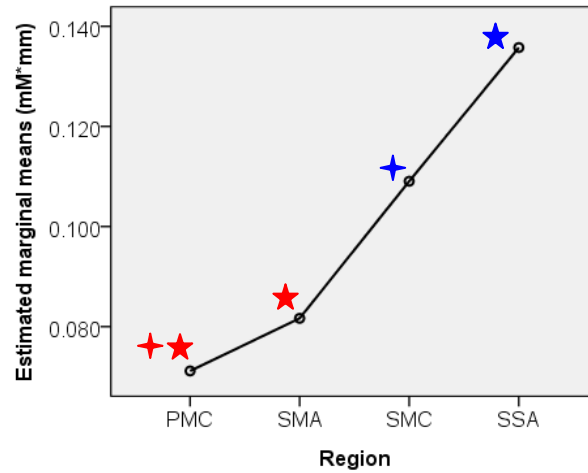
Fig. 4-13 Estimated marginal means in four motor related regions. For the factor of 'region', the cerebral activation concentration in SSA (attached with blue five-pointed star) was significantly greater than that in PMC and SMA (attached with red five-pointed stars); the cerebral activation concentration in SMC (attached with blue four-pointed star) was significantly greater than that in PMC (attached with red four-pointed star).
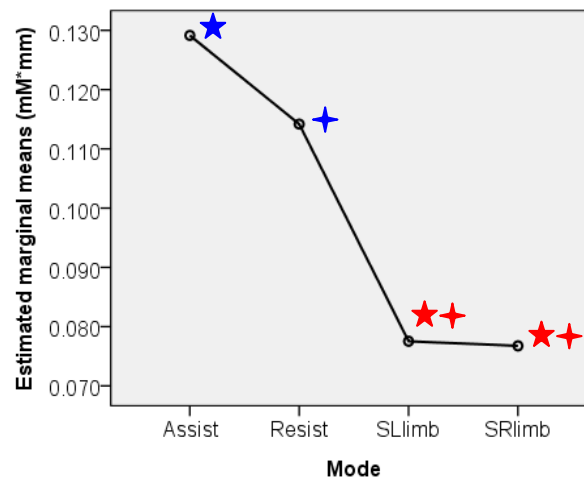
Fig. 4-14 Estimated marginal means in four training modes. For the factor of 'mode', the cerebral activation concentration induced in active-assisted mode (attached with blue five-pointed star) was significantly greater than those induced in single right-limb and left-limb modes (attached with red five-pointed stars); the cerebral activation concentration induced in active-resisted mode (attached with blue four-pointed star) was significantly greater than those induced in single right-limb and left-limb modes (attached with red four-pointed stars).

amount in different regions and modes were presented in Fig. 4-13 and Fig. 4-14, respectively.

Post-hoc analysis on 'region' revealed significant differences between SSA and PMC ($p = 0.000$),

between SSA and SMA ($p = 0.002$), and between SMC and PMC ($p = 0.033$). Post-hoc analysis on 'mode' revealed significant differences between bimanual assist and single left-limb modes ($p = 0.004$), between bimanual assist and single right-limb modes ($p = 0.003$), between bimanual resist and single left-limb modes ($p = 0.039$), and between bimanual resist and single right-limb modes ($p = 0.035$).

B. Motion Tracking Precision

Considering the motion tracking precision in assisted and resisted training modes, the volunteers-average results in six tasks are shown in Fig. 4-15. Overall, position mean deviation decreased as the increase of task number in both resisted mode and assisted mode. However, velocity mean deviation had no obvious change in two training modes. Two-way multivariate ANOVA analysis revealed a significant main effect of 'time' ($p = 0.005$) when considering $\overline{\theta_{MD}}$ and $\overline{\omega_{MD}}$ together. As for the independent variables, the position mean deviation was significantly reduced in the last task compared to that in the first task ($p = 0.017$, estimated marginal means in the first and last tasks were 1.768 and 1.359 degrees), whereas the velocity mean deviation had no significant decrease in the last task ($p = 0.06$, estimated marginal means in the first and last tasks were 2.448 and 2.268 degrees per second). No significant main effect of 'mode' was presented. Besides, the interaction between 'time' and 'mode' was not significant for both the position and velocity tracking precisions. But from Fig. 4-15 it can be seen that the reductions of mean deviations in resisted mode (0.452 degree and 0.234 degree per second) were greater than those in assisted mode (0.366 degree and 0.126 degree per second).
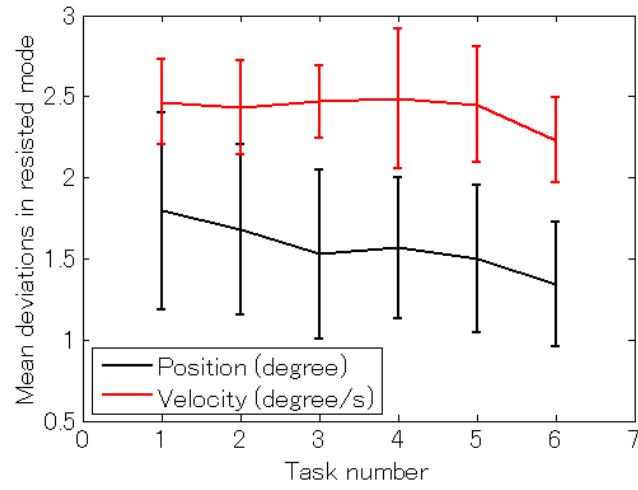
(a) Active-resisted mode
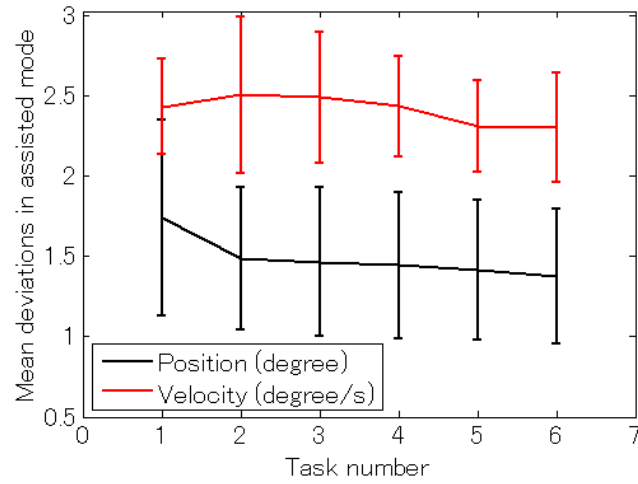
(b) Active-assisted mode

Fig. 4-15 Volunteers-average results of motion tracking precision in 6 tasks. Figures (a) and (b) display mean deviations in active-resisted and active-assisted training modes, respectively.

4.2.7 Discussion

Overall, the experiments demonstrated that the robot can support healthy subjects to perform motion tracking training in different modes with safety. After training, the significant increased CAL ($p = 0.027$) and motion tracking precision ($p = 0.005$) revealed that the proposed bimanual coordinated training implemented with our designed robot can improve the bimanual coordination capability of the healthy subjects. A greater increase in CAL was achieved in the left

hemisphere compared to in the right hemisphere (Fig. 4-11). This result was in good agreement with previous studies [24, 41], which verified that the left hemisphere can achieve an increased brain activation more easily than the right hemisphere. However, no significant difference between the two hemispheres was found in CAL increment. This may be explained with that our proposed bimanual training tasks also motivated and trained the right hemisphere greatly (no significant main effect of 'hemisphere' was obtained from the three-way ANOVA on 'time' × 'hemisphere' × 'mode' in CAL comparison). In addition, a greater increase in CAL was achieved in the active-resisted mode compared to in the active-assisted mode (Fig. 4-12). This result may be correlated with the results that greater reductions in the mean deviations of positions and velocities were achieved in active-resisted mode compared to in active-assisted mode. However, no significant difference between the two bimanual training modes was found in CAL increment (the interaction between 'time' and 'mode' of the three-way ANOVA on 'time' × 'hemisphere' × 'mode' in CAL comparison) and in the reduction of motion tracking precision (the interaction between 'time' and 'mode' of the two-way multivariate ANOVA on 'time' × 'mode' in movement precision comparison). Thus, the correlation between the enhancements of CAL and the improvement of movement performance should be further confirmed in our future study.

On the other hand, considering the motion tracking precision, a significant improvement was revealed only in position tracking ($p = 0.017$) but not in velocity tracking ($p = 0.06$). This results was consistent with that obtained in training experiment No. 1. During the task periods, the volunteers mainly focused on position tracking rather than velocity tracking. Therefore, in the short training period, the position tracking achieved a greater enhancement in accuracy compared to velocity tracking.

Significantly higher CAL in SSA compared to in PMC ($p = 0.000$) and SMA ($p = 0.002$) may be correlated with the bilateral force sensing capability of the system. However, this preliminary

conclusion should be further verified by performing more experiments on more subjects. Significantly higher CAL induced in active-assisted and active-resisted modes than that induced in single right-limb mode ($p = 0.003$ and $p = 0.035$) and single left-limb mode ($p = 0.004$ and $p = 0.039$) confirmed that bimanual training motivated brain activation to greater extent than single limb training. This may be explained by the coordination of two limbs and the planning of movement procedures in bimanual training modes.

4.3 Motion Tracking Training No. 3

In training experiment 2, no resistant or assistant force comparative to that exerted in active-resisted or active-assisted mode was provided in single-limb tasks. This reduced the reliability of our preliminary conclusion that bimanual training induced greater brain activation than single-limb training, because single-limb movement was always performed with other persons providing a resistant or assistant force. Therefore, in motion tracking training No. 3, a resistant or assistant force was attached to the other site by another person in single-limb tasks.

4.3.1 Subject

18 healthy volunteers (eleven male and seven female, age: 27.2±1.42 years old) at Kochi University of Technology participated in the motion tracking training. All the volunteers were right-handed. No volunteers had a history of physical or psychiatric disorder. Informed consent was obtained from each volunteer.

4.3.2 Training Task

Based on haptic and visual feedback, the volunteers performed elbow flexion and extension movements and controlled the master and slave terminals to track desired movements in four patterns: (1) the right limb provided an active force and the left limb exerted an auxiliary force to assist the left one in movement tasks (bimanual active-assisted mode); (2) the right limb started the movement actively while the left limb attached a resistant force to increase the impedance of the left one (bimanual active- resisted mode); (3) the right limb actively exerted a driving force on

the right handle and another person (an experiment supervisor) attached a small assistant force on the left handle to reduce the workload of the subject (unilateral-limb active-assisted mode); (4) the right limb actively exerted a driving force on the right handle while another person attached a small resistant force on the left handle to motivate the maximum effort of the subject (unilateral-limb active-resisted mode). In order to compare the difference between two control directions (right to left and left to right), training tasks in the four patterns were also performed with the left limb providing an active force, and the right limb or another person providing an assistant or resistant force in the contra-lateral side. 18 volunteers were randomly distributed to four groups (Table VII). They performed tasks in four patterns and two control directions with different training orders. This was aimed at eliminating the effects caused by the order of training patterns.

TABLE VII
FOUR GROUPS OF VOLUNTEERS IN DIFFERENT TRAINING ORDERS

Group	Male	Female	Mode	Control direction
1	3	2	Resisted	Left
			Assisted	Left
			Resisted	Right
			Assisted	Right
2	2	2	Assisted	Left
			Resisted	Left
			Assisted	Right
			Resisted	Right
3	2	2	Resisted	Right
			Assisted	Right
			Resisted	Left
			Assisted	Left
4	4	1	Assisted	Right
			Resisted	Right
			Assisted	Left
			Resisted	Left

Mode: 'resisted' or 'assisted' includes both bimanual and unilateral-limb modes;

Control direction: 'left' means from left to right, the left limb provided an active force; 'right' means from right to left, the right limb provided an active force.

A training pattern together with a control direction was defined as a training phase. Each training phase included six 20-s specific tracking tasks in a pattern of alternate bimanual-coordinated

tasks (TA) and unilateral-limb tasks (TB). Each task period was alternated with a 30-s rest period, as shown in Fig. 4-16. There was a beep to remind the volunteers of the start and end of each task. In each bimanual training task, the assistant or resistant force provided by a subject himself/ herself in the slave terminal was recorded, and in the following unilateral-limb task, another person tried to repeat the recorded force and provided a comparative assistant or resistant force. Therefore, the effect caused by obviously different slave-terminal forces in bimanual and unilateral-limb tasks could be avoided. Before the recorded experiment in each training phase, the volunteers practiced the corresponding bimanual tracking task three times to get familiar with the operation. Following was a 50-s rest period. Then, the training was performed simultaneously with the hemoglobin concentration of the volunteers and the movement information in the master and slave terminals being recorded (measurement method was the same as that introduced in training No. 2, an elastic gauze hat with 30 holes was used to fix two probe holders.). In order to present an objective evaluation, training tasks were videotaped for all the volunteers.
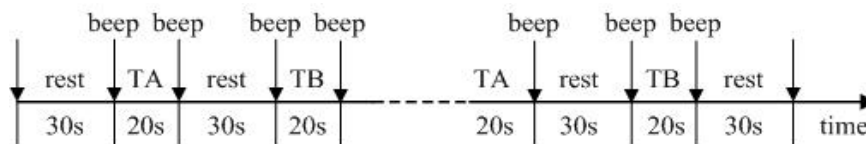
Fig. 4-16. Time sequence in one phase. TA denotes bimanual task, TB denotes unilateral-limb task.

4.3.3 Instructions for Subjects

(1) Track desired movement carefully during the whole process;

(2) Sit up straight and avoid head tilt;

(3) Try to keep head and legs stationary during the whole period of each phase;

(4) During a rest period, stop movement and maintain the same posture, close eyes and fully relax
    the brain without thinking, movement, and language before a new task.

(5) Open and close mouth or speaking is prohibited during the experimental phases;

(6) In unilateral-limb mode, perform task actively and do no not follow the movement of another person passively (exert a larger force than the assistant or resistant force of another person);

(7) In bimanual mode, keep one limb providing a larger force for both the upward and downward movement (keep the same control direction in one task).

4.3.4 Statistical Analyses

Firstly, the sampled data was analyzed in "integral mode" with ETG-7100 software. The pre time, recovery time and post time those determine a baseline for calculating a relative hemoglobin concentration in task period were 9s, 14s, and 7s, respectively. However, if a volunteer achieved a better rest of brain obviously different from the defined post time or pre time period, the lengths of pre time, recovery time, and post time were adjusted for the volunteer. The obtained relative value of Oxy-Hb was recorded with ΔOxy-Hb. Secondly, average ΔOxy-Hb in each channel was respectively calculated for different training phases. Thirdly, average ΔOxy-Hb in two hemispheres and motor related regions of SMC, SMA, PMC, and SSA were calculated. Finally, laterality index (LI) that defined as (ΔOxy-Hb in the left hemisphere $-$ ΔOxy-Hb in the right hemisphere) / (ΔOxy-Hb in the left hemisphere $+$ ΔOxy-Hb in the right hemisphere) was calculated. Positive LI indicates the left hemisphere is predominantly activated, negative LI indicates the right hemisphere is predominantly activated.

To compare the amount of hemispherical ΔOxy-Hb and regional ΔOxy-Hb induced in different training patterns (resisted and assisted modes, as well as bilateral and unilateral limb (UBlimb) operation patterns), four-way ANOVA on 'Mode' × 'UBlimb' × 'Hemisphere' × 'Region' was performed for the two control directions (CtlDir: right to left and left to right, respectively with right and left for short). The analysis model included the main effect of each factor and the interactions between two factors except that between 'Hemisphere' and 'Region'. To evaluate inter-hemispheric asymmetry of cerebral activation in different training patterns, three-way ANOVA on 'Mode' × 'UBlimb' × 'CtlDir' was also performed using the calculated LI. The

analysis model included the main effect of each factor and the interactions between two factors except that between 'Mode' and 'UBlimb'. In above analyses, if the interactions between two or three factors were significant, simple main effect for the interaction would be analyzed. If no significant interactions were obtained but the main effect of a factor was significant, post-hoc multiple comparison analysis using Tukey's honestly significant difference criterion will be further performed. The analyses were performed with SPSS software (PASW Statistics 18). Statistical significance was set at $p < 0.05$.

4.3.5 Results

All the 18 volunteers were included in data analyses. Four-way ANOVA for the amount of hemispherical ΔOxy-Hb and regional ΔOxy-Hb showed that there was a significant main effect of 'UBlimb' for the right control direction ($p \approx 0.000$, estimated marginal means in bilateral and unilateral limb patterns were 0.105 and 0.072, respectively), a main effect of 'Mode' ($p \approx 0.056$, estimated marginal means in assisted and resisted modes were 0.067 and 0.077, respectively) and a significant main effect of 'UBlimb' ($p \approx 0.000$, estimated marginal means in bilateral and unilateral limb patterns were 0.085 and 0.059, respectively) for the left control direction. However, there was no significant main effect of any other factor or significant interactions. Estimated marginal means of ΔOxy-Hb for the interactions between 'UBlimb' and 'region' is given in Fig. 4-17. For the two control directions, bimanual training achieved a higher CAL in all the motor related regions.

Three-way ANOVA for LI revealed that there was a significant main effect of 'CtlDir' ($p \approx 0.010$, estimated marginal means in the right and left control directions were 0.001 and -0.127). The main effects of other two factors had no meanings. Significant interactions between 'Mode' and 'CtlDir' ($p \approx 0.057$), and between 'BUlimb' and 'CtlDir' ($p \approx 0.007$) were also presented. The corresponding interactive graphs of estimated marginal means are given in Fig. 4-18 and Fig. 4-19. For the interaction between 'Mode' and 'CtlDir', simple main effect of 'CtlDir' was only

significant in assisted mode ($p \approx 0.002$, estimated marginal means of LI in the right and left control directions were 0.050 and -0.173). However, in resisted mode, no significant simple main effect of 'CtlDir' was presented. The corresponding estimated marginal means of LI in the right and left control directions were -0.048 and -0.082. For the interaction between 'BUlimb' and 'CtlDir', simple main effect of 'CtlDir' was only significant in unilateral limb pattern ($p \approx 0.000$, estimated marginal means of LI in the right and left control directions were 0.064 and -0.199). However, in bimanual pattern, no significant simple main effect of 'CtlDir' was presented. And the estimated marginal means of LI in the right and left control directions were -0.061 and -0.055.

4.3.6 Discussion

The main effect of 'mode' for the left control direction preliminarily evidenced that resisted mode may require more movement coordination command and thus motivated greater brain activation than assisted mode. However, no difference of resisted and assisted modes in inducing brain activation was observed for the right control direction. Therefore, the merits of resisted training mode should be further confirmed in future study.

(a)   (b)
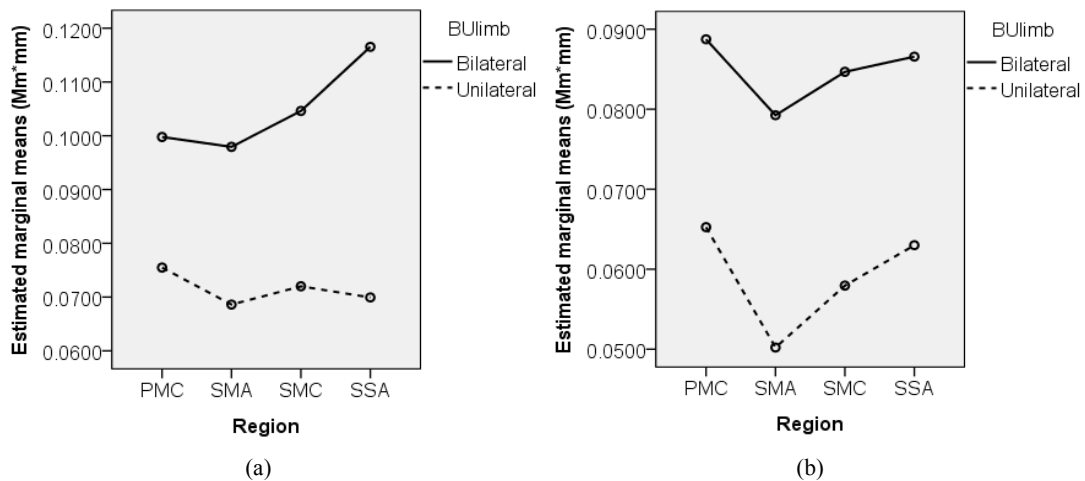
Fig. 4-17. Estimated marginal means of Δ Oxy-Hb concentration for the interaction between 'BUlimb' and 'region' direction. For the two control directions, bimanual training achieved a higher CAL in all the motor related regions.
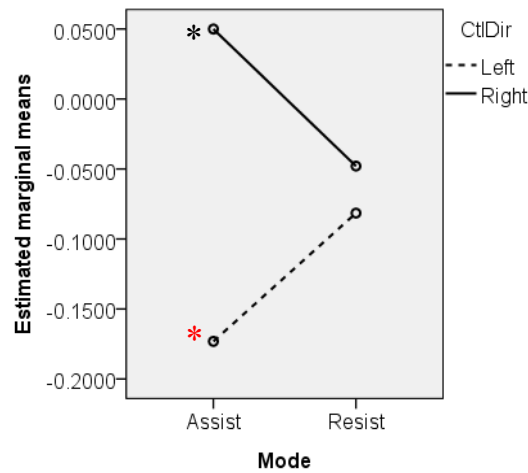
Fig. 4-18. Estimated marginal means of LI for the interaction between mode and control direction. Simple effect of control direction was significant in assisted mode (black asterisk denotes a positive LI, and red asterisk denotes a negative LI).
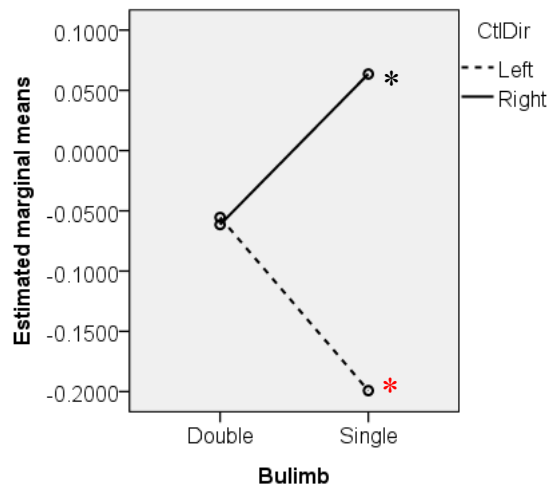
Fig. 4-19. Estimated marginal means of LI for the interaction between BUlimb and control direction. Simple effect of control direction was significant in uni-limb pattern (black asterisk denotes a positive LI, and red asterisk denotes a negative LI).

Considering four-way ANOVA on CAL, the significant main effect of 'UBlimb' and insignificant interaction between 'UBlimb' and 'hemisphere' revealed that bimanual training induced higher CAL than unilateral limb training in the both hemispheres. Bimanual training may induce the functional integrity of two hemispheres and thus activated the both hemispheres to a greater extent. The estimated marginal means for the interaction between 'UBlimb' and 'Region' (Fig.

4-17) showed that bimanual training induced higher CAL than unilateral limb training in all the motor related regions. This confirmed that bimanual training fully motivated motor-control related regions (SMC, SMA, and PMC) and movement sensation region (SSA) in brain. Higher CAL in two hemispheres and all the motor related regions evidenced the proposed bimanual training have a potential for promoting motor function recovery in rehabilitation therapy.

As for assisted training mode, the positive LI in the right control direction (0.050) indicated that when an active force with a larger magnitude provided by the right limb, greater cerebral activation was induced in the left hemisphere; the negative LI in the left control direction (-0.173) indicated that when an active force with a larger magnitude provided by the left limb, greater cerebral activation was induced in the right hemisphere. As for resisted training mode, the negative LI in both the right and left control directions (-0.048 and -0.082) revealed no matter that which limb provided an active force with a larger magnitude, the right hemisphere was predominantly activated. Considering unilateral limb training pattern, the positive LI in the right control direction (0.064) and negative LI in the left control direction (-0.199) demonstrated that unilateral limb training mainly activated the contra-lateral hemisphere. But in bimanual training pattern, the LI in both the right and left control directions were negative (-0.061 and -0.055). This indicated that bimanual training activated the right hemisphere to a greater extent for the both control directions. Overall, the simple effects of two interactions between 'Mode' and 'CtlDir' and between 'BUlimb' and 'CtlDir' preliminarily revealed that assisted training activated the contra-lateral hemisphere to a greater extent compared to resisted training, and unilateral limb training activated the contra-lateral hemisphere to a greater extent compared to bimanual training. That is, relatively easier tasks inclined to induce an obvious inter-hemispheric asymmetry of cerebral activation, and more difficult tasks inclined to activate the right hemisphere, which is less active than the left hemisphere for the right-handed volunteers. This result was consistent with that observed in the previous study [42], which showed that the complex motor tasks were usually accompanied by a bilateral hemisphere activation of cerebral cortices, and the easy tasks

usually only activated contra-lateral activation.

5. Conclusions

5.1 Summary

5.1.1 Master-Slave Rehabilitation Robot

This paper introduced a new master-slave rehabilitation robot with two DC motors and an H-bridge driver constructing a closed-loop circuit. The master motor works in generating state and supplies energy for the slave motor, which is driven to reproduce the movement of the master motor and to support the connected limb in motion imitation.

The system is capable of mirroring the force from the slave to the master without a force sensor, thus the hardware mounting difficulty can be reduced greatly. Accurate motion tracking was achieved within the velocity's frequency response range of around 30 Hz. The maximum velocity error was 0.5987 degree per second and the maximum angular position error was 0.0719 degree. The tracking precision is comparative with the system introduced in [7]. It satisfies the application requirement for a rehabilitation robot. Force sensing and motion tracking are realized simultaneously with only a master-slave motion tracking controller. This reduces the control complexity significantly. Besides, the characteristic of energy recycling makes a lightweight battery be able to supply enough power for the system, thus, reduces the design burden of the power supply unit. Additionally, self-controlled operation, together with the force sensing capability, will enable patients to adjust the force of the healthy limb timely according to the feel of the impaired limb and the movement intent of the impaired one, further avoiding pain and unpredictable reactions. As well, bidirectional controllability (right to left or left to right) makes the system capable of delivering treatment for patients no matter which limb is impaired, and without any demand for hardware reconfiguration.

Moreover, the force sensing coefficient mainly depends on the gear ratios of the gearboxes. Based

on the effects of different gear ratio combinations, the system hardware configuration can be considered according to the emphases in applications. For example, when the healthy limb possesses sufficient power, and patients want to exercise the healthy limb simultaneously while carrying out rehabilitation training, the master/gear unit can select a gearbox with a larger gear ratio. Then, the energy of the power supply unit, such as a battery, can be saved greatly. However, the gear ratio is not allowed to be very large since the gearbox in the master site works in the back-drivable state and it is easy to destroy it when the gear ratio is too large. In contrast, if patients are older subjects and the healthy limb has not enough power due to the weak motor function, the gearbox in the master site with a smaller gear ratio will be preferable.

Furthermore, different operating modes can be achieved by coordinating the forces of the two limbs. The clinical trial with MIME [43, 44] has proved that the treatments with patient's active participation (robot-assisted treatment) can produce larger improvements on a motor impairment scale, and active-constraint training can achieve a greater strength gains. However, the bilateral training has no advantage over the unilateral training except that hypertonia and abnormal synergies can be reduced. In this system, the required control force, assistant force, or resistant force is from the healthy limb rather than the robot. This is different from MIME, in which the healthy limb provides a reference movement while the robot gives an assistant force for bilateral exercises. This means that the healthy limb not just provides a reference but also produces a suitable force (in-phase or reverse in direction) for the impaired one. Therefore, much more cognitive processing will be involved in training tasks. The proposed bimanual training make the robot may support bimanual-constrained tasks that prevalently exist in daily life and advance the adaption of patients in dealing with daily tasks.

Since the master and the slave units have a wired connection, the relative position of the two units can be regulated if they are designed with independent and position-adjustable base plates. Based on this characteristic, the system will be able to support multiple movements, such as wrist/ elbow/shoulder flexion/extension, shoulder abduction/adduction, forearm pronation/supination

and so on, by adjusting the positions of the two units and replacing the handles in the two terminals. This will be an advantage over some conventional systems that achieve a mechanical coupling between the unimpaired and impaired arms, such as the system introduced in [45].

However, the no-load torques of motors and the efficiency of gearboxes increased the requirement for the input power from the healthy limb or another person. Thereby, motors and gearboxes with higher efficiency should be employed, whereas the system cost will be increased relatively. Besides, the device has only one degree of freedom (DOF) and a different mechanism with human limbs. Otherwise, the current device has not additional Velcro fasteners attached to the handles. It can not strap the wrist of the impaired limb that does not have enough power to hold a handle. These deficits make the robot unfavorable for supporting rehabilitation therapy on patients.

5.1.2 Training Experiments

Bimanual training experiment No. 1 verified a positive training effect based on the improvement of motion tracking precision. Further, training experiment No. 2 fully confirmed a positive training effect based on the enhancement of both the movement performance and cerebral activation level. The corresponding results preliminarily revealed that bimanual training motivated greater cerebral activation than single-limb training. And active-resisted mode, which was a particular training method supported by our designed robot, achieved a greater enhancement in CAL and movement performance compared to active-assisted mode. However, no significant difference was presented.

In training experiment No. 3, a resistant or assistant force was provided by another person in single-limb tasks. This increased reliability of the comparison in cerebral activation amount between bimanual and single-limb training patterns. In addition, the training was performed in different control directions (right to left and left to right) for fully analyzing the asymmetry of two hemispheres in cerebral activation. Statistical analysis results in the third experiment completely

confirmed that bimanual coordinated tasks induced significantly greater cerebral activation than single-limb tasks in both hemispheres and all the motor related regions. Besides, active-resisted training motivated brain activation to an obviously greater extent than active-assisted training in the left (left to right) control direction. Combining with experiment No. 2's result that active-resisted exercise achieved a greater enhancement in CAL and movement performance than active-assisted exercises, it is indicated that the proposed active-resisted training mode may be more preferable for promoting motor function improvement. In addition, active-resisted training and bimanual exercises achieved a better symmetry of two hemispheres in cerebral activation. The results preliminarily reflected that relatively easier tasks in active-assisted or unilateral limb training pattern activated the contra-lateral hemisphere predominantly and thus induced an obvious inter-hemispheric asymmetry of cerebral activation; while relatively difficult tasks in active-resisted or bimanual training pattern induced cerebral activation in both hemispheres to a certain extent, and the right hemisphere that is not predominantly used for the right handed volunteers was fully activated in our experiments. Overall, bimanual coordinated training may induce the functional integrity of two hemispheres, and thus may be more favorable for activating brain and promoting motor function recovery and enhancement. The designed robot supports both bimanual and unilateral limb training tasks, this makes it has a great potential for delivering rehabilitation therapy and improving motor function in a large scale.

Furthermore, the analyses on oxygenated hemoglobin concentration objectively assessed the training effect in view of cerebral activation level. This evaluation method can avoid subjective factors those existed in traditional assessment methods, such as Fugl-Meyer (FM) scale, Motor status score (MSS), Modified Ashworth Scale (MAS) score, and so on.

However, the training experiments were only performed on healthy subjects, and the number of the subjects was limited. The current conclusions should be further confirmed on more subjects and hemiplegic patients.

5.2 Future Work and Prospect

(1) This one D.O.F. (degree of freedom) robotic system will be expanded to a multiple D.O.F. mechanism with multi-motor combinations so as to make it conform to the mechanism of human limbs and more suitable for upper limb rehabilitation training in daily life.

(2) Motion tracking controller and the hardware design should be improved for enabling the robot to support both mirror-symmetric and anti-symmetric movement. And light-weight motors and gearheads should be applied in order that make the robot portable and capable of supporting self-powered rehabilitation therapy with one less impaired limb assisting more impaired limb, no matter that the coordinated two limbs are upper or lower limbs, such as walking, stair climbing, and riding.

(3) Training task should be improved more practical in daily life so as to achieve a better recovery effect. Tests on more volunteers will be performed to fully confirm the relation between the enhancement of brain activation and the improvement of movement performance. As well, training experiments on hemiplegic patients should be performed so as to confirm the effectiveness of the designed robotic system and advantages of the proposed bimanual training methods in rehabilitation therapy.

(4) We are considering applying myoelectric signal of limbs in the master-slave motion controller, in order that enable the robot to support patients in performing tasks in terms of the patients' movement intent even though the both limbs have weak residual motor function.

The characteristics force sensing without using a force sensor, give the proposed new master-slave mechanism great potential in application fields of rehabilitation, minimally invasive surgery, manipulation, and so on. If proper components are selected for the slave site, this working mechanism can also be applied in isolated environments (high temperature, radiation, toxic).

References

[1] Hogan, N.; Krebs, H.I. Interactive robots for neuro-rehabilitation. J. Restorative Neurology and Neuroscience. **2004**, 22(3), pp. 349–358.

[2] Krebs, H.I.; Volpe, B.T.; Aisen, M.L.; Hogan, N. Increasing productivity and quality of care: Robot-aided neuro-rehabilitation. J. Rehabil Res Develop. **2000**, 37 (6), pp. 639–652.

[3] Reinkensmeyer, D.J.; Kahn, L.E.; Averbuch, M.; McKenna-Cole, A.; Schmit, B.D.; Zev Rymer, W. Understanding and treating arm movement impairment after chronic brain injury: progress with the ARM Guide. J. Rehabil Res Develop. **2000**, 37 (6), pp. 653–662.

[4] Reinkensmeyer, D.J.; Dewald, J.P.A.; Rymer, W.Z. Guidance-based quantification of arm impairment following brain injury: a pilot study. IEEE Trans Rehabil Eng. **1999**, 7 (1), pp. 1–11.

[5] Lum, P.S.; Burgar, C.G.; Shor, P.C.; Majmundar, M.; Van der Loos, M. Robot-assisted movement training compared with conventional therapy techniques for the rehabilitation of upper-limb motor function after stroke. Arch Phys Med Rehabil. **2002**, 83 (7), pp. 952-959.

[6] Lum, P.S.; Burgar, C.G.; Shor, P.C. Evidence for improved muscle activation patterns after retraining of reaching movements with the MIME robotic system in subjects with post-stroke hemiparesis. IEEE Trans. Neural Syst. Rehabil. Eng. **2004**, 12 (2), pp. 186-194.

[7] Nef, T.; Mihelj, M.; Riener, R. ARMin: A robot for patient-cooperative arm therapy. Medical and Biological Engineering and Computing. **2007**, 45 (9), pp. 887–900.

[8] van Exel, N.J.A.; Koopmanschap, M.A.; Scholte op Reimer, W.; Niessen, L.W.; Huijsman, R. Cost-effectiveness of integrated stroke services. QJM - Monthly Journal of the Association of Physicians. **2005**, 98 (6), pp. 415-425.

[9] Park, H.-S.; Peng, Q.; Zhang, L.-Q. A Portable Telerehabilitation System for Remote Evaluations of Impaired Elbows in Neurological Disorders. IEEE Trans. Neural Syst. Rehabil. Eng. **2008**, 16 (3), pp. 245-254.

[10] Peng, Q.; Park, H.-S.; Zhang, L.-Q. A Low-Cost Portable Tele-Rehabilitation System for the Treatment and Assessment of the Elbow Deformity of Stroke Patients. Proc. 2005 IEEE 9th Int. Conf. on Rehabilitation Robotics, Chicago, Illinois, USA. **2005**, 28 June-1 July, pp.149-151.

[11] Park, H.-S.; Peng, Q.; Zhang, L.-Q. Causality-Based Portable Control System Design for Tele-Assessment of Elbow Joint Spasticity. Proc. 2005 IEEE 9th Int. Conf. on Rehabilitation Robotics, Chicago, Illinois. **2005**, 28 June-1 July, pp.303-306.

[12] Reinkensmeyer, D.J.; Pang, C.T.; Nessler, J.A.; Painter, C.C. Web-based telerehabilitation for the upper extremity after stroke. IEEE Trans. Neural Syst. Rehabil. Eng. **2002**, 10 (2), pp. 102-108.

[13] Jadhav, C.; Nair, P.; Krovi, V. Individualized interactive home-based haptic telerehabilitation. IEEE Multimedia. **2006**, 13 (3), pp. 32-39.

[14] Perry, J.C.; Rosen, J.; Burns, S. Upper-limb powered exoskeleton design. IEEE/ASME Trans. Mechatronics. **2007**, 12 (4), pp. 408-417.

[15] Feng, X.; Winters, J.M. An interactive framework for personalized computer-assisted neurorehabilitation. IEEE Trans. Inf. Technol. Biomed. **2007**, 11 (5), pp. 518-526.

[16] Popescu, V.G.; Burdea, G.C.; Bouzit, M.; Hentz, V.R. A Virtual-Reality-Based Telerehabilitation System with Force Feedback. IEEE Trans. Inf. Technol. Biomed. **2000**, 4 (1), pp. 45-51.

[17] Colombo, R.; Pisano, F.; Micera, S.; Mazzone, A.; Delconte, C.; Chiara Carrozza, M.; Dario, P.; Minuco, G. Robotic Techniques for Upper Limb Evaluation and Rehabilitation of Stroke Patients. IEEE Trans. Neural Syst. Rehabil. Eng. **2005**, 13 (3), pp. 311-324.

[18] Whitall, J.; Waller, S.M.; Silver, K.H.C.; Macko, R.F. Repetitive bilateral arm training with rhythmic auditory cueing improves motor function in chronic hemiparetic stroke. Stroke, **2000**, 31 (10), pp. 2390-2395.

[19] Luft, A.R., McCombe-Waller, S., Whitall, J., Forrester, L.W., Macko, R., Sorkin, J.D., Schulz, J.B., Hanley, D.F., *et al*. Repetitive Bilateral Arm Training and Motor Cortex Activation in Chronic Stroke: A randomized controlled trial. JAMA, **2004**, 292 (15), pp. 1853-1861.

[20] Hesse, S.; Schulte-Tigges, G.; Konrad, M.; Bardeleben, A.; Werner, C. Robot-assisted arm trainer for the passive and active practice of bilateral forearm and wrist movements in hemiparetic subjects. Archives of Physical Medicine and Rehabilitation, **2003**, 84 (6), pp. 915-920.

[21] Hesse, S.; Werner, C.; Pohl, M.; Rueckriem, S.; Mehrholz, J.; Lingnau, M.L. Computerized arm training improves the motor control of the severely affected arm after stroke: A single-blinded randomized trial in two centers. Stroke, **2005**, 36 (9), pp. 1960-1966.

[22] Lloyd-Fox, S., Blasi, A., Elwell, C.E. Illuminating the developing brain: The past, present and future of functional near infrared spectroscopy. Neuroscience and Biobehavioral Reviews, **2010**, 34 (3), pp. 269-284.

[23] Kato, H., Izumiyama, M., Koizumi, H., Takahashi, A., Itoyama, Y. Near-infrared spectroscopic topography as a tool to monitor motor reorganization after hemiparetic stroke: A comparison with functional MRI. Stroke, **2002**, 33 (8), pp. 2032-2036.

[24] Watanabe, A., Matsuo, K., Kato, N., Kato, T. Cerebrovascular Response to Cognitive Tasks and Hyperventilation Measured by Multi-Channel Near-Infrared Spectroscopy. J Neuropsychiatry Clin Neurosci, **2003**, 15 (4), pp. 442-449.

[25] Imai, I., Takeda, K., Shiomi, T., Taniguchi, T., Kato, H. Sensorimotor cortex activation during mirror therapy in healthy right-handed subjects: A study with near-infrared spectroscopy. Journal of Physical Therapy Science, **2008**, 20 (2), pp. 141-145.

[26] Niide, W., Tsubone, T., Wada, Y. Identification of moving limb using near infrared spectroscopic signals for brain activation. Proc. Int. Joint Conf. Neural Networks, Atlanta, GA, **2009**, pp. 2264-2271.

[27] Amemiya, K., Ishizu, T., Ayabe, T., Kojima, S. Effects of motor imagery on intermanual transfer: A near-infrared spectroscopy and behavioural study. Brain Research, **2010**, 1343 (C), pp. 93-103.

[28] Miyai, I., Yagura, H., Hatakenaka, M., Oda, I., Konishi, I., Kubota, K. Longitudinal Optical Imaging Study for Locomotor Recovery after Stroke. Stroke, **2003**, 34 (12), pp. 2866-2870.

[29] Takeda, K., Gomi, Y., Imai, I., Shimoda, N., Hiwatari, M., Kato, H. Shift of motor activation areas during recovery from hemiparesis after cerebral infarction: A longitudinal study with near-infrared spectroscopy. Neuroscience Research, **2007**, 59 (2), pp. 136-144.

[30] Biernaskie, J., Szymanska, A., Windle, V., Corbett, D. Bi-hemispheric contribution to functional motor recovery of the affected forelimb following focal ischemic brain injury in rats. European Journal of Neuroscience, **2005**, 21 (4), pp. 989-999.

[31] Zatsiorsky, Vladimir M., Seluyanov, V.N. Mass and Inertia Characteristics of the Main Segments of the Human Body. International Series on Biomechanics, **1983**, 4 (B), pp.1152-1153. Available: http://www.dh.aist.go.jp/bodyDB/m/k-05.html

[32] Jiang, Y., Wang, S. Speed dependency of cerebral blood volume changes during visual cognitive activation measured with NIRS. Proc. 3rd Int IEEE. EMBS Conf. on Neural Engineering, Kohala Coast, HI, **2007**, pp. 306-309.

[33] Lin, P.-Y., Lin, S.-I., Penney, T., Chen, J.-J.J. Applications of near infrared spectroscopy and imaging for motor rehabilitation in stroke patients. Journal of Medical and Biological Engineering, **2009**, 29 (5), pp. 210-221.

[34] Boas, D.A., Dale, A.M., Franceschini, M.A. Diffuse optical imaging of brain activation: Approaches to optimizing image sensitivity, resolution, and accuracy. NeuroImage, **2004**, 23 (SUPPL. 1), pp. S275-S288.

[35] Klem, G.H., Lüders, H.O., Jasper, H.H., Elger, C. The ten-twenty electrode system of the International Federation. Electroencephalogr Clin Neurophysiol, **1999**, Suppl 52, pp. 3-6.

[36] Okamoto, M., Dan, H., Sakamoto, K., Takeo, K., Shimizu, K., Kohno, S., Oda, I., Dan, I., *et al*. Three-dimensional probabilistic anatomical cranio-cerebral correlation via the international 10-20 system oriented for transcranial functional brain mapping. NeuroImage, **2004**, 21 (1), pp. 99-111.

[37] 田中謙次. ブレインコンピュータインタフェースのためのモデル選択に関する研究. 筑波大学大学院博士課程, システム情報工学研究科, **2006.**

[38] 渡辺 茂, 坂井克之, ヴィラヤヌル S. ラマチャンドラン. 宇宙にまで進出した知的生命体 ヒト **Homo sapiens** ヒトのずば抜けた'頭脳', そのしくみは? Newton graphic seisence magzine, **2010**, 30 (12), pp. 22-53.

[39] Plichta, M.M., Herrmann, M.J., Baehne, C.G., Ehlis, A.-C., Richter, M.M., Pauli, P., Fallgatter, A.J. Event-related functional near-infrared spectroscopy (fNIRS): Are the measurements reliable? Neuroimage, **2006**, 31 (1), pp. 116–124.

[40] Optical topography basic course: analysis guide. In: Optical topography user conference, Hitachi Med. Corp. Japan **2009**, 1-36.

[41] Kim, S.-G., Ashe, J., Hendrich, K., Ellermann, J.M., Merkle, H., Ugurbil, K., Georgopoulos, A.P., Functional magnetic resonance imaging of motor cortex: hemispheric asymmetry and handedness. Science, **1993**, 261 (5121), pp. 615–617.

[42] Shibasaki, H., Sadato, N., Lyshkow, H., Yonekura, Y., Honda, M., Nagamine, T., Suwazono, S., Konishi, J, *et al.* Both primary motor cortex and supplementary motor area play an important role in complex finger movement. Brain, **1993**, 116 (6), pp. 1387-1398.

[43] Lum, P.S.; Burgar, C.G.; Van Der Loos, M.; Shor, P.C.; Majmundar, M.; Yap, R. The MIME robotic system for upper-limb neuro-rehabilitation: Results from a clinical trial in subacute stroke. Proc. 2005 IEEE 9th Int. Conf. on Rehabilitation Robotics, Chicago, Illinois. **2005**, 28 June-1 July, pp. 511-514.

[44] Lum, P.S.; Burgar, C.G.; Van Der Loos, M.; Shor, P.C.; Majmundar, M.; Yap, R. MIME robotic device for upper-limb neurorehabilitation in subacute stroke subjects: A follow-up study. J. Rehabil Res Develop. **2006**, 43 (5), pp. 631-642.

[45] Hesse, S.; Schmidt, H.; Werner, C. Machines to support motor rehabilitation after stroke: 10 Years of experience in Berlin. J. Rehabil Res Develop. **2006**, 43 (5), pp. 671-678.

Appendix

Appendix A

Derivation of Transfer Function Diagram

The Laplace transform of vlotage balance equantion of the closed-loop circuit is:

$$E_{\text{sup}}(s) + E_1(s) - E_2(s) = (Ls + R)I(s) \tag{29}$$

where

$$\begin{cases} E_{\text{sup}}(s) = [W_{in}(s) - W_{out}(s)]C(s) \\ E_1(s) = C_T W_1(s) \\ E_2(s) = C_T W_2(s) \end{cases} \tag{30}$$

$$W_1(s) = NW_{in}(s), W_2(s) = NW_{out}(s) \tag{31}$$

The meanings of all the symbols are listed in Table VIII. The electro-megnetic torque of the motors is expressed as:

$$T_M(s) = C_T I(s) \tag{32}$$

Combining Eqs. (6), (7), (8), and (9), we can get the expression of electro-megnetic torque:

$$T_M(s) = \frac{C_T}{Ls + R}\{[W_{in}(s) - W_{out}(s)]C(s) + NC_T W_{in}(s) - C_T W_2(s)\} \tag{33}$$

The torque balance equations of the two motors are written as:

$$\frac{T_{in}(s)}{N} = T_M(s) + (Js + B)W_1(s) \tag{34}$$

$$\frac{T_{out}(s)}{N} = T_M(s) - (Js + B)W_2(s) \tag{35}$$

Based on Eqs. (8) and (12), the output velocity in the slave terminal can be expressed as:

TABLE VIII: SYMBOL MEANINGS.

Symbol	Meaning
L	Armature inductance summation of the two motors
R	Armature resistance summation of the two motors
J	Equivalent inertial moment
B	Equivalent viscous friction coefficient
C_T	Motor torque constant
N	Gear ratio of gearheads
T_0	Unload torque
T_M	Motor electromagnetic torque
i	Current in the closed-loop circuit
α	Duty cycle of the PWM signal
u_s	Supply voltage of the H-bridge driver
$e_{\sup}$	Supplementary energy
e_1, e_2	Motor armature voltage
ω_1, ω_2	Rotational velocity of motors
ω_{in}, ω_{out}	Angular velocity in terminals
T_{in}, T_{out}	Terminal torque
$C(s)$	Motion tracking controller

$$W_{out}(s) = \frac{1}{N} W_2(s) = \left[T_M(s) - \frac{T_{out}(s)}{N} \right] \frac{1}{Js+B} \frac{1}{N} \tag{36}$$

By combining Eqs. (8), (11), and (12), the input velocity in the master terminal can be written as:

$$W_{in}(s) = \left[T_{in}(s) - T_{out}(s) \right] \frac{1/N^2}{Js+B} - W_{out}(s) \tag{37}$$

The transfer function diagram of the system is set up based on Eqs. (10), (13), and (14). In addition, we can get the expression of velocity difference by adding Eqs. (11) and (12):

$$W_1(s) - W_2(s) = \frac{\left[T_{in}(s) + T_{out}(s) \right]/N - 2T_M(s)}{Js+B} \tag{38}$$

When the system achieves symmetric movement accurately, $\omega_1 = \omega_2$, the electro-megnetic torque can be expressed with the input and output torques as:

$$NT_M(s) = \frac{T_{in}(s) + T_{out}(s)}{2} \tag{39}$$

If a resistant force is attached to the slave terminal, T_{out} will be positive; while if an assistant force is attached to the slave terminal, T_{out} will be negative.

Acknowledgments

To my advisor Prof. Yoshio Inoue, who provided me with his enthusiastic suggestions and advice to support my research works. If I am one day a nice researcher, much of it will be his doing.

To my vice-advisor Prof. Kyoko Shibata, who gave me so many useful suggestions and much support in the process of developing my project.

To my vice-advisor Prof. Koichi Oka, an experienced researcher, his precious suggestions on motion control help me so much.

To Prof. Shuoyu Wang, who gave me many valuable advices on the analysis of brain activation and supported me in performing experiments with NIRS system. His support made me generate considerable interest in studying the brain activation of humans.

To assistant teacher Tao liu, who gave me a lot of help in my research and in my daily life. Many experiences in system design and article writing obtained from him endowed me confidence in my future research and work.

To assistant teacher Yinlai Jiang, who taught me how to use NIRS system and gave me instruction on NIRS data analysis.

To all the other members of SSP students, make me feel so fine and happy. Particularly, they helped me to finish many training experiments.

To all the other members of Robotics and Dynamic Lab. They make me feel so comfortable and happy. Special acknowledgments to my tutor Nozomu Imanishi who helped me to deal with a lot of probelmes when I just cam Japan.

At last but no least, thank SSP of KUT and Kokuhi Scholarship of Japanese Government (Monbukagaku-sho) for kind supports.